

Development of Improved Reactive Power Optimization Schemes for PV and Wind Penetrated Grids using Advanced Electronic Compensators

Thesis submitted by
Swati Suman

Doctor of Philosophy (Engineering)

Department of Electrical Engineering
Faculty Council of Engineering & Technology
Jadavpur University
Kolkata, India

November-2022

Development of Improved Reactive Power Optimization Schemes for PV and Wind Penetrated Grids using Advanced Electronic Compensators

Thesis submitted by
Swati Suman

Doctor of Philosophy (Engineering)

Department of Electrical Engineering
Faculty Council of Engineering & Technology
Jadavpur University
Kolkata, India

November-2022

**JADAVPUR UNIVERSITY
KOLKATA-700032, INDIA**

INDEX NO.: 282/18/E

- 1. Title of the Thesis:** **Development of Improved Reactive Power Optimization Schemes for PV and Wind Penetrated Grids using Advanced Electronic Compensators**
- 2. Name, Designation & Institution of the Supervisor:** **Name: Dr. Debashis Chatterjee**
Designation: Professor,
Department: Electrical Engineering,
Institution: Jadavpur University,
Kolkata 700032, West Bengal, India.

3. List of Publications:

- I. **S. Suman**, D. Chatterjee, & R. Mohanty, “Development of Improved Harmonic Compensation Technique for PV-wind Hybrid Distributed Generator Connected to Microgrid”, **Electric Power Systems Research**, 210, pp. 108071,2022. **DOI: <https://doi.org/10.1016/j.epsr.2022.108071>**.
- II. **S. Suman**, D. Chatterjee, & R. Mohanty, “A Novel Approach for Mitigating Power Quality Issues in a PV Integrated Microgrid System Using an Improved Jelly Fish Algorithm. **Journal of Bionic Engineering**, pp. 1-17, 2022. **DOI: <https://doi.org/10.1007/s42235-022-00252-7>**.
- III. **S. Suman**, D. Chatterjee, M. Anand, R. Mohanty & A. Bhattacharya, “An Improved Harmonic Reduction Technique for the PV-Wind Hybrid Generation Scheme using Modified Whale Optimization Algorithm (MWOA)”, **U.P.B. Sci. Bull., Series C**, 84(1), ISSN 2286-3540, 2022.
- IV. **S. Suman**, D. Chatterjee, & R. Mohanty, “Improved Performance for Microgrid Connected PV-based Converters under Partial Shading Conditions by using a Cuckoo Search Algorithm Integrated with Improved Particle Swarm Optimization. **International Journal of Bio-Inspired Computation**, pp. 123-136, 21(3), 2023.

4. List of Patents:

NIL.

5. List of Presentations in National/International/Conferences/Workshops:

- I. **S. Suman**, D. Chatterjee, & R. Mohanty, “Comparison of PSO and GWO Techniques for SHEPWM Inverters”, **In 2020 International Conference on Computer, Electrical & Communication Engineering (ICCECE)**, IEEE, pp. 1-6, 2020. **DOI: [10.1109/ICCECE48148.2020.9223108](https://doi.org/10.1109/ICCECE48148.2020.9223108)**.
- II. **S. Suman**, D. Chatterjee, & R. Mohanty, “Speed Range Improvement of Induction Generator for wind Power Applications. **In 2020 International**

Conference on Computational Intelligence for Smart Power System and Sustainable Energy (CISPSSE), IEEE, pp. 1-6, 2020. DOI: 10.1109/CISPSSE49931.2020.9212277.

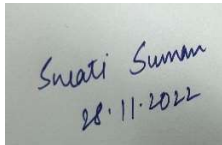
- III. **S. Suman, S., R. Mohanty, & D. Chatterjee, “Comparison of Multi-carrier MLI, CHB-MLI, SHEPWM and SPWM Inverters for PV-Grid Integration”, In: Mahanta, P., Kalita, P., Paul, A., Banerjee, A. (eds) Advances in Thermofluids and Renewable Energy, Lecture Notes in Mechanical Engineering, Springer, Singapore, pp. 669-681, 2022. DOI: https://doi.org/10.1007/978-981-16-3497-0_54.**
- IV. **S. Suman, R. Mohanty, D. Chatterjee, and G. Sengupta, “PV Based Multi Output Boost Converter Fed AC-DC hybrid Distribution System for Residential/Industrial Application”, In 2020 International Conference on System, Computation, Automation and Networking (ICSCAN), IEEE, pp. 1-6, 2020. DOI: 10.1109/ICSCAN49426.2020.9262418.**

“Statement of Originality”

I **Swati Suman** registered on **23rd May’ 2018** do hereby declare that this thesis entitled **“Development of Improved Reactive Power Optimisation Schemes for PV and wind Penetrated Grids using Advanced Electronic Compensators”** contains literature survey and original research work done by the undersigned candidate as part of Doctoral studies.

All information in this thesis have been obtained and presented in accordance with existing academic rules and ethical conduct. I declare that, as required by these rules and conduct, I have fully cited and referred all materials and results that are not original to this work.

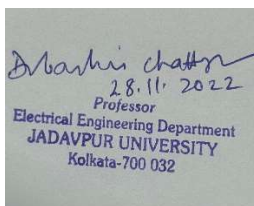
I also declare that I have checked this thesis as per the “Policy on Anti Plagiarism, Jadavpur University, 2019”, and the level of similarity as checked by iThenticate software is **2%**.



Swati Suman
28.11.2022

Signature of Candidate:

Date:



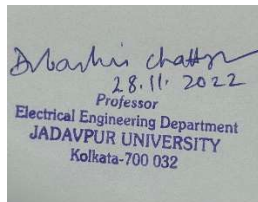
Dr. Barshis Chatterjee
28.11.2022
Professor
Electrical Engineering Department
JADAVPUR UNIVERSITY
Kolkata-700 032

Certified by Supervisor:

(Signature with date, seal)

CERTIFICATE FROM THE SUPERVISOR/S

This is to certify that the thesis entitled “**Development of Improved Reactive Power Optimisation Schemes for PV and wind Penetrated Grids using Advanced Electronic Compensators**” submitted by **Swati Suman**, who got her name registered on **23rd May, 2018** for the award of Ph.D. (Engineering) degree of Jadavpur University, is absolutely based upon her own work under the supervision of **Dr. Debashis Chatterjee**, Professor, Electrical Engineering Department, Jadavpur University and that neither her thesis nor any part of the thesis has been submitted for any degree/diploma or any other academic award anywhere before.



Debashis Chatterjee
28.11.2022
Professor
Electrical Engineering Department
JADAVPUR UNIVERSITY
Kolkata-700 032

(Signature of the Supervisor
and date with Office Seal)

Acknowledgement

The research work and the current thesis are outcomes of constant inspiration and help from a number of persons at various spheres of my association. I would like to convey my most sincere recognition to each and every one for their respective assists.

At the onset, I would like to convey my heartfelt gratitude and deepest regards to my supervisor, Dr. Debashis Chatterjee, member of the research advisory committee for his valuable guidance, advice, encouragement and warm support at every step of my doctoral program. In spite of his busy schedules and even at odd hours of the day, they always lent me a patient listening and helped me to the fullest extent. I do consider myself very lucky for working under such helpful gentle person. He is an outstanding thinker blessed with sharp intellect and generosity of heart. He has been a true mentor and guided me throughout my Jadavpur University journey concerning academics, health, and well-being. He stood with me against all odds and has put all possible efforts to smoothen this doctoral journey. His unparalleled insights have helped me immensely improve my otherwise naïve research attempts.

I am thankful to other research advisory committee members Dr. Saswati Mazumdar, Prof. Sugata Munshi and Dr. Suparna Kar Choudhary for their constant encouragement and patience with my limitations. I admire their positivity and encouraging personalities and consider myself fortunate for getting a chance to work with them. I am indebted for their unwavering trust in my capabilities and guidance through all the stages of my research. They have provided me with much needed valuable reviews and unequalled insights.

I am grateful to the Head of Electrical Engineering Department, and Doctoral Committee members of Electrical Engineering Department, Jadavpur University, for their kind support and concern regarding my academic requirements.

I have been privileged to spend my years as a doctoral student at JU. I am grateful to different faculty members across departments and laboratories I interacted over through courses and casual conversations. I whole-heartedly express my thankfulness to nurture me as a scholar and develop academic acumen in me.

My thanks and appreciation also go to the staffs of office, IT department, library and administration that have supported me through thick and thin in whatever manner they can. Finally, my sincere thanks to my fellow friends and colleagues for their help in completing this degree. They have provided technical assistance at various fronts and always being a constant companion. They have become more like a family who always encouraged and supported me through their thoughts, words and deeds. I would also like to express my deep sense of gratitude to seniors to help me with methodologies and study analysis. No word, howsoever perfect would be sufficient to thank everyone.

Dept. of Electrical Engineering
Jadavpur University, Kolkata –700032.

Swati Suman

Dedication

I dedicate this thesis to the almighty

and

To my father, Sudhir Kumar Singh and my mother Suman Singh, they have always supported my dream for higher studies and have stood by me without fail. They are the persons who show me the joy of intellectual pursuit ever since I was a child. They are the backbone and inspiration for me to accept challenges and excel in all the endeavors of life.

To my grandfather Lt. Basant Prasad Singh and grandmother Lt. Chandrakanta Devi for their constant encouragement, motivation and blessings that not only helped me in academic career but also throughout my life journey. Enthusiastic and curious, my grandmother was always keen to know what I was doing and how I was advancing, although it is likely she could grasp only a little of what it was all about! I always admire her inquisitiveness about my work.

To my uncle Subodh Kumar and aunt Bobby Singh, they have always showered me with their love and blessings, which further amplified whenever a significant milestone was reached.

To my brother, Shekhar Suman, for always supporting me in all the ups and downs over these years. His continuous cooperation and valuable advice extended to me on numerous occasions has made this journey a lot easier. I would also like to thank my cousins Aditya Harsh and Akansha Priya for their love and support.

Above all, my husband, Mr. Shashank Shekhar deserves special mention for his exemplary support, constant encouragement, and patience throughout my studies. He has been understanding of the zeal for my passion. I'd also like to thank my parents' in-laws, Girish Chandra Singh and Manju Rai, and my sisters-in-law Jyoti Rai and Jyotsna Rai, for their blessings, unconditional love, and help in accomplishing my dream. Also,

I would like to extend my thanksgiving to all my relatives and friends for their unwavering love, kind and motivating words and being pillars in this journey. Lastly, I would like to extend whole-hearted thanks to everyone who supported me in any way for the completion of the thesis.

Preface

Fossil fuels are the conventional source of energy in order to meet the power demands. The disadvantages associated with these fuels are it possess harmful effects on environment such as global warming, pollution etc. Since last decade there was a major shift of electricity production countries towards renewable or alternative source of energy. The benefits related to it are its clean and green source, inexhaustible and easily available. However, PV and wind sources of energy make the power extraction little difficult as it depends on irradiance and wind speed. For high power extraction series connection can't, be done as it can lead to imbalance and high in cost. PV generates low voltage which is inefficient to single phase 230V RMS AC voltage. Therefore, a boost converter is connected to increase the voltage to high values so that it can supply to inverter and which can convert to 230V RMS AC voltage. The proposed circuits solve the common problems which arises due to power quality issues. The thesis has dealt with the issue of wider voltage variation, harmonics, partial shading condition, losses due to higher switching's. The proposed techniques have used recent and modified metaheuristics techniques to extract the gating pulses for driving the inverters in PV and PV- wind hybrid distributed generation system connected to microgrid. Thus, the system can be applied to large power plants, can also work in standalone or islanded mode. Resolving these problems of power quality can improve the standards of living. The proposed schemes are also verified with the laboratory setup thus concluding that it can be used for practical purposes. A detailed discussion of the problems and the process or techniques involved has been discussed in detail.

Dept. of Electrical Engineering
Jadavpur University
Kolkata –700032.

Swati Suman

Table of Contents

Publication.....	i
Statement of Originality.....	iv
Certificate of supervisor.....	v
Acknowledgement.....	vi
Dedication.....	vii
Preface.....	viii
Table of contents.....	ix
List of abbreviations.....	xiv
List of symbols.....	xv
List of tables.....	xvi
List of figures.....	xvii

Chapter 1 Introduction

1.1 Context and purpose of research.....	1
1.2 Literature survey.....	2
1.3 Renewable energy sources.....	6
1.3.1 Different Induction Generators.....	6
1.3.1.1 DFIG.....	7
1.3.1.2 SCIG.....	8
1.3.1.3 WRIG.....	9
1.3.2 Power Electronics Converters for Microgrid.....	9
1.3.2.1 SPWM.....	9
1.3.2.2 MLI.....	10
1.3.2.3 SHEPWM.....	10
1.4 Reactive power optimization.....	11
1.5 Motivation of the thesis.....	13
1.6 Objective and contribution of thesis.....	15
1.7 Thesis organization.....	15
References.....	17

Chapter 2 Mitigating power quality issues for PV-grid integration

2.1 Introduction.....	20
-----------------------	----

2.2 Switching strategies of inverters.....	20
2.2.1 Existing schemes.....	20
2.2.2 Proposed configuration.....	20
2.2.2.1 System in detail.....	20
2.2.3 Comparison of different types of switching techniques.....	22
2.2.3.1 Sinusoidal Pulse Width Modulation Inverter.....	22
2.2.3.2 Multicarrier MLI.....	23
2.2.3.3 Selective Harmonic Elimination PWM Inverter.....	23
2.2.3.3.1 Need of metaheuristic technique.....	25
2.2.3.3.1.1 Grey Wolf Algorithm implementation for driving inverters.....	25
2.2.3.3.1.2 Particle Swarm Optimization implementation for driving inverters.....	26
2.2.3.4 Cascade H bridge MLI.....	27
2.2.4 Simulative result analysis.....	27
2.2.4.1 Comparative details for different switching parameters.....	31
2.2.5 Conclusion.....	32
Publication.....	32
References.....	32
2.3 Power quality issues for PV integrated microgrid system.....	33
2.3.1 Introduction.....	33
2.3.2 Existing topologies and its drawbacks.....	34
2.3.3 Proposed configuration.....	35
2.3.3.1 Topology in detail.....	35
2.3.4 Existing and proposed switching techniques for harmonic elimination.....	37
2.3.4.1 Existing switching approaches.....	37
2.3.4.1.1 Sinusoidal Pulse Width Modulation Inverter (SPWM).....	37
2.3.4.1.2 Using the direct solution method for the conventional 180 switching strategy.....	38
2.3.4.1.3 Using the direct solution method for the conventional 120 switching strategy.....	39
2.3.4.2 Proposed switching approaches.....	39
2.3.4.2.1 SHE implemented IJFA in a conventional 180° switching strategy.....	39
2.3.4.2.2 SHE implemented IJFA in a conventional 120° switching strategy.....	40
2.3.5 Application of metaheuristic technique for angle generation and tracking of GMPP.....	41
2.3.5.1.1 Jelly Fish Algorithm (JFA) metaheuristic technique.....	41
2.3.5.1.2 Improved Jelly Fish Algorithm (IJFA) in detail and JFA limitations.....	42
2.3.5.1.2 Application of IJFA in proposed compensation technique.....	43

2.3.5.1.2.1 Angle obtained for the Main SHEPWM inverter in detail.....	43
2.3.5.1.2.2 Angle calculation for Auxiliary SHEPWM inverter to suppress higher orders in detail..	43
2.3.5.2 Partial Shading Condition (PSC): concern for PQ issues.....	44
2.3.6 Implementation of the control technique.....	45
2.3.7 Results.....	46
2.3.7.1 Simulation results.....	46
2.3.7.2 Experimental setup.....	48
2.3.7.3 Comparison with the existing and the proposed scheme.....	51
2.3.8 Conclusion.....	57
Publication.....	57
References.....	58

Chapter 3 Mitigating power quality issues for the PV-wind hybrid system

3.1 Introduction.....	61
3.2 Power quality improvement for the microgrid connected PV-wind hybrid generation scheme without series compensation.....	61
3.2.1 Existing schemes.....	62
3.2.2 Proposed topology.....	62
3.2.2.1 Its features in detail.....	62
3.2.3 SHEPWM application in converters for harmonic analysis.....	63
3.2.4 Application of metaheuristic technique in SHEPWM based inverter.....	63
3.2.4.1 Whale Optimization Algorithm (WOA).....	64
3.2.4.1.1 Steps for WOA for food hunt.....	64
3.2.4.1.2 Limitation of WOA and implementation of MWOA.....	65
3.2.4.1.3 MGWO application to the proposed compensation technique.....	65
3.2.5 Wind characteristics equations.....	66
3.2.5.1 Wind turbine characteristics.....	66
3.2.5.2 Mathematical modelling of DFIG.....	67
3.2.5.3 Reactive power compensation.....	69
3.2.6 Result analysis.....	72
3.2.6.1 MATLAB Simulation discussion.....	72
3.2.6.2 Comparison with the existing schemes.....	73
3.2.7 Conclusion.....	75

Publication.....	76
References.....	76
3.3 Power quality issues for PV-wind hybrid distributed generator with series compensation integrated to microgrid.....	78
3.3.1 Introduction.....	78
3.3.2 Existing topologies.....	78
3.3.3 Proposed scheme.....	79
3.3.3.1 Configuration in detail.....	79
3.3.4 Harmonic investigation in a DFIG system.....	81
3.3.4.1 Generation of stator harmonics by rotor speed.....	82
3.3.5 Comparison of conventional and proposed improved switching strategies for inverters.....	84
3.3.5.1 Traditional method.....	84
3.3.5.1.1 In the case of 180° switching strategy.....	84
3.3.5.1.2 In the case of SHEPWM switching strategy.....	85
3.3.5.2 Improved approach.....	85
3.3.5.2.1 In the case of 180° switching strategy.....	85
3.3.5.2.2 In the case of the SHEPWM switching strategy.....	86
3.3.5.2.2.1 SHE implemented SAR in unipolar case.....	86
3.3.5.2.2.2 SHE implemented SAR in bipolar case.....	86
3.3.6 Application of optimization technique for harmonic mitigation.....	87
3.3.6.1 Search and rescue optimization algorithm in detail.....	87
3.3.6.1.1 Phases of the SAR.....	87
3.3.6.1.2 Control Parameters of SAR.....	89
3.3.6.2 SAR Application for harmonic compensation in detail.....	91
3.3.6.2.1 Angle obtained for RSC and GSC SHEPWM inverter.....	91
3.3.6.2.2 Angle generation for compensating SHEPWM converter to suppress higher order.....	91
3.3.7 Control strategy used.....	92
3.3.7.1 Reactive power compensation.....	94
3.3.8 Results.....	95
3.3.8.1 MATLAB Simulation results.....	95
3.3.8.2 Experimental results.....	98
3.3.8.3 Comparative analysis of existing schemes with the state-of-the-art.....	100
3.3.9 Conclusion.....	104
Publication.....	104

References.....	104
Chapter 4 Conclusion	
4.1 Introduction.....	108
4.2 Outline of the contributions.....	108
4.3 Recommendation for future work.....	110
Appendices	

List of Abbreviations

RES	Renewable Energy Source
PV	Photovoltaic panel
VSI	Voltage Source Inverter
MLI	Multilevel Inverter
PWM	Pulse Width Modulation
EMI	Electromagnetic Interference
FACTS	Flexible AC Transmission System
UPFC	Unified Power Factor Conditioner
CHB	Cascaded H-Bridge
THD	Total Harmonic Distortion
VAR	Volt Ampere Reactive
DC	Direct Current
AC	Alternating Current
IGBT	Insulated Gate bipolar Transistor
MOSFET	Metal Oxide Semiconductor Field Effect Transistor
SPV	Solar Photo Voltaic
DSO	Digital Storage Oscilloscope
V	Voltage
S	Switch
MPPT	Maximum Power Point Tracking
PEC	Power Electronic Converter
FPGA	Field Programmable Gate Array
Gan-FET	Gallium Nitride Field Effect Transistor
PSC	Partial Shading Condition
GMPP	Global Maximum Power Point
SHEPWM	Selective Harmonic Elimination Pulse Width Modulation Inverter

List of Symbols

N_{switch}	Number of Switches
N_{level}	Number of Level
P	Active power
Q	Reactive power
R	Resistance
L	Inductance
N	Number of Diodes
T	Time
N	Harmonic order
$\alpha_1 \dots \alpha_d$	Switching angles
θ	Phase angle of AC voltage
ϕ	Phase angle difference
s	slip
w_r	rotor speed
f	frequency
$b_1 \dots b_{29}$	voltage harmonics amplitude

List of Tables

Table 2.1 Switching pattern for phase- A

Table 2.2. Comparative analysis of CHB-MLI, Multicarrier, SPWM, SHEPWM inverter

Table 2.3 Switching angles obtained for different values of firing angles

Table 2.4 A comparison of the proposed MPPT techniques with the existing MPPT techniques

Table 2.5 Comparison of different evolutionary techniques

Table 2.6 Comparison of voltage harmonic amplitudes of standards with the proposed techniques

Table 2.7 Comparative analysis of existing and proposed schemes

Table 3.1 Comparison of voltage harmonic amplitudes of literature survey with the proposed technique

Table 3.2 Comparison of metaheuristic techniques with the proposed technique

Table 3.3 Stator harmonics generation for a wide range of rotor speed due to the rotor harmonics presence

Table 3.4 Ratings of the model used

Table 3.5 Different Parameters used for various search-based optimization techniques

Table 3.6 Comparison of voltage harmonic amplitudes of the literature survey with the proposed technique

Table 3.7 Comparison of existing schemes with the State-of the-Art

Table 4.1 Comparison of different proposed schemes proposed in this thesis.

List of Figures

Fig. 1.1 DFIG system connected to wind turbine

Fig. 1.2 SCIG system connected to wind turbine

Fig. 1.3 WRIG system connected to wind turbine

Fig. 1.4 Series connected FACTS controller

Fig. 1.5 Series connected FACTS controller

Fig. 1.6 Series-series connected FACTS controller

Fig. 1.7 Series-shunt connected FACTS controller

Fig. 2.1 Proposed topology of PV integrated (a) Multicarrier MLI (b) SPWM inverter (c) SHEPWM inverter (d) Multilevel inverter

Fig. 2.2 (a) Pulse generation for SPWM (b) Pulse generation for Multicarrier MLI (c) Unipolar voltage output for SHEPWM inverter (d) Output voltage waveform for CH-MLI

Fig. 2.3 Output voltage waveform of Boost converter

Fig. 2.4 (a) Three-phase output voltage of SPWM inverter (b) FFT spectrum of the output voltage waveform

Fig. 2.5 (a) Output voltage of Multicarrier MLI inverter (b) FFT spectrum of the output voltage waveform

Fig. 2.6 (a) Output voltage of SHEPWM inverter (b) Convergence behavior of GWO search-based techniques (c) FFT spectrum of the output voltage waveform for GWO obtained by MATLAB Simulink (d) FFT spectrum obtained by MATLAB program

Fig. 2.7 (a) Output voltage of CHB-MLI inverter (b) Convergence behavior of GWO search-based techniques (c) FFT spectrum of the output voltage waveform for GWO obtained by MATLAB Simulink (d) FFT spectrum obtained by MATLAB program

Fig. 2.8 Proposed prototype

Fig. 2.9 (i) Pulse generation for a) 180° conventional b) 120° conventional

Fig. 2.10 (ii) Pulse generation for a) IJFA implemented in 180° b) IJFA implemented in 120°

Fig. 2.11 Flowchart for the IJFA

Fig. 2.12 For tracking power (a) Flowchart of the IJFA-PO (b) Solar irradiance at various times of the day, c) PV curve with Partial Shading conditions (PSC) and uniform isolation in a general scenario

Fig. 2.13 Control unit

Fig. 2.14 (a) PSC power curve versus time (b) System voltage at the grid side

Fig. 2.15 Voltage waveform for unipolar switching at the main inverter side a) SPWM b) 180° conventional c) IJFA implemented in 180° d) 120° conventional e) IJFA implemented in 120°

Fig. 2.16 Experimental setup

Fig. 2.17 Gate pulses of switches a) SHEPWM-based 120° conduction in the main inverter (scale: CH1: Y-axis: 5V/div.) b) SHEPWM-based 120° conduction in the auxiliary inverter (scale: CH1: Y-axis: 5V/div.)

Fig. 2.18 Output voltage waveform a) SHEPWM based 120° conduction in main inverter (scale: CH1: Y-axis: 60V/div.) b) SHEPWM based 120° conduction in auxiliary inverter (scale: CH1: Y-axis: 12V/div.) c) at the grid side after series compensation (scale: CH1: Y-axis: 120V/div.)

Fig. 2.19 Voltage harmonics spectra up to the 29th harmonic order a) before series compensation (scale: CH1: Y-axis: 60V/div; X-axis: 250Hz/div) b) after series compensation (scale: CH1: Y-axis: 120V/div; X-axis: 250Hz/div) at MI=0.5. c) at MI=0.8, after series compensation (scale: CH1: Y-axis: 120V/div; X-axis: 250Hz/div) d) The output current waveform (scale: CH1: Y-axis: 1A /div.; X-axis: 250 ms/div), e) MPP tracking (scale: CH1: Y-axis: 212W /div.; X-axis: 50 ms/div).

Fig. 2.20 Analysis of system output a) FFT analysis of the main SHEPWM inverter b) FFT analysis at the grid side c) voltage THD variation over iterations for various metaheuristic techniques d) Switching angle behaviour vs. MI for conventional and optimised pulses (e) Convergence vs. number of iterations plot (f) Run time vs. population size plot.

Fig. 2.21 Behaviour of switching angles vs. modulation index a) for three switching angles b) for five switching angles c) for seven switching angles

Fig. 2.21 Voltage output analysis for the variation of THD vs. MI a) IJFA implemented in 180° b) IJFA implemented in 120° c) characteristics of different metaheuristic techniques

Fig. 3.1 Proposed model

Fig.3.2 Turbine power output versus speed of the shaft.

Fig. 3.3. DFIG (a) Equivalent circuit (b) Dynamic equivalent circuit in q axis frame

Fig. 3.4 Dynamic equivalent circuit in d axis frame

Fig 3.1 (a) RSC controller

Fig. 3.1(b) GSC controller

Fig. 3.5 System output at 1450 rpm (a) rotor voltage output without harmonic elimination (b) rotor voltage output with harmonic elimination

Fig. 3.6 System output at 1450 rpm (a) stator output voltage without harmonic elimination (b) stator output voltage with harmonic elimination

Fig. 3.7 Characteristics behavior (a) THD vs. modulation index for various switching angles (b) THD vs. no. of iterations for various algorithms used

Fig. 3.8 DFIG harmonic spectra with and without harmonic (a) at rotor side (b) for three switching angles at stator side (c) for seven switching angles at stator side

Fig. 3.9 Proposed Scheme with the control unit

Fig. 3.10 Switching techniques used a) 180° conventional b) SHE in 180° c) SHE for unipolar d) SHE for bipolar

Fig. 3.11 Flowchart for the controller used

Fig. 3.12 DFIG outputs at a speed of 1250 rpm a) Rotor voltage and current in 180° conduction mode (a1) without harmonic elimination (a2) with harmonic elimination (a3) with harmonic elimination b) Rotor voltage and current in SHE unipolar (b1) without harmonic elimination (b2) with harmonic elimination (b3) with harmonic elimination (c) Rotor voltage and current in SHE bipolar (c1) without harmonic elimination (c2) with harmonic elimination (c3) with harmonic elimination (d) Stator voltage and currents with quasi sine rotor injection in 180° conduction mode (d1) without harmonic elimination (d2) with harmonic elimination (d3) with harmonic elimination (e) Stator voltage and current in SHE (e1) without harmonic elimination (e2) with harmonic elimination (e3) with harmonic elimination

Fig. 3.13 Laboratory setup

Fig. 3.14 Stator side voltage waveform for three switching (channels 1, 2 and 3: Y-axis: 500 V/div.)

Fig. 3.15 Voltage harmonic spectra at the stator side a) simulation results b) experimental results i) without harmonic elimination, ii) with harmonic elimination

Fig. 3.16 DFIG outputs a) switching angle variation vs. modulation index for 180° conduction mode. b) SHE switching angle vs. modulation index variation c) Changes in voltage THD over iterations for various metaheuristic techniques

Fig. 3.17 FFT analysis of the output voltage at a speed of 1250 rpm for three switching angles a) at the rotor side b) at the stator side for 180° conduction c) at the stator side in SHE

INTRODUCTION

1.1 INTRODUCTION

This modern civilization is highly dependent on electricity. Excessive use of conventional source of energy has resulted in its depletion thus causing crisis of electricity. Therefore, the world has now started to shift towards the use of renewable source of energy [1.1]. It has proved to be a major source of energy with major advantages over the fossil fuels. Its clean and green source as well with availability in abundance and inexhaustible advantages has made organisations to start investing these power generation projects [1.2].

Renewable energy source is not a constant and stable source in terms of solar and wind. The sun's irradiance can vary significantly during the day in solar photovoltaic (PV) systems. Another important renewable energy source and a good substitute for producing electricity is wind energy. Similarly, here also wind speed is varying throughout which in turns varies the bus voltage.

To provide uninterrupted power to the consumers a reliable grid interfaced renewable energy source is required. Mostly, solar photovoltaic (SPV) systems interface to the grid. Therefore, a stable grid interface is required to feed the grid without any fluctuations [1.3]. Photovoltaic cells provide DC voltage. This DC is converted into AC by power electronic converters.

There are numerous inverter topologies for renewable energy systems projected in research. The voltage source (VS) and current source (CS) inverter are the main types of inverter. They have their own merits and demerits however in the renewable energy system VSI is more appropriate compared to CSI. There are different techniques available to control the inverters. Depending on the circuit topology inverters can be operated in two or higher number of levels of DC voltages. In recent years, multilevel inverters are commonly used due to the numerous advantages over other traditional two level inverters. To drive these inverters various new and modified metaheuristic techniques are used to fetch angle as gating pulses.

It needs rigorous improvement in the field of power semiconductor switches, topologies to satisfy the harmonic standard set by IEEE. So, that it can deal with power quality issues like harmonics, voltage unbalance, power fluctuations, frequency variations etc. For these purposes reactive power demands has also to be taken care of by using advanced electronic compensators. Therefore, this thesis attempts to address these important issues in order to make power quality better in a PV-wind integrated microgrid system. On overcoming these challenges, the proposed schemes can be implemented easily in a large power plant, grid-secluded regions or even in islanded mode of operation in order to make life better.

1.2 LITERATURE SURVEY

Various articles and journals were investigated to develop a better proposed scheme or real time implementation. The reviewed literatures related to the topics of the thesis work has been studied in detail which are given as follows:

[1] Memon, M. A., Mekhilef, S., Mubin, M., & Aamir, M. (2018). Selective harmonic elimination in inverters using bio-inspired intelligent algorithms for renewable energy conversion applications: A review. *Renewable and Sustainable Energy Reviews*, 82, 2235-2253.

The review paper presents various optimization techniques and discusses different objective function. It has been used in inverters for harmonic application. Various comparative analysis has been done to draw a conclusion on the basis of information extracted from the literature and evaluation results with future recommendations [1.4].

[2] Ray, R. N., Chatterjee, D., & Goswami, S. K. (2010). Reduction of voltage harmonics using optimisation-based combined approach. *IET power electronics*, 3(3), 334-344.

A basic module is developed for voltage harmonics in a sine pulse-width modulation (PWM) inverter connected microgrid system. The dominant harmonics are obtained in phase opposition to nullify them. This is validated both by simulation and by experimentation [1.5].

[3] Al-Quraan, A., & Al-Qaisi, M. (2021). Modelling, design and control of a standalone hybrid PV-wind micro-grid system. *Energies*, 14(16), 4849.

In this paper, a Permanent Magnet Synchronous Generator (PMSG) based standalone micro-grid system is designed. The sources of energy used are Photovoltaic (PV) and Wind Energy Conversion System (WECS) with a battery connection. When the electricity generated by the PV panels is insufficient to meet the load's demands, the extra power is extracted from the charged batteries. A controller is designed to protect the battery banks in all conditions, including normal, overcharging, and overdischarging conditions. Different cases are considered for to check proper working of these conditions [1.6].

[4] Krishnamurthy, K., Padmanaban, S., Blaabjerg, F., Neelakandan, R. B., & Prabhu, K. R. (2019). Power electronic converter configurations integration with hybrid energy sources—a comprehensive review for state-of the-art in research. *Electric Power Components and Systems*, 47(18), 1623-1650.

This paper reviews various PEC configurations available for integration of renewable energy sources. It emphasizes on coordination power control, maximum power point, and grid integration challenges related to the hybrid energy system [1.7].

[5] Sarker, K., Chatterjee, D., & Goswami, S. K. (2017). Grid integration of photovoltaic and wind based hybrid distributed generation system with low harmonic injection and power quality improvement using biogeography-based optimization. *Renewable Energy Focus*, 22, 38-56.

In this paper, authors have introduced FACTS based hybrid model with microgrid connection. PV-DFIG were connected to DVR, STATCOM and UPQC (with and without transformer) switching improve grid power quality and voltage interruption. Metaheuristic techniques has been used for offline computation of angles for harmonics elimination [1.8].

[6] Balamurugan, M., Sahoo, S. K., & Sukchai, S. (2017). Application of soft computing methods for grid connected PV system: a technological and status review. *Renewable and Sustainable Energy Reviews*, 75, 1493-1508.

This paper summarizes various metaheuristic techniques to different stages of a grid connected PV system such as panel reconfiguration, Maximum Power Point Tracking (MPPT) technique in the converter, harmonic elimination in inverter and islanding detections. This paper highlights better results obtained from SPWM technique than from space vector modulation in modular multilevel converters for balancing sub modules capacitor [1.9].

[7] Ghodelbourk, S., Azar, A. T., Dib, D., & Omeiri, A. (2020). Selective harmonic elimination strategy in the multilevel inverters for grid connected photovoltaic system. *International Journal of Advanced Intelligence Paradigms*, 15(3), 317-339.

This paper describes multilevel inverters for PV applications integrated in distribution grids so as to reduce THD. The proposed control strategy implements SHE modulation for a 5 to 11 levels. This helps to reduce harmonics for multilevel converter sources both for equal and unequal DC voltages cases [1.10].

[8] Ramesh, A., & Sait, H. H. (2020). An approach towards selective harmonic elimination switching pattern of cascade switched capacitor twenty nine-level inverter using artificial bee colony algorithm. *Microprocessors and Microsystems*, 79, 103292.

In this paper switched capacitor multilevel inverter based artificial bee colony (ABC) method has been used. The twenty nine level inverter gets input from the SEPIC converter powered by PV. A comparative analysis of ABC harmonics elimination technique has been carried out with genetic algorithm based SHE method [1.11].

[9] Ray, S., Gupta, N., & Gupta, R. A. (2021). Power quality improvement using multilevel inverter-based active filter for medium-voltage high-power distribution system: a comprehensive review. *International Journal of Power Electronics*, 14(1), 1-36.

In this paper, authors have discussed that MLI-based active filter (AF) is having more potential and thus, can replace two-level inverter-based AF in medium-voltage distribution sector. It has reviewed different possible configurations, control techniques and their different applications [1.12].

[10] Sarker, K., Chatterjee, D., & Goswami, S. K. (2018). Modified harmonic minimisation technique for doubly fed induction generators with solar-wind hybrid system using biogeography-based optimisation. IET Power Electronics, 11(10), 1640-1651.

A PV-wind hybrid connected distributed generation has been developed in the present paper. A modified switching strategy is developed for mitigating stator harmonics at different speeds based on operating rotor speed [1.13].

[11] Blooming, T. M., & Carnovale, D. J. (2006, June). Application of IEEE Std 519-1992 harmonic limits. In Conference Record of 2006 Annual Pulp and Paper Industry Technical Conference (pp. 1-9), IEEE, DOI: 10.1109/PAPCON.2006.1673767.

This paper discusses the IEEE standard 519-1992 for understanding harmonics and applying harmonic limits in power systems [1.14].

[12] Beaulieu, G., Bollen, M. H. J., Malgarotti, S., & Ball, R. (2002, July). Power quality indices and objectives. Ongoing activities in CIGRE WG 36-07. In IEEE Power Engineering Society Summer Meeting, 2, pp. 789-794. IEEE.

This literature elaborates the need for power quality indices and objectives in the context of deregulation of the electricity industry. Voltage quality monitoring such as harmonics, flicker, unbalance and voltage dips are also discussed [1.15].

[13] Alkahtani, A. A., Alfalahi, S. T., Athamneh, A. A., Al-Shetwi, A. Q., Mansor, M. B., Hannan, M. A., & Agelidis, V. G. (2020). Power quality in microgrids including supraharmonics: Issues, standards, and mitigations. IEEE Access, 8, 127104-127122.

This review study contributes towards the mitigation and development of PQ issues mainly superharmonics in connection to microgrid. Its characteristics, causes, consequences, and measurements are discussed. Also, the control strategies to overcome the power quality issues, and the devices used has been detailed [1.16].

[14] Khosravi, N., Abdolmohammadi, H. R., Bagheri, S., & Miveh, M. R. (2021). Improvement of harmonic conditions in the AC/DC microgrids with the presence of filter compensation modules. Renewable and Sustainable Energy Reviews, 143, 110898.

In this paper authors have designed filter compensation devices for harmonic reduction. The green plug filter compensator (GPFC) and active power filter module (APFM) has been used to stabilize the transient voltage in the DC side and the latter has been used to reduce voltage and current harmonics at the AC side. Comparison of various optimization techniques has been carried out to obtain best answer to the problem statement [1.17].

[15] Reddy, C., Goud, B. S., Aymen, F., Rao, G. S., & Bortoni, E. C. (2021). Power quality improvement in HRES grid connected system with FOPID based atom search optimization

technique. *Energies*, 14(18), 5812.

An optimum power quality for grid connected hybrid system has been proposed by the authors. A Unified Power Quality Conditioner with Active and Reactive power (UPQC-PQ) has been designed with Atom Search Optimization (ASO) based Fractional-order Proportional Integral Derivative (FOPID) controller. It is used to control the real and reactive power, voltage, Total Harmonic Distortion (THD) etc [1.18].

[16] Alhato, M. M., & Bouallègue, S. (2019). Direct power control optimization for doubly fed induction generator based wind turbine systems. *Mathematical and Computational Applications*, 24(3), 77.

In this literature, a Thermal Exchange Optimization (TEO) algorithm has been proposed which is used to tune the PI controller for direct power control of Doubly Fed Induction Generator (DFIG) based Wind Turbine systems. It also regulates the active/reactive power and DC-link voltage simultaneously. A topology is developed based on basic modules. It has different levels which increases after series connection of basic module [1.19].

[17] Aljendy, R., Nasyrov, R. R., Abdelaziz, A. Y., & Diab, A. A. Z. (2022). Enhancement of power quality with hybrid Distributed generation and FACTS device. *IETE Journal of Research*, 68(3), 2259-2270.

In this paper, the voltage profile has been improved by determining the size of distributed generators using the Salp Swarm algorithm (SSA). To do so, an Active Power Filter (APF) has been used which also compensates reactive power and harmonics [1.20].

[18] Guichi, A., Mekhilef, S., Berkouk, E. M., & Talha, A. (2021). Optimal control of grid-connected microgrid PV-based source under partially shaded conditions. *Energy*, 230, 120649.

This objective of this paper is to design a microgrid connected PV system which can deliver the power needed. Particle swarm optimization algorithm and the proposed intermediate power point tracker algorithm combine has been used as a controller of the DC-DC boost converter. The voltage source inverter is controlled with the phase-locked loop algorithm to keep the DC bus voltage constant and carry out the voltage synchronization [1.21].

[19] Motahhir, S., El Hammoumi, A., & El Ghzizal, A. (2020). The most used MPPT algorithms: Review and the suitable low-cost embedded board for each algorithm. *Journal of cleaner production*, 246, 118983.

In this manuscript the authors reviews the most used MPPT algorithms. It is categorized into three which are direct (traditional ones), Indirect, and lastly the soft computing ones. Each of its implementation has also been carried out in low-cost embedded board [1.22].

[20] Yadav, R. S., Dhaked, D. K., & Jaiswal, A. (2021). Comparative study of MPPT techniques for solar PV-based system. *International Journal of Environment and Sustainable Development*, 20(3-4), 366-380.

The literature objective is to increase the output power from the solar PV system. The comparative analysis has been studied in aspect of efficiency for the perturb and observe (P&O) and variable step size incremental conductance (VSS-IC)-based optimization techniques in a MATLAB simulation environment [1.23].

1.3 RENEWABLE ENERGY SOURCES

Renewable energy source as the name itself denotes its characteristics of alternative energy/sustainable form of energy. It has zero carbon emission, freely available in plenty and of course inexhaustible. The most popular sources are wind, solar, tidal, hydro, biomass, geothermal etc. Solar and wind has been focusses in the present thesis. The manufacturing cost of solar panels has declined in past few years thus, making them more affordable and cheapest form of electricity. Wind turbines (WT) converts the kinetic energy of moving air to electrical energy. They can be found in on land (onshore) or in sea or freshwater (offshore) in which the offshores ones has tremendous potential. It has basically two types horizontal and vertical. Former being the most common as well as older. The advantage of vertical WT is that it does not need to be facing straight into the wind to be more efficient.

The focus is to obtain maximum power out of the solar panel or wind turbine which is to be boosted on the later stage for meeting the grid demands. For this purposes, previously traditional methods like Perturb and Obserb (P&O), incremental conductance method etc. [1.18] were used. But they didn't worked well under non-uniform irradiance condition. Therefore, the studies [1.20] shows that the various metaheuristic techniques has been combined with these traditional methods as well these soft computing methods have been applied separately to get the desired maximum power output.

1.3.1 Induction Generators and its types

Induction machines are commonly used in a large-scale in the power industry. Mostly they are used as motors due to various benefits such as their simple and robust design, cost-effective, low maintenance requirements. It gets excited without any DC source and performs even with increased transient state. It has built-in protection against short circuit faults, overloading effects which make them more popular to be used a generator. One of the major concerns is that it requires external reactive power source for stator magnetization current which is not applicable in case of synchronous generators. The source for the reactive power is capacitor banks, synchronous generators etc. By the process of self-excitation magnetic field is induced in the rotor. When the magnetic field interacts with the stator magnetic field it induces an electric field and produces rotor winding current. The current is caused due to the relative movement of

these fields, known as “slip.” Wind turbines is categorised based on the operating turbine speed: fixed speed wind turbines (FSGs) and adjustable speed generators (ASGs).

The adjustable speed generators outperform fixed-speed generators in terms of lower cost, simpler pitch control. When the wind speed is low the pitch control is fixed but at higher wind speed pitch control is used to limit maximum output power. It also reduces mechanical stresses from gusts of wind. Due to the elasticity of the wind turbine system power quality is improved with reduced torque pulsations which in turn reduces/eliminates power fluctuations. With this the systems efficiency is improved. Turbine speed is the function of wind speed which maximizes output power result. Last but not the least, low-speed operation is possible at low power conditions which also reduces the acoustic noise. In addition, most ASG-based wind turbines can also operate in island mode which is hence, difficult in the Danish concept.

1.3.1.1 Doubly fed Induction generator (DFIG)

Contrary to SCIGs, doubly fed induction generators (DFIGs) with wound rotor and slip rings offer more flexibility and variable speed operation made possible by a supplementary rotor port via which energy can be fed or withdrawn. These generators fall under the (ASG) category. By changing the direction of power flow through the rotor, the machine can run in driving and generating modes at both sub-synchronous and super-synchronous speeds. A DFIG is made of a three-phase stator winding and a three-phase rotor winding, similar to a wound rotor induction machine (IM) which are fed through slip rings. As the inverter rating is typically 25% of the total system power and the speed range of the ASG is only 33% around synchronous speed, DFIG has the benefit over other IGs because of decreased inverter cost and size.

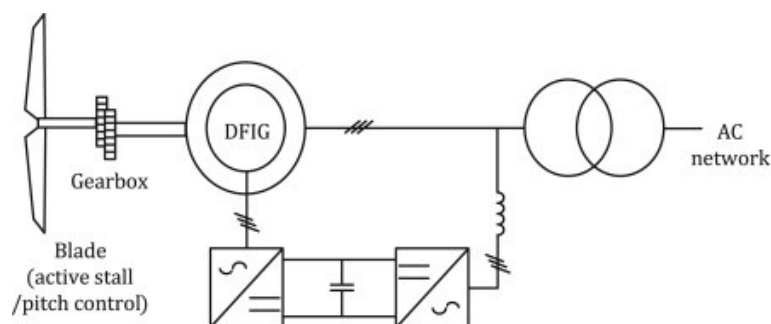


Fig. 1.1 DFIG system connected to wind turbine (Courtesy: Google Image)

Since inverter harmonics contributes very less of the overall system harmonics than EMI harmonics therefore, inverter filters and EMI filters are less expensive as they are rated only for 0.25 p.u. of system power [1.10]. An increase of 2% to 3% has been observed in terms of efficiency. Since the DFIG system (four-quadrant converter and induction machine) functions essentially like a synchronous generator,

power-factor control can be accomplished more affordably. The excitation energy is needed from the converter only. Additionally, this simultaneously manages the generator's reactive and active power.

1.3.1.2 Squirrel Cage Induction Generator (SCIG)

Fixed speed wind turbines produce rated power to a very small range, corresponding to less than 1% of the rated wind speed. Consequently, any variation in wind speed will result in a change in the output power. This category includes squirrel cage induction generators (SCIGs). These wind turbines' benefits include minimal cost, great efficiency, straightforward construction, and no maintenance. The drawbacks are low conversion efficiency, significant mechanical stress, and power fluctuation. Through a coupling transformer, these particular wind turbines are directly connected to the grid. A capacitor bank will be included as reactive power correction since the fixed speed wind turbine absorbs a significant quantity of reactive power during the excitation process.

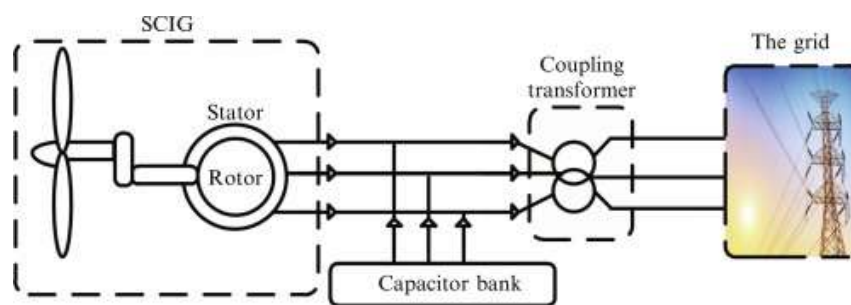


Fig. 1.2 SCIG system connected to wind turbine (Courtesy: Google Image)

As a result of the rotor's construction, which places conducting bars in slots and uses end rings to short both ends, it is also known as a short-circuit rotor machine. The electrical properties can be controlled without an external device whereas a generator's slip is affected by the wind speed, a CIG operates very closely to its rated speed [1.24]. In the face of changing wind speeds, speed deviation is incredibly modest. The use of reactive power which rises with wind speed, is a significant linked disadvantage. The delicate starter mechanism is therefore usually mentioned in order to offset this effect.

Wind turbines with SCIG bases will provide more active power at higher wind speeds, but this will also result in a greater need for reactive power. In their absence, the grid is used to compensate, which causes the system as a whole to become unstable [1.24]. This is often provided by the power electronics equipment or capacitor banks. When wind turbines are operating in the grid-connected mode the fluctuation in wind speed cause transients in the form of inrush current which is forwarded to the grid. As a result, this inrush current causes serious voltage disturbances and device damage.

1.3.1.3 Wound Rotor Induction Generator (WRIG)

The connection between WRIG and a wind turbine is identical to that of SCIG, with the exception that WRIG also has an external mechanism for controlling electrical characteristics or rotor output.

Power electronics, slip rings, and brushes, or both, may be coupled to the rotor windings.

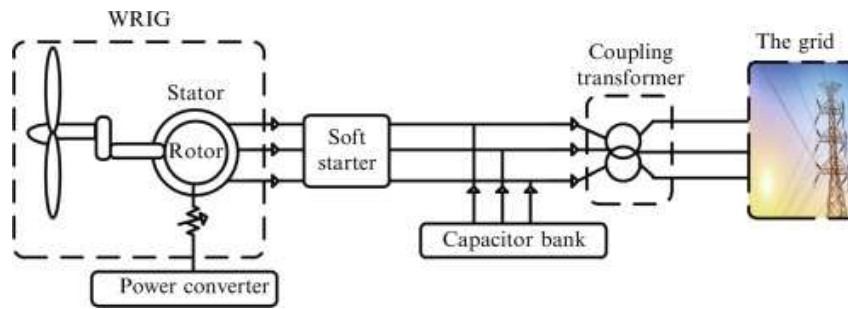


Fig. 1.3 WRIG system connected to wind turbine (Courtesy: Google Image)

The necessity for slip rings in the rotor is eliminated by the use of resistors and power electronic converters that are placed inside the rotor. To keep the electricity flow continuous, the variable resistors can swiftly adjust the rotor voltage. These are more expensive than the SCIG, though, and their structure is less sturdy and straightforward. Rotor resistance can be regulated with 10% slip using optically controlled converters.

1.4 POWER ELECTRONICS CONVERTERS FOR MICRO-GRID

Power electronic converters serve as the connecting device between different loads and power sources. A lot of the time, the power source is the utility grid directly, which provides AC sinusoidal voltage. However, in some situations (like adjustable speed motor drives), it is necessary to first convert AC power into DC power. This process is known as rectification. Different proposed schemes are presented and various DC/AC converters are verified to check which performed their best in the given scheme. The inverters are given as under:

1.4.1 SPWM Inverter

The SPWM is mostly used in industrial applications and is based on a comparison of the carrier and modulation signals. A common PWM approach is sinusoidal PWM. To calculate the switching states for each pole in the inverter using this PWM technique, the sinusoidal AC voltage reference (V_{ref}) is compared with the high-frequency triangular carrier wave (V_c) in real time. Following a comparison, the switching states for each pole can be calculated using the formula:

- Voltage reference > Triangular carrier: upper switch is turned on (pole voltage = $(V_{dc}/2)$)
- Voltage reference < Triangular carrier: lower switch is turned on (pole voltage = $(-V_{dc}/2)$)

The DC-link voltage is specified here as the triangle carrier wave's peak to peak value. The voltage reference's amplitude in this PWM technique must be kept below the triangle carrier's peak (1.26) in order to achieve linear modulation.

1.4.2 Multilevel Inverter

The use of multi-level inverters in industrial settings with high power and voltage ranges has grown to be interesting. For a variety of high-power applications, it is simple to interface with renewable energy sources. Batteries, capacitors, renewable energy systems, etc. serve as the sources for the input side dc voltage. Reduced harmonic distortion, more voltage levels, staircase waveform quality, operation at both fundamental and high switching frequency PWM, lower switching losses, improved electromagnetic compatibility, and higher power quality are therefore some of MLI's appealing qualities. This has the drawback of requiring a lot of power semiconductor switches. Large switching results in losses, which lower system efficiency. The gate driver circuits connected to each switch add complexity to the system of the system [1.27]. The overall cost of the system will escalate. The term "reduced MLI" refers to the current focus on reducing circuit complexity by reducing the amount of power electronic switches and gate driver circuits. The gating pulses are produced by metaheuristic methods using Grey Wolf Optimisation (GWO) and Particle Swarm Optimization (PSO), which are both covered in more detail later in the chapters. The problem statement directs the employment of bio-inspired algorithms to extract the best answer from the search space.

1.4.3 SHEPWM Inverter

In 1973, Patel and Hoft introduced the SHEPWM approach. The basic square-wave output, which is obtained by accurate off-line calculations, is "chopped" a number of times in this process. The outcomes are then either immediately recorded in look-up tables or interpolated for real-time execution using straightforward procedures. The greatest quality output among all PWM techniques can theoretically be produced with SHEPWM-based technologies. The drawback of this method is that a huge amount of memory is needed for the lookup table as the number of switching angles increases. To apply this method in multilayer inverters, it is further developed. In comparison to other PWM approaches, the Multilevel SHEPWM methodology offers the maximum output power quality at low switching frequencies [1.4].

In the chapters that follow, these switching methods as well as the metaheuristic methods covered for getting the gate pulses for MLI and SHEPWM switching patterns are covered in more detail. A comparison analysis has been done to determine whether metaheuristic technique is best for a given issue statement or suggested solution. According to claims made about bio-inspired algorithms, their performance is optimal due to smoother and more accurate convergence, faster speeds, lower levels of computational complexity, less memory usage, and finally, fewer tuning parameters. Of all the switching methods mentioned, SHEPWM switching has been used most frequently for the schemes discussed in the chapters to come.

1.5 REACTIVE POWER OPTIMISATION

These are connected in series with the line as they are meant for injecting voltage in series with the line. If the injected voltage is in phase quadrature with the line current, then only supply or consumption of variable reactive power is possible. In order to handle real power also, any other phase relationship has to be involved. These types of controllers include Static Synchronous Series Compensator (SSSC), Interline Power Flow Controller (IPFC), Thyristor Controlled Series Capacitor (TCSC), Thyristor Switched Series Capacitor (TSSC), Thyristor Controlled Series Reactor (TCSR), Thyristor Switched Series Reactor (TSSR). In all of these TCSC is commonly used. These all comprises of capacitor, reactor, power electronic based variable source. In order to improve the networks' ability to transfer power, stability, and controllability through series and/or shunt compensation, FACTS devices are static power-electronic devices used in AC transmission networks. Additionally, these devices are used for loss optimization and congestion management.

Four groups of FACTS controllers can be distinguished:

- **Series Controllers:** As they are designed to inject electricity in series with the line, they are linked to it in series. It is only possible to provide or consume variable reactive power if the injected voltage is in quadrature phase with the line current. To manage actual power any other phase interaction is also to be incorporated. These controllers come in various forms, such as the Static Synchronous Series Compensator (SSSC), Interline Power Flow Controller (IPFC), Thyristor Controlled Series Capacitor (TCSC), Thyristor Switched Series Capacitor (TSSC), Thyristor Controlled Series Reactor (TCSR), and Thyristor Switched Series Reactor (TSSR). TCSC is frequently employed in all of these. Each of them is an electronic-based variable source with a capacitor, reactor, and power source.

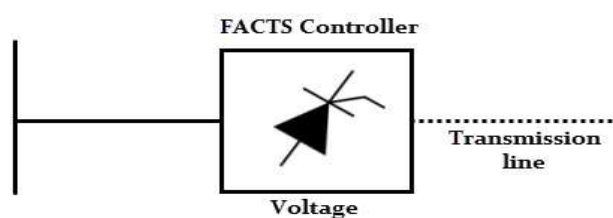


Fig. 1.4 Series connected FACTS controller (Courtesy: Google Image)

- **Shunt Controllers:**

It is shunt connected to the line in order to inject current into the system at the connection point. They could also be variable source or variable impedance, or a combination of the two. Variable reactive power supply or consumption could be achieved if the injected line current and line voltage are in quadrature, but any other phase relationship could also entail real power management. Static VAR Compensator and Static Synchronous Compensator (STATCOM) are examples of this (SVC).

Thyristor switched capacitors (TSC), thyristor-controlled reactors (TCR), and other SVCs are common. The majority of the uses for STATCOM, SVC, and TCR are industrial.

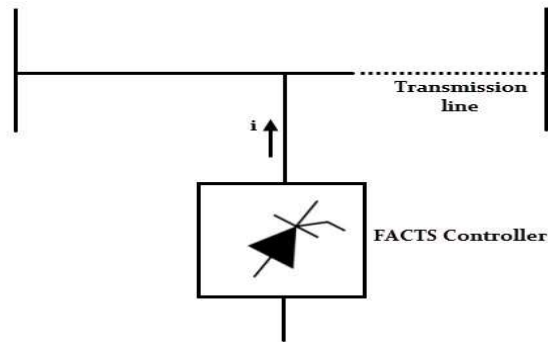


Fig. 1.5 Shunt connected FACTS controller (Courtesy: Google Image)

- **Combined series-series Controllers:** These controllers combine various series controllers that are co-ordinately controlled in various power transmission systems. Alternately, these might be a unified controller in which independent series controllers are used in each line to compensate for series reactive power and transfer real power between the lines via proper link. As an illustration, the IPFC controller balances the actual and reactive power flow in the lines to increase the amount of power being transmitted.

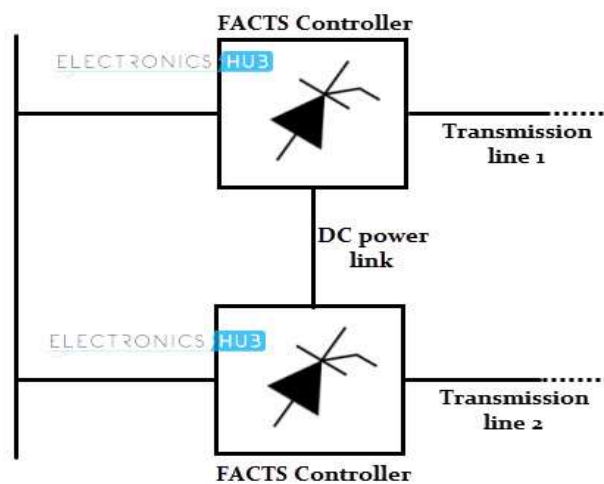


Fig. 1.6 Series-series connected FACTS controller (Courtesy: Google Image)

As an illustration, the IPFC controller balances the actual and reactive power flow in the lines to increase the amount of power being transmitted.

- **Combined series-shunt Controllers:** A coordinated series and shunt controller is used, or a unified power flow controller could be used instead. Shunt and series components of the controller respectively inject current and voltage into the system and when everything is functioning as intended real power exchange via the power link occurs.

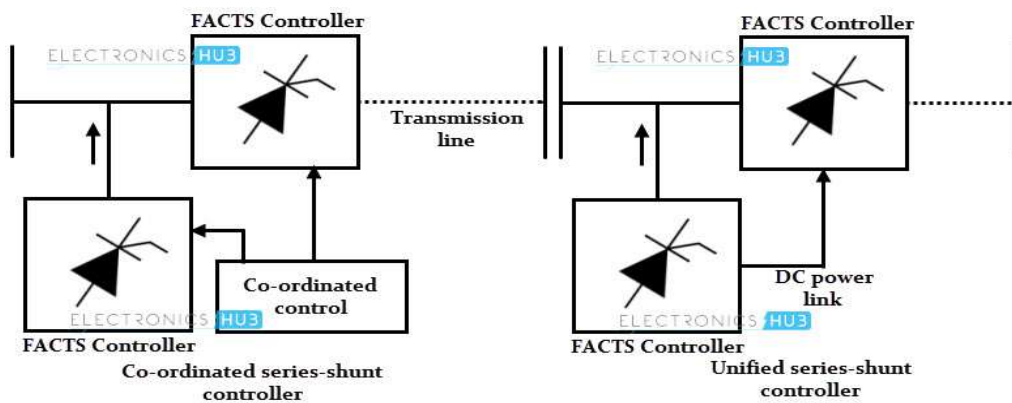


Fig. 1.7 Series-shunt connected FACTS controller (Courtesy: Google Image)

Unified Power Flow Controller (UPFC), Thyristor Controlled Phase Shifting Transformer (TCPST), and Interphase Power Controller are three examples of combine series and shunt controllers (IPC). According to a study [1.13], UPFC is frequently used for higher load flow and voltage control, whereas STATCOM is used for voltage control in small distribution systems. The UPFC also exhibits better results for improving power system stability compared to other FACTS devices like SVC, TCSC, and SSSC.

1.6 MOTIVATION OF THE THESIS

Due to the increase in population, the electricity demand has also increased. To meet the increased demand for electricity, renewable sources of energy are the best alternative, as conventional fossil fuel-based generation has a limited reserve and is one of the major sources of global warming and other environmental hazards. The advantages of renewable energy are many. However, the sole reason for switching is that it is a clean and green source with no negative effect on the environment. This has motivated many researchers to work and advance in this field. In today's scenario, photovoltaic (PV) and wind-based power generation have become popular choices as a replacement for the usual fossil fuel-based schemes because of their several advantageous features. It has minimal maintenance, is inexhaustible and less costly compared to fossil fuels.

Due to non-uniform irradiance, MPP tracking in these renewable energy sources is difficult. The conventional methods of tracking the global maximum power peak (GMPP) are inefficient in tracking the GMPP as it gets trapped in the local maximum. Therefore, hybrid algorithms have been developed to deal with Partial Shading Conditions (PSC). The effectiveness of the algorithms must be judged on the basis of faster and smoother convergence, precise tracking in the lowest time, lower computational complexity, and fewer tuning parameters without any processing units, etc. The motivation was developed after studying various recent research papers on power quality improvement using renewable-based energy generation [1.3].

From the aforesaid reports' investigation, it was found that the existing schemes suffer from the issue that with variable isolation throughout the day, along with partial shading conditions, it can be difficult

to keep the DC bus and output voltage constant with a single boost converter. Although extensive literature was referred to, it lacks the desired result for wider voltage variations. Therefore, the proposed schemes have dealt with the issue of wider voltage variation by means of novel series compensation. The literature survey [1.5]- [1.9] has given immense ideas and assistance regarding the systems, but it lacked in terms of maintaining wider voltage variation and simpler system design in practical scenarios. Therefore, an initiative was taken to develop a robust, durable, stable, simple, and cheaper real-time implementation system. A laboratory setup has also been developed for the given proposed schemes to verify the systems' working conditions in real time. The schemes are based on PV and PV-wind hybrid based microgrid connections. The proposed schemes involve DFIG-based systems which have efficient working even at lower wind speeds and voltage fluctuations. The converter on the rotor side should guarantee sinusoidal input at a slip frequency with the stator frequency maintained at 50 Hz. Since then, RSC has used a six-step switching method, which causes ripples in the output. For nearly sinusoidal output, a high switching frequency is required, which causes higher losses in the converters. Also, induction generators have limitations over speed range due to magnetic circuit saturations, high reactive power requirements, etc. With high wind speeds, the excess power availability can affect the shaft, which is to be taken care of. However, due to renewable energy's random nature and with current methods, uncertainties like these pose significant challenges for power quality maintenance in microgrids. A control strategy should be developed to control the converters at higher wind speeds and the generator not exceed the limiting torque. These points are also to be overcome, which are the source of motivation for the development of proposed schemes. The control algorithm should be easier for implementation and should occupy less memory space so that it can be widely used for domestic and industrial purposes. Various switching approaches have also been carried out to determine proper converter selection for the conversion from DC to AC and vice-versa. The inverters are operated at a lower switching frequency and with the least number of switches in order to maintain the efficiency of the whole system. Efforts are made to acquire the desired voltage pattern and enhance the quality of power by reducing the switching frequency of operation. The main goal was to improve and maintain power quality issues such as harmonics, power fluctuation, frequency and voltage variation. Both the lower and higher order harmonics have been efficiently taken care of by the help of novel series compensation, which has simply given the best results. This has been shown in the comparative analysis on various parameters with the existing schemes presented later in the chapters.

1.7 OBJECTIVE OF THESIS

The topologies are developed keeping in mind to upgrade the level of or improve power quality.

The objectives are as follows:

- Minimization and mitigation of injected harmonics by PV and wind-based hybrid DGs and enhance power quality when the microgrid will be connected with non-linear loads.
- Improve power quality issues (lower and higher order harmonics, frequency and voltage fluctuation, unbalance), power fluctuation (small time power fluctuations, long time or seasonal power fluctuations).
- To implement various new and modified metaheuristic techniques in order to eliminate undesirable harmonic and the optimized result gave the minimum possible THD.
- To use reduced number of triggering angles which gives equivalently good results as that of higher switching angles thus reducing the harmonics. Hence, this leads to reduced conduction and switching losses and higher efficiency.
- To overcome the effects of Partial Shading Conditions (PSC) in order to cater the issues of the real time scenarios.
- To test and compare the existing schemes with the proposed ones on the basis of various parameters.
- A novel series compensation strategy in proposed PV integrated microgrid and PV-Wind hybrid system to mitigate harmonics and maintain voltage profile under wide voltage variation at the grid side detailed later in the thesis.
- Comparison of different switching techniques for inverters was carried out to judge which serves the industrial/domestic demand better.
- To implement easier and effective control strategy discussed later in the thesis.
- To prioritise development of an easier simple, cost-effective proposed system which uses least components like IGBTs and driver circuit's hence the installation space.
- Proposed configurations are simulated to verify the operation of proposed topologies.
- Prototype verification of proposed topologies is also being developed for all the separate topologies reported in the thesis.

1.8 THESIS ORGANIZATION

The organization of thesis has been designed as follows:

Chapter 1 presents the highlights of overall research papers referred, under the topic of literature survey. These papers gave an idea of the shortcomings which motivated for the development of proposed topologies in order to deal with them efficiently. It assisted in deciding the objective of the present work

and also consists of brief highlights of all the topics covered in the thesis. Finally, it ends up with thesis organization.

Chapter 2 is divided into two schemes, the first of which introduces the suitable power converter selection for the grid integration of renewable energy sources. Cascaded architecture with a multilevel idea is most frequently utilized to incorporate PV sources into the grid due to its many benefits. Four alternative converter solutions have been compared in this study in order to examine the compatibility of PV-grid integration. Converters include SHEPWM with multilevel topology, two-level SPWM inverter, conventional Cascade H Bridge MLI (CHB-MLI), multicarrier PWM-based cascaded Multilevel inverter, and cascaded Multilevel inverter. Comparison criteria include output voltage THD, scheme complexity, effectiveness, performance, and other significant elements. The chapter also emphasizes harmonic mitigation in order to preserve power quality. Using the Perturb and Observe (P&O) approach, the Maximum Power Point from the PV source has been reached. For a multilayer inverter, two carrier waves were used to generate the gate pulse, which was then compared to a sinusoidal and an inverse sinusoidal reference wave. The switching angles of the cascaded MLI and SHEPWM inverters have been calculated using a metaheuristic method. It also exposes a number of intriguing properties, including convergence, output voltage behavior, and THD variance. Further consideration was given to the appropriate minimal THD angles. By comparing the reference and carrier waves at various modulation indices, SPWM was performed. The proposed topology has been validated by simulation using MATLAB/Simulink 2016b.

In Scheme 2, a novel two-step methodology is presented that tackles and enhances power quality issues for the PV integrated microgrid system. In order to address the real-time concerns, partial shading was first included. Next, it has been suggested to use the Improved Jelly Fish Algorithm with Perturb and Observe (IJFA-PO) to track the Global Maximum Power Point (GMPP). The main unit, which is powered by a DC-AC converter, is also synchronized with the grid. An auxiliary unit goes through a revolutionary series compensation technique to deal with the wide voltage variation and harmonic mitigation. This chapter has tested a number of switching strategies in an effort to identify the best one. The chapter goes into detail on the suggested system's superior performance in terms of convergence, metaheuristics, and efficiency.

Chapter 3, uses MWOA search-based SHEPWM for a microgrid system, which contributes to the field of power quality. It went into detail on how higher-order harmonics are typically not addressed, increasing switching losses and decreasing system efficiency. Instead, a large number of switching angles are typically used to remove harmonics. Different switching angles were used to analyse the performance. An experimental setup was created to support the findings after the model was run in MATLAB 2016b.

In order to get rid of lower-order harmonics and maximize higher-order harmonics, Scheme 2 offers a better framework for a microgrid-connected system based on PV-DFIG. Additionally, it provides

voltage to meet grid demand during periods of low wind speed and greater voltage swings. To reduce stator harmonics caused by switching at the rotor side, dependent on rotor speed, a novel series compensation approach has been implemented. The piecewise mixed model has been used online in conjunction with the SHEPWM approach to manage a wider spectrum of harmonics with a minimal amount of switching pulses. This was achieved with just three triggering angles, which produces results as excellent as seven switches, resulting in lower switching losses and greater efficiency. In order to manage these harmonics with the fewest switches possible each cycle, the SHEPWM technique has been used. Additionally, different search-based optimization methods have been contrasted to see which performed the best for the issue statement. Finally, a lab prototype was created to test the simulations, and the findings section includes further information on this. After conducting a comparison with other works of literature, it was discovered that the SAR-based SHEPWM performs better when subjected to the proposed series compensation in order to fulfil the goal of the current chapter.

In **Chapter 4**, the endeavor of this research is finally summarized and concluded. It also includes the perspective for future work and the constraints of the thesis work.

References

- [1.1] Solanki, C. S. (2015). Solar photovoltaics: fundamentals, technologies and applications. Phi learning pvt. Ltd, ISBN-13: 978-81-203-5111-0.
- [1.2] Kamal, W. A. (1997). Improving energy efficiency—The cost-effective way to mitigate global warming. *Energy conversion and management*, 38(1), 39-59.
- [1.3] Demirbas, M. F., & Balat, M. (2006). Recent advances on the production and utilization trends of bio-fuels: a global perspective. *Energy conversion and Management*, 47(15-16), 2371-2381.
- [1.4] Memon, M. A., Mekhilef, S., Mubin, M., & Aamir, M. (2018). Selective harmonic elimination in inverters using bio-inspired intelligent algorithms for renewable energy conversion applications: A review. *Renewable and Sustainable Energy Reviews*, 82, 2235-2253.
- [1.5] Ray, R. N., Chatterjee, D., & Goswami, S. K. (2010). Reduction of voltage harmonics using optimisation-based combined approach. *IET power electronics*, 3(3), 334-344.
- [1.6] Al-Quraan, A., & Al-Qaisi, M. (2021). Modelling, design and control of a standalone hybrid PV-wind micro-grid system. *Energies*, 14(16), 48-49.
- [1.7] Krishnamurthy, K., Padmanaban, S., Blaabjerg, F., Neelakandan, R. B., & Prabhu, K. R. (2019). Power electronic converter configurations integration with hybrid energy sources—a comprehensive review for state-of-the-art in research. *Electric Power Components and Systems*, 47(18), 1623-1650.

- [1.8] Sarker, K., Chatterjee, D., & Goswami, S. K. (2017). Grid integration of photovoltaic and wind-based hybrid distributed generation system with low harmonic injection and power quality improvement using biogeography-based optimization. *Renewable Energy Focus*, 22, 38-56.
- [1.9] Balamurugan, M., Sahoo, S. K., & Sukchai, S. (2017). Application of soft computing methods for grid connected PV system: a technological and status review. *Renewable and Sustainable Energy Reviews*, 75, 1493-1508.
- [1.10] Ghodelbourk, S., Azar, A. T., Dib, D., & Omeiri, A. (2020). Selective harmonic elimination strategy in the multilevel inverters for grid connected photovoltaic system. *International Journal of Advanced Intelligence Paradigms*, 15(3), 317-339.
- [1.11] Ramesh, A., & Sait, H. H. (2020). An approach towards selective harmonic elimination switching pattern of cascade switched capacitor twenty-nine-level inverter using artificial bee colony algorithm. *Microprocessors and Microsystems*, 79, 103292.
- [1.12] Ray, S., Gupta, N., & Gupta, R. A. (2021). Power quality improvement using multilevel inverter-based active filter for medium-voltage high-power distribution system: a comprehensive review. *International Journal of Power Electronics*, 14(1), 1-36.
- [1.13] Sarker, K., Chatterjee, D., & Goswami, S. K. (2018). Modified harmonic minimisation technique for doubly fed induction generators with solar-wind hybrid system using biogeography-based optimisation. *IET Power Electronics*, 11(10), 1640-1651.
- [1.14] Blooming, T. M., & Carnovale, D. J. (2006, June). Application of IEEE Std 519-1992 harmonic limits. In *Conference Record of 2006 Annual Pulp and Paper Industry Technical Conference* (pp. 1-9). IEEE, DOI: 10.1109/PAPCON.2006.1673767.
- [1.15] Beaulieu, G., Bollen, M. H. J., Malgarotti, S., & Ball, R. (2002, July). Power quality indices and objectives. Ongoing activities in CIGRE WG 36-07. In *IEEE Power Engineering Society Summer Meeting*, 2, pp. 789-794. IEEE.
- [1.16] Alkahtani, A. A., Alfalahi, S. T., Athamneh, A. A., Al-Shetwi, A. Q., Mansor, M. B., Hannan, M. A., & Agelidis, V. G. (2020). Power quality in microgrids including supraharmonics: Issues, standards, and mitigations. *IEEE Access*, 8, 127104-127122.
- [1.17] Khosravi, N., Abdolmohammadi, H. R., Bagheri, S., & Miveh, M. R. (2021). Improvement of harmonic conditions in the AC/DC microgrids with the presence of filter compensation modules. *Renewable and Sustainable Energy Reviews*, 143, 110898.
- [1.18] Reddy, C., Goud, B. S., Aymen, F., Rao, G. S., & Bortoni, E. C. (2021). Power quality improvement in HRES grid connected system with FOPID based atom search optimization technique. *Energies*, 14(18), 5812.

- [1.19] Alhato, M. M., & Bouallègue, S. (2019). Direct power control optimization for doubly fed induction generator-based wind turbine systems. *Mathematical and Computational Applications*, 24(3), 77.
- [1.20] Aljendy, R., Nasyrov, R. R., Abdelaziz, A. Y., & Diab, A. A. Z. (2022). Enhancement of power quality with hybrid Distributed generation and FACTS device. *IETE Journal of Research*, 68(3), 2259-2270.
- [1.21] Guichi, A., Mekhilef, S., Berkouk, E. M., & Talha, A. (2021). Optimal control of grid-connected microgrid PV-based source under partially shaded conditions. *Energy*, 230, 120649.
- [1.22] Motahir, S., El Hammoumi, A., & El Ghzizal, A. (2020). The most used MPPT algorithms: Review and the suitable low-cost embedded board for each algorithm. *Journal of cleaner production*, 246, 118983.
- [1.23] Yadav, R. S., Dhaked, D. K., & Jaiswal, A. (2021). Comparative study of MPPT techniques for solar PV-based system. *International Journal of Environment and Sustainable Development*, 20(3-4), 366-380.
- [1.24] Parida, A., & Chatterjee, D. (2017). Integrated DFIG–SCIG-based wind energy conversion system equipped with improved power generation capability. *IET Generation, Transmission & Distribution*, 11(15), 3791-3800.
- [1.25] Abdelateef Mostafa, M., El-Hay, E. A., & ELkholy, M. M. (2023). Recent Trends in Wind Energy Conversion System with Grid Integration Based on Soft Computing Methods: Comprehensive Review, Comparisons and Insights. *Archives of Computational Methods in Engineering*, 30(3), 1439-1478.
- [1.26] Suman, S., Chatterjee, D., & Mohanty, R. (2020, July). Speed Range Improvement of Induction Generator for wind Power Applications. In *2020 International Conference on Computational Intelligence for Smart Power System and Sustainable Energy (CISPSSE)* (pp. 1-6). IEEE, DOI: 10.1109/CISPSSE49931.2020.9212277.
- [1.27] Suman, S., Mohanty, R., & Chatterjee, D. (2022). Comparison of Multi-carrier MLI, CHB-MLI, SHEPWM and SPWM Inverters for PV-Grid Integration. In *Advances in Thermofluids and Renewable Energy* (pp. 669-681). Springer, Singapore, DOI: 10.1007/978-981-16-3497-0_54.

MITIGATING POWER QUALITY ISSUES FOR PV-GRID INTEGRATION

2.1 INTRODUCTION

Among the various source of alternative energy, solar energy is the most efficient and reliable that can be applied to the smart grids. The factors that have made them more popular over conventional energy are abundance, less cost, pollution free and easily availability. To put these renewable energies to use, converters are required to supply the demand side. Therefore, in order to fulfill the need efficiently, a comparative analysis of different type of inverters has been carried by Mohan et al. in [2.1]. Challenges related to the power quality issues in a microgrid connected system are mostly power fluctuations, voltage unbalance, frequency deviation. Voltage unbalance can be caused due to dips, swell, sags and interruptions giving rise to harmonics. Issues and its mitigation have been discussed in detail in the present chapter.

2.2 SWITCHING STRATEGIES OF INVERTERS

2.2.1 Existing Schemes

There are diversified topologies related to MLI such as symmetrical and asymmetrical dc sources for ach bridge, reduced switch MLI, Bridges connection with transformers addressed by Mohanty et al. and Mohammad in [2.2]- [2.5]. There are different papers which includes several other optimization techniques which was used for CHB-MLI inverters stated by Kangarlu and Babaei in [2.6]. Ye et al. and Laali et al. in [2.7]- [2.8] introduces the hybrid multicarrier PWM scheme to satisfy the deficiencies provided by carrier phase shift and in phase disposition.

A set of transcendental equations has been used to find the optimal solution using metaheuristic techniques. Fundamental component is assigned the desired values and harmonics are set to zero. It generates multiple solutions and makes the process problematic which was described by Ray et al. and Wells et al. in [2.9]- [2.15].

2.2.2 PROPOSED CONFIGURATION

2.2.2.1 System in detail

Solar panel has been used in the present scheme as a source of generation. It was connected to the boost converter to increase the voltage which was controlled by Perturb and Observe (P&O) method. The dc voltage obtained was used as an input to the inverter. Inverters that are chosen for comparison are CHB-MLI, Multicarrier MLI, SHEPWM, and SPWM. Constant dc voltage was obtained by the DC-DC boost converter which was given to the inverters. Different topologies can be seen in Fig. 2.1 (a), (b), (c) and

(d). GWO techniques was used to calculate switching angles in SHEPWM and CHB-MLI. The PWM pulses are obtained by sinusoidal and triangular comparison whereas, in Multicarrier MLI switching, different carrier signal was compared with Sinusoidal and inverse sinusoidal reference wave. This Multicarrier topology has been inspired by the survey of carrier level shifted like Phase Disposition (PD), and carrier phase shifted techniques such as Modified Reference Phase Disposition PWM (MRPD- PWM) etc.

The system has been obtained for three phases. In this case, triple-n harmonics are absent in line-to-line voltage. As the level of output voltage increases in MLI, THD decreases as it almost reflexes equivalent to sinusoidal wave. Hence, no filter requirement is there. RL load signifies the grid in the present scheme. This system is apt for wide range of application thus reliable for serving industrial and domestic demands.

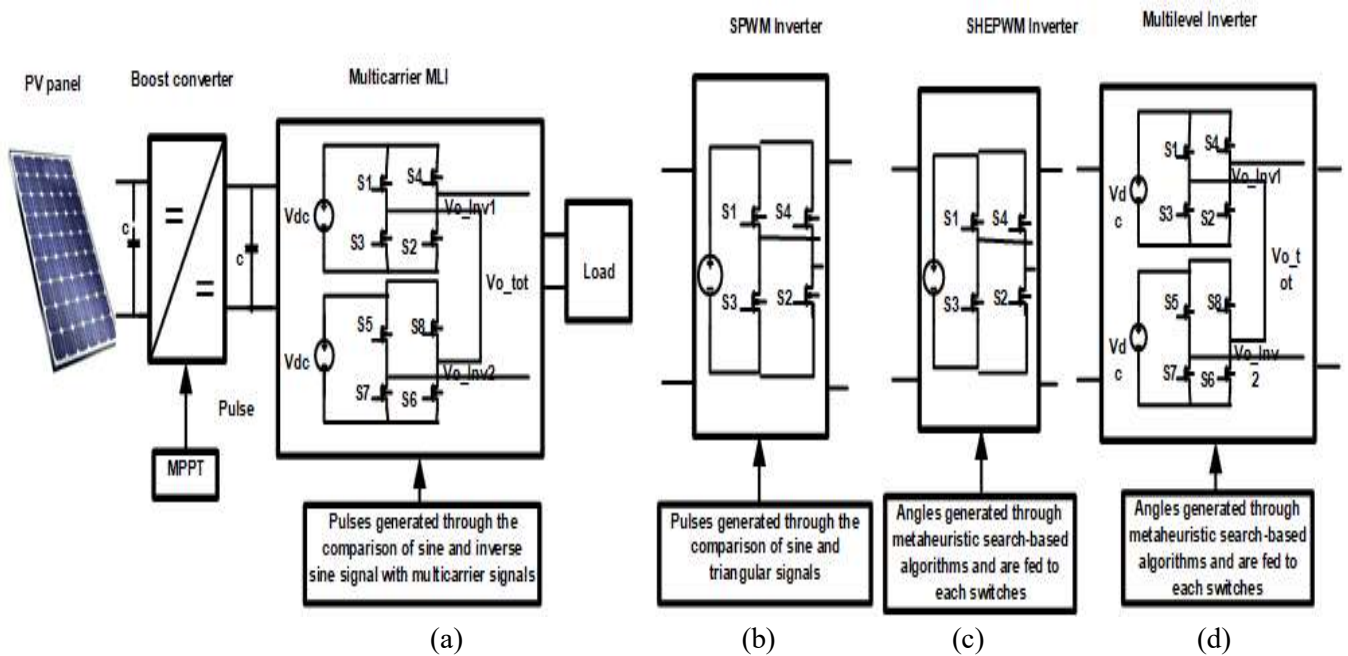


Fig. 2.1 Proposed topology of PV integrated (a) Multicarrier MLI (b) SPWM inverter (c) SHEPWM inverter (d) Multilevel inverter

As in MLI topologies level of voltage decides the number of components e.g., dc sources, diodes and MOSFET/ IGBTs to be used. As the level of inverter increases complexity, cost, size and installation area also increases. Losses also increases as no. of switch used increases; therefore, the efficiency of the system decreases. In the present chapter, the inverter used from the MLI family are Multicarrier MLI and conventional CHB-MLI topology. The proposed multicarrier MLI technique has addressed these issues and managed to give better result which marks the novelty of the scheme. Metaheuristic technique has been used to produce angles which can drive the SHEPWM and CHB-MLI inverters. These optimization technique uses an objective function which reduces or eliminates the undesired harmonics to large extent

which plummets the THD. Apart from that the other motive was to maintain the power quality with least voltage and current harmonics to be fed in the demand side which has been included.

2.2.3 COMPARISON OF DIFFERENT TYPES OF SWITCHING TECHNIQUES

2.2.3.1 Sinusoidal Pulse Width Modulation Inverter

In the present chapter, SPWM inverter is designed for the two level. These gating pulses are used to control the triggering of the switches as shown in Fig. 2.2 (a). If the value of M is selected wisely then it could also minimize the THD by reducing or eliminating harmonics to large extent.

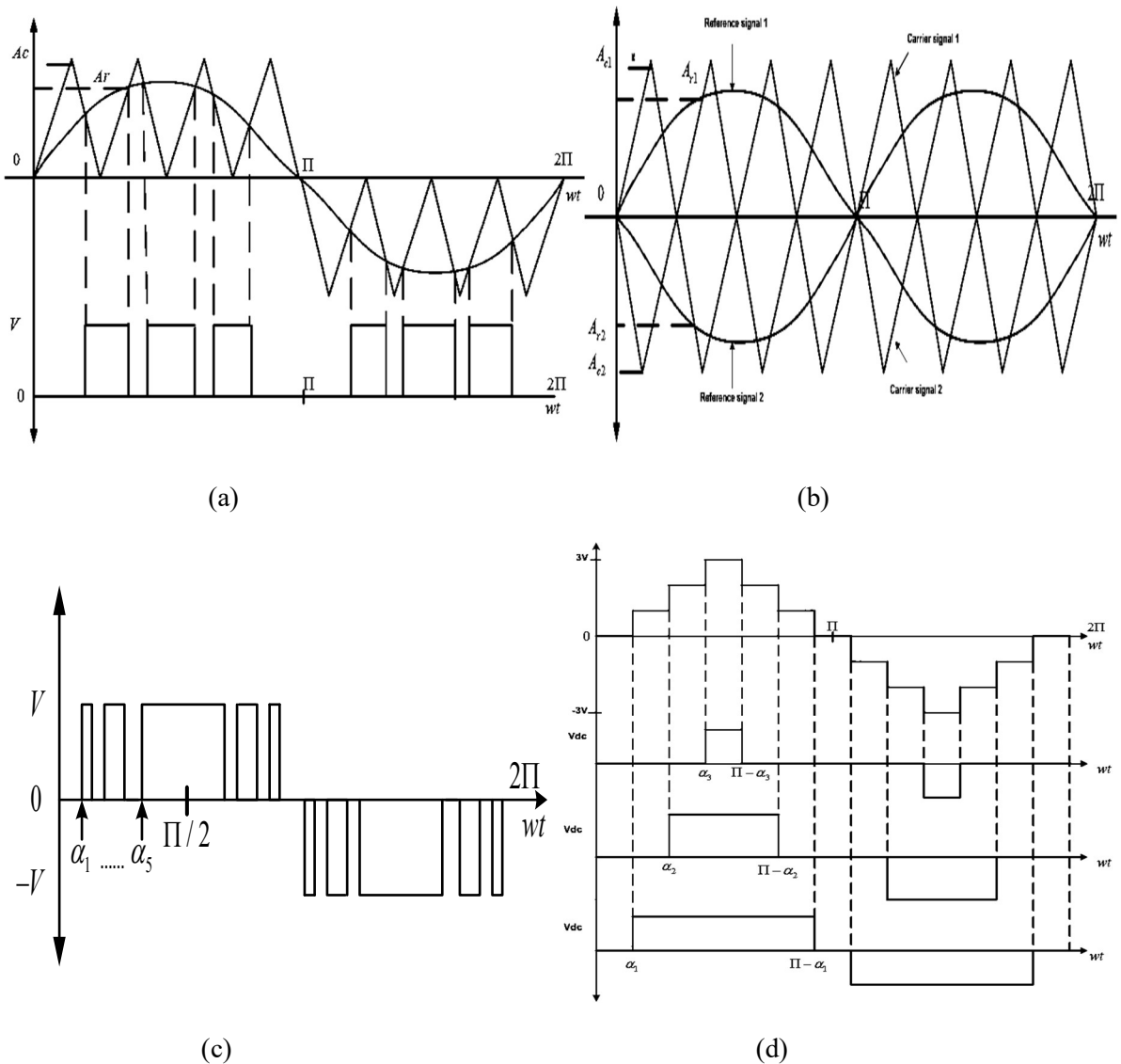


Fig. 2.2 (a) Pulse generation for SPWM (b) Pulse generation for Multicarrier MLI (c) Unipolar voltage output for SHEPWM inverter (d) Output voltage waveform for CH-MLI

The THD of unipolar is found out to be better than bipolar because the levels are more obtained for same number of carriers and Reference signals given by Ray et al. and Wells et al. in [2.10], [2.15]. The switching pattern has been shown in Fig 2.2 (a).

2.2.3.2 Multicarrier MLI

In the present chapter, dc sources used were symmetrical in nature. In this topology, for generating 'N' level inverters, no of carrier signals used would be 'N-1'. number of dc sources can be calculated by ((N-1)/2), and the no. of switches is given by 2 (N-1). In the conventional techniques single sine wave (reference) was compared with triangular (carrier) wave to generate pulses. But, for multilevel topologies it got extended to multi carrier waves with a single reference wave therefore called Multicarrier MLI as shown in Fig. 2.2 (b). This type of topology was considered to generate multilevel in the output voltage waveform which would automatically reduce the THD which was addressed by Laali et al. in [2.8]. As per the conventional methods the harmonics are obtained in the sidebands around carrier frequency 'Fc' which are resolved by using filters, but in this case, it is solved automatically.

2.2.3.3 Selective Harmonic Elimination PWM Inverter

SHEWPM works at low switching frequency which is having the benefit of lower switching loss as compared to the conventional converters. Angles are calculated by solving the non-linear equations given by Ray et al. in [2.9], [2.10]. If the switching angles are considered to be of 'd' number then it is efficient enough to remove '(n-1)' no of harmonics.

Generally, odd harmonics are present and even harmonics are mostly zero. In the present case, harmonics such as 5th, 7th, 11th, and 13th would be taken care by the five switching angles and rest of higher order harmonics would be controlled by the objective function in (2.3). Three-phase inverter has been taken into consideration for the unipolar case of output voltage as shown in Fig. 2.2 (c).

The output voltage, shown in Fig. 2.2, can be illustrated in terms of the Fourier series. According to the quarter-wave symmetry, only odd harmonics are present, i.e., ($a_n=0$).

$$v(\omega t) = \sum_{n=1}^{\infty} (a_n \cos n\omega t + b_n \sin n\omega t) \quad (2.1)$$

Where,

$$b_n = -\frac{4}{n\pi} \sum_{d=1}^m (-1)^d \cos n\alpha_d \quad (2.2)$$

On expanding (2.2) we get,

$$b_1 = \cos \alpha_1 - \cos \alpha_2 + \cos \alpha_3 - \cos \alpha_4 + \cos \alpha_5 = M \quad (2.2 (a))$$

$$b_5 = \cos 5\alpha_1 - \cos 5\alpha_2 + \cos 5\alpha_3 - \cos 5\alpha_4 + \cos 5\alpha_5 = 0$$

$$b_7 = \cos 7\alpha_1 - \cos 7\alpha_2 + \cos 7\alpha_3 - \cos 7\alpha_4 + \cos 7\alpha_5 = 0$$

:

$$b_{29} = \cos 29\alpha_1 - \cos 29\alpha_2 + \cos 29\alpha_3 - \cos 29\alpha_4 + \cos 29\alpha_5 = 0$$

The objective function can be given as

$$y(\alpha) = (b_1 - M)^2 + K_{17} * (b_{17} - e_{17})^2 + \dots + K_n * (b_n - e_n)^2 \quad (2.3)$$

Subjected to

$$0 < \alpha_1 < \alpha_2 \dots < \alpha_m < \frac{\pi}{2} \quad (2.4)$$

where, n is the harmonic order; $\alpha_1 \dots \alpha_d$ are the five triggering angles; y is the objective function; e is a value close to zero, so that the harmonics value should be close to it; k is known as the priority setter value, because it prioritizes the harmonic that is too high and urgently needs to be reduced; $b_1, b_5, b_7 \dots b_n$ = amplitude of harmonic voltage., in the case of line-to-line voltage triple-n and the even harmonics are non-existent.

The fundamental component was adjusted within the range set for the modulation index. Lower order harmonics such as $b_1, b_5, b_7 \dots$ were removed by finding the five numbers of triggering angles. These angles were calculated by b_5, b_7, b_{11} , and b_{13} , equating the non-linear equations to zero. If the switching angles are considered to be of 'd' number, then it is efficient enough to remove the '(d-1)' number of harmonics. Generally, odd harmonics are present, and even harmonics are mostly zero. In the present case, five switching angles were found which dealt with the lower order harmonics such as 5th, 7th, 11th, and 13th, and the rest of the higher-order harmonics were controlled by the objective function in (2.3) by following the condition mentioned in (2.4). In the present case, harmonics of up to twenty-nine were taken into consideration. On considering an odd number of switching angles, such as three, the harmonics such as the 5th and 7th were removed. Similarly, by considering an even number of switching angles like four, the harmonics of the 5th, 7th, and 11th would be mitigated. So, the advantage is that by using the least number of triggering angles, a wider number of harmonics can be removed, as that would decrease the switching losses and would increase the performance capability and efficiency of the system. By using (2.2), (2.3), and (2.24) in the search-based algorithm, the minimum THD possible was generated with corresponding angles, which were further considered. As shown later, the harmonics up to the 29th order were decreased with five triggering pulses, reducing the switching losses. This limits the use of a higher number of triggering pulses and maintains the efficiency of the system.

$$\%THD = \sqrt{\frac{b_5^2 + b_7^2 + \dots + b_{29}^2}{b_1^2}} \quad (2.5)$$

2.2.3.3.1 NEED OF METAHEURISTIC TECHNIQUE

It helps in solving the optimization problem. Problem statements are taken from daily life aspects. The algorithms are chosen which are applied to similar kind of problem in existing schemes. The same has been used to justify the proposed schemes. There are various kinds of optimization techniques such as ant colony optimization (ACO), genetic algorithm (GA), and particle swarm optimization (PSO) etc. It is used according to the problem statement to find the optimal solution. On analyses with several other algorithms, it was found that IJFA suits best to the present case in terms of faster convergence, fewer tuning parameters, lower computational effort and easier implementation etc. shown later in the chapter. Metaheuristic technique was used to find angles for SHEPWM and CH-MLI inverter.

2.2.3.3.1.1 Grey Wolf Algorithm implementation for driving inverters

Mirjalili et al. in 2014, [2.11] has invented this algorithm which involves searching and hunting by grey wolves for the survival of their pack. There are different levels which defines the position and power of wolves. ‘Alpha’ is strongest and superior amongst the whole group basically the decision maker. ‘Beta’ holds the next position which helps alpha in decision making and then comes the delta who listens to the order placed by the dominant members and rest candidate comes under the grade of ‘Omega’ given by Dzung in [2.12]. Delta is the lowest member in priority according to the hierarchy. Its performance was enhanced by the variable, which decreases from 2 to 0. The main process of fetching the food is by three steps, which is encircling, hunting and attacking the prey. The deriving equations for GWO are:

$$A = 2ar_1 - a \quad (2.6)$$

$$C = 2r_2 \quad (2.7)$$

$$\begin{aligned} D &= |C \cdot G_p(t) - G(t)| \\ G(t+1) &= G_p(t) - A \cdot D \end{aligned} \quad (2.8)$$

Steps related to GWO algorithm are:

Step1: Random initialization of search agents, where (i=1, 2...n).

Step2: Initialization of GWO parameters using (2.6) and (2.7) and initialize iter = itermax.

Step3: Start iteration loop using (2.8).

Step4: Calculation of $G_\alpha, G_\beta, G_\omega$ hunt agents.

Step5: Update the current position using step4.

Step6: Program gets terminated when iter = itermax and minimum THD is obtained using the corresponding switching angles.

When $|\vec{A}| > 1$ the wolves leave the prey in search of better prey which is called global search in optimization, but when $|\vec{A}| < 1$ grey wolf converges to the prey they found. The values \vec{a} decreases linearly from 2 to 0.

2.2.3.3.1.2 Particle Swarm Optimization Algorithm (PSO) optimization technique used

The algorithm is developed by Dr. Eberhart and Dr. Kennedy in 1995 [2.31]. It is inspired by bird's flocks or fish school behavior to search food. It is like GA, but crossover and mutation don't occur in PSO. The deriving equations are as follows:

$$v_i^{k+1} = wv_i^k + c_1 \text{rand}(pbest_i^k - x_i^k) + c_2 \text{rand}(gbest_i^k - x_i^k) \quad (2.9)$$

$$x_i^{k+1} = x_i^k + v_i^{k+1} \quad (2.10)$$

Where, c1 and c2 are the constriction factors which is considered 2 respectively, rand () is the random variable between 0 and 1; w is the inertia weight factor; v_i is the current particle velocity; x_i is the current particle position and k is the iteration number.

The Pseudocode algorithm for PSO

1. The parameters such as population matrix and iteration vector are initialized. The counter was set as 1 for iteration vector
2. Particle position was assigned from 0 to $\pi/2$ for switching angles and velocity vector was considered as voltage.
3. The vectors are updated using (2.9) and (2.10).
4. Fitness value of each particle was checked and calculated using (2.4).
2. Best result gbest would be displayed by replacing itself with best values of angles by using the fitness function.
6. If the condition is satisfied the process ends, otherwise it repeats from step 4 until convergence.

Each particle is initialized by group of random particles, which searches for optimal solution. There are two best solutions, pbest solution is the solution obtained so far and the other best solution is the gbest solution, which is obtained so far by any particle in population.

2.2.3.4 Cascade H bridge MLI

In the present chapter, MLI are powered by a set of PV panel and boost converter. The switches are fed using the angles found by metaheuristic technique. According to CHB-MLI topology, if the no. of levels is ‘m’, number of bridges can be found by ‘(m-1)/2’ for each phase. The number of angles can be calculated by, $A_i=i*180/m$, where. $i=1, 2, 3, \dots (m-1)/2$ by kala and Arora in [2.3]. The switching pulses can be seen in the Fig. 2.2 (d). Table 2.1 shows the switching pattern of Phase-A. In case of three-phase, it would be shifted by 120 degrees. As the input voltage (V_{dc}) is symmetric in nature for each cells/ bridge so the voltage can be expressed in terms of Fourier series

$$V(\omega t) = \sum_{n=1,5,7\dots}^{\infty} \frac{4V_{dc}}{n\pi} (\cos(n\alpha_1) + \cos(n\alpha_2) + \dots + \cos(n\alpha_n)) \sin(\omega t) \quad (2.11)$$

With the condition applied as mentioned in (4.4) the objective function or the fitness function in the search-based algorithm is to minimize the THD as far as possible as given in (2.4).

$$V_{ph} = V_{o1} + V_{o2} + \dots + V_{on} \quad (2.12)$$

As the bridges are series connected phase voltage (V_{ph}) is the sum total of individual output voltage of each bridge.

Table 2.1 Switching pattern for phase- A

Switching states	Output voltage levels								
	0 V	V	2V	V	0	-V	-2V	-V	0
S1	0	1	1	1	0	0	0	0	0
S2	0	1	1	1	0	0	0	0	0
S3	0	0	0	0	0	0	1	0	0
S4	0	0	0	0	0	1	1	1	0
S5	0	0	1	0	0	0	0	0	0
S6	0	1	1	1	0	0	0	0	0
S7	0	0	0	0	0	1	1	1	0
S8	0	0	0	0	0	1	1	1	0

2.2.4 SIMULATIVE RESULT ANALYSIS

There are two blocks one is the supply block i.e., PV panel connected to the boost converter and other block i.e., the inverter connected load as shown in Fig. 2.1. The simulation was carried out for a load

resistance and inductance of 50Ω and 0.01 mH respectively. The output waveform of the DC-DC Boost converter can be seen in Fig. 2.3.

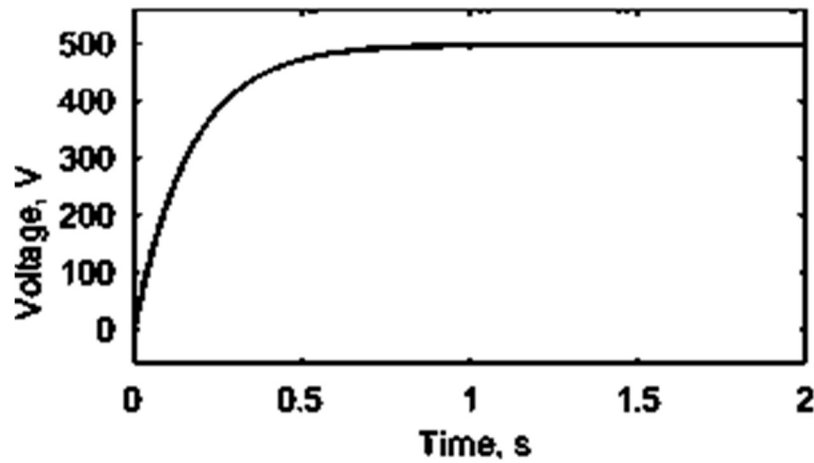


Fig. 2.3 Output voltage waveform of Boost converter

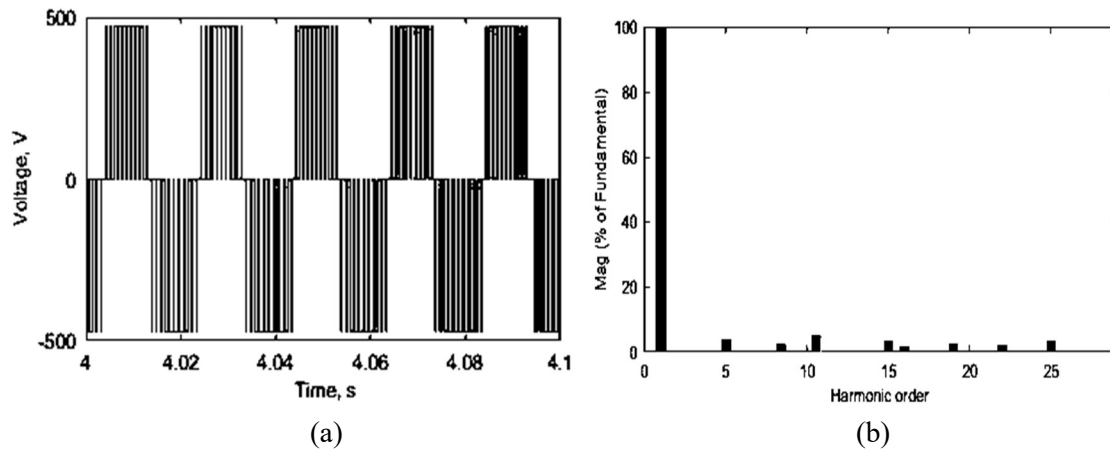


Fig. 2.4 (a) Three-phase output voltage of SPWM inverter (b) FFT spectrum of the output voltage waveform

The output voltage waveform and the FFT spectrum for the full bridge SPWM inverter can be seen in Fig. 2.4 (a) and (b) respectively. THD was found out to be 9.32%. It was found that in the over-modulation case, THD gets better. It can be observed that in the unipolar output voltage waveform lower order harmonics are mostly dominant. The seven-level output voltage waveform for multicarrier MLI can be observed in Fig 2.5 (a) and its corresponding THD was found to be 1.56% as shown in Fig 2.5 (b).

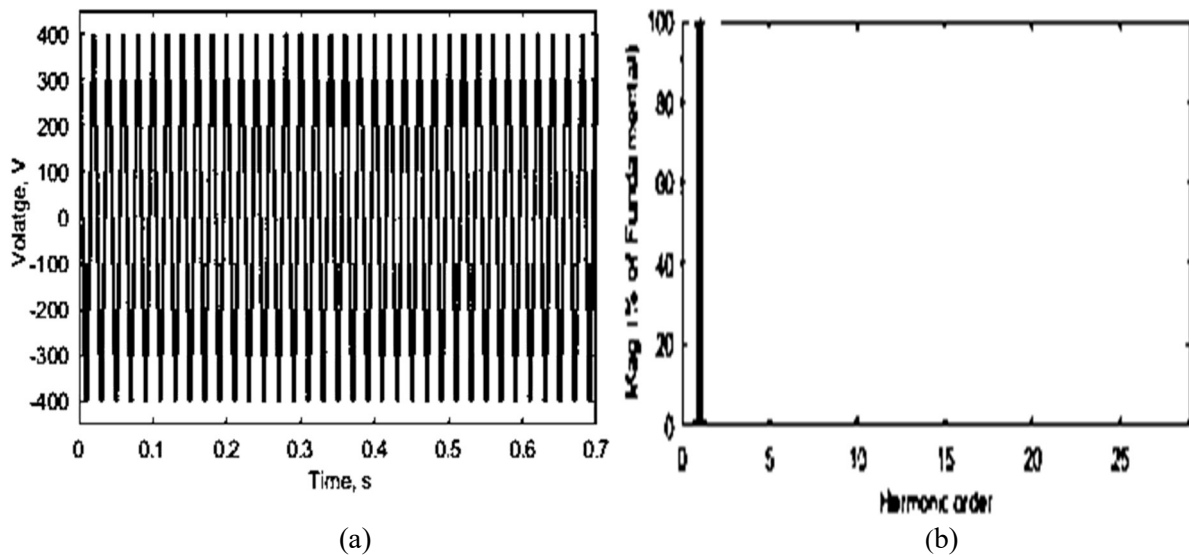
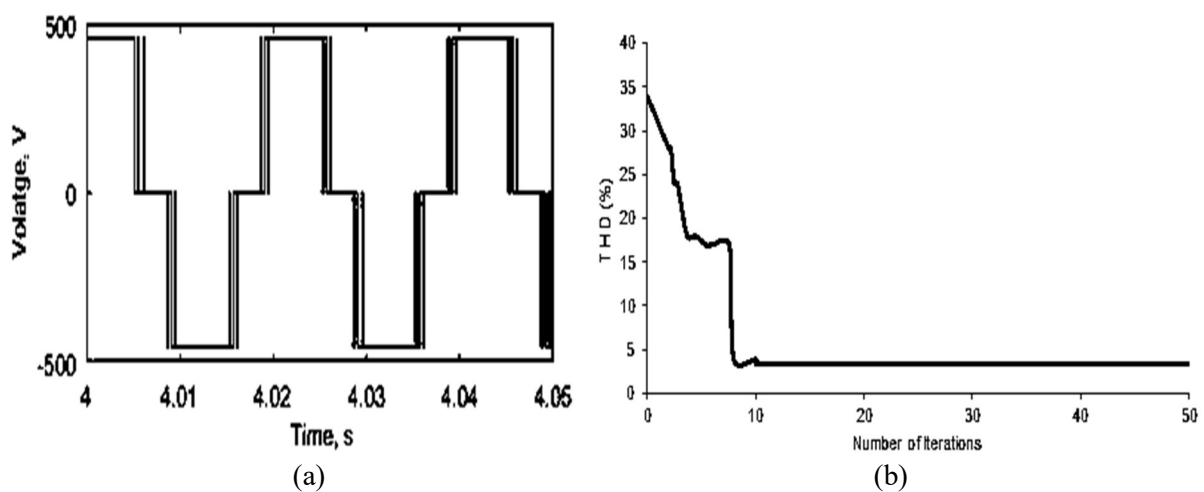


Fig. 2.5 (a) Output voltage of Multicarrier MLI inverter (b) FFT spectrum of the output voltage waveform

As the level of the output voltage increases, THD gets decreased. FFT spectrum was considered up to 29th order for all cases. Lower and higher order harmonics are mostly reduced or eliminated by the three-phase multicarrier MLI. In case of SHEPWM inverter, search-based techniques were used for angle calculation which was determined using MATLAB program. Angles generated using GWO are $\alpha_1 = 44.40^\circ, \alpha_2 = 54^\circ, \alpha_3 = 67^\circ, \alpha_4 = 82^\circ, \alpha_5 = 105^\circ$ at a modulation index ($M = V_1/V_{max}$) of 0.82. The output voltage using SHEPWM inverter can be seen in Fig. 2.6 (a). The iteration curve for GWO is shown in Fig. 2.6 (b). It attains the convergence in merely 0.28 seconds. THD found out was 3.05% as seen in Fig. 2.6 (c). Fig. 2.6 (c) and (d) shows the FFT analysis of the output voltage waveform taken by MATLAB /Simulink and MATLAB program. It was found that the FFT analysis by calculated values of MATLAB program and simulated values of Simulink are almost matching.



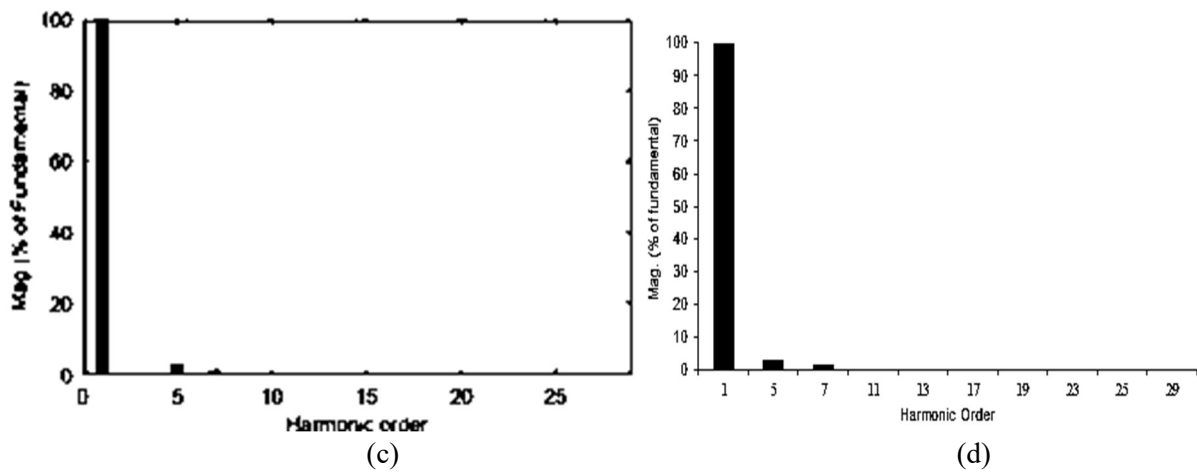


Fig. 2.6 (a) Output voltage of SHEPWM inverter (b) Convergence behavior of GWO search-based techniques (c) FFT spectrum of the output voltage waveform for GWO obtained by MATLAB Simulink (d) FFT spectrum obtained by MATLAB program

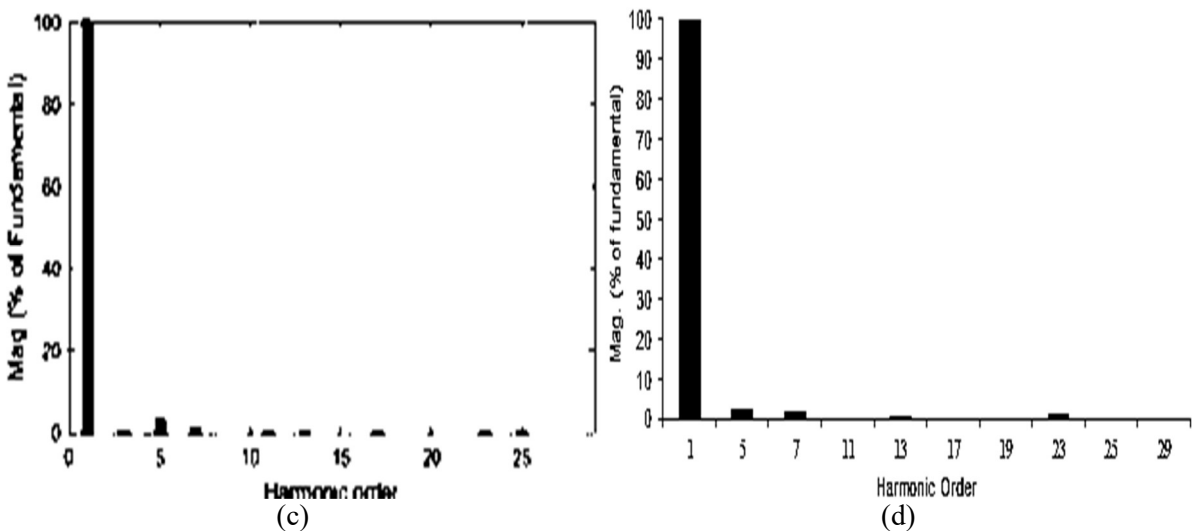
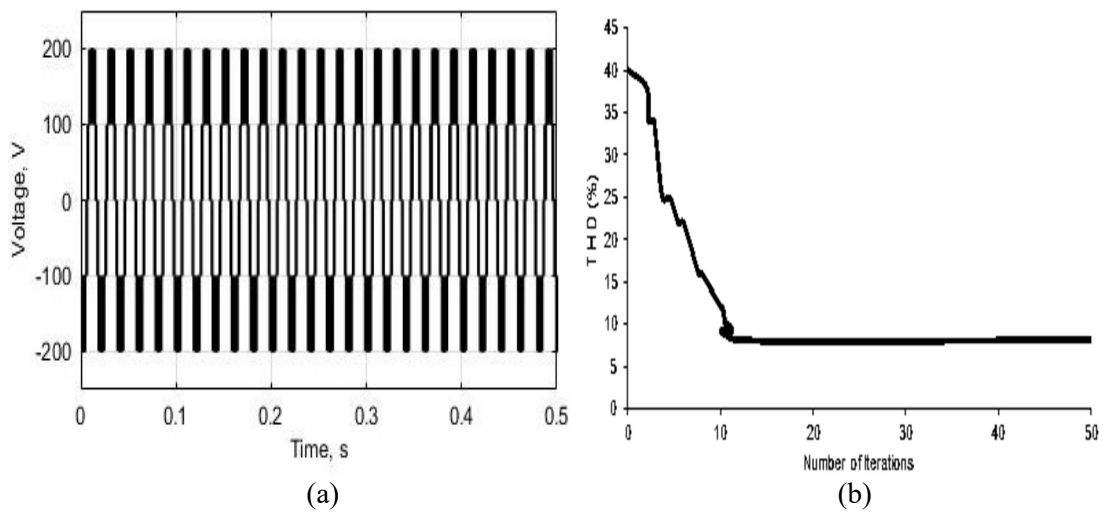


Fig. 2.7 (a) Output voltage of CHB-MLI inverter (b) Convergence behavior of GWO search-based techniques (c) FFT spectrum of the output voltage waveform for GWO obtained by MATLAB Simulink (d) FFT spectrum obtained by MATLAB program

In case of H bridge CHB-MLI inverter, for generating five-level output, the no of angles considered were two. This was calculated by using same optimization techniques as used in the SHEPWM case. For the three-phase inverter it was appropriate enough to reduce or eliminate the lower order harmonics such as 5th, 7th and the higher order are reduced. The angles calculated using GWO are $\alpha_1 = 36^\circ, \alpha_2 = 72^\circ$; $\alpha_1 = 28^\circ, \alpha_2 = 64^\circ$. Output line voltage can be seen in Fig. 2.7 (a). THD obtained by the FFT analysis was 3.1% at the modulation index of 0.82. The iteration curve for GWO is shown in Fig. 2.7 (b). It attains the convergence in merely 0.45 seconds. The values of the harmonics calculated using the MATLAB Simulink and program was found to be similar as shown in Fig. 2.7 (c), Fig. 2.7 (d).

2.2.4.1 Comparative details for different switching parameters

A comparative analysis can be observed in Table 2.2. A closed loop feedback controller was connected with inverters to keep a check on the response for the change in load. In case of SHEPWM and CHB-MLI, if there was any change in load then the angles would automatically tune itself to maintain low THD.

Table 2.2. Comparative analysis of CHB-MLI, Multicarrier, SPWM, SHEPWM inverter

Parameters	CHB-MLI	Multicarrier MLI	SPWM	SHEPWM
No. of levels of inverter	5	7	3	3
No. of switches used (in single phase)	24	24	6	6
No. of DC sources	6	6	1	1
No. of bridges	6	6	-----	-----
Filter	Not required	Not required	Can be used	Not required
Performance	Better	Best	Could have been better	Better
No. of components Requirements	Higher	Higher	Lesser compared to others	Lesser compared to others
Power quality	Could have been better	Best	Could have been better	Best
Switching frequency	High	High	Low	Low
THD	3.1%	1.56%	9.32%	3.05%
Convergence time	0.45 sec	-----	-----	0.28 sec

2.2.5 CONCLUSION

A comparative analysis of different inverters has been carried out in various aspects such as harmonic compensation, THD minimization etc. has been taken into consideration to evaluate the performance of inverter. Multicarrier MLI was found to give the out of all with THD of only 1.56% when considered up to 29th order harmonic. Both simulation and MATLAB program justifies the similarity of the THD for the five- level inverter. For SHEPWM and CHB-MLI H-bridge inverters, GWO switching scheme works better for removing undesirable harmonics. The controller would automatically adjust itself with the variation in load. The proposed method shows benefits in terms of power quality and switching frequency and the complex circuits designs thus, reducing the overall costing. The purpose to find the best inverter for the proposed topology was successfully attained.

Publication

- ❖ Suman, S., Mohanty, R., & Chatterjee, D. (2022). Comparison of Multi-carrier MLI, CHB-MLI, SHEPWM and SPWM Inverters for PV-Grid Integration. In *Advances in Thermo-fluids and Renewable Energy* (pp. 669-681). Springer, Singapore. DOI: 10.1007/978-981-16-3497-0_54.

References

- [2.1] Mohan, N., Undeland, T. M., & Robbins, W. P. (2003). *Power electronics: converters, applications, and design*. John Wiley & sons, ISBN: 978-0-471-22693-2.
- [2.2] Mohanty, R., Chatterjee, D., Suman, S., & Sengupta, G. (2019, July). PSO based improved topology for MLI considering low THD and low switching loss. In *2019 10th International Conference on Computing, Communication and Networking Technologies (ICCCNT)* (pp. 1-5). IEEE, DOI: 10.1109/ICCCNT45670.2019.8944546.
- [2.3] Kala, P., & Arora, S. (2017). A comprehensive study of classical and hybrid multilevel inverter topologies for renewable energy applications. *Renewable and Sustainable Energy Reviews*, 76, 905-931.
- [2.4] Hasan, N. S., Rosmin, N., Osman, D. A. A., & Musta'amal, A. H. (2017). Reviews on multilevel converter and modulation techniques. *Renewable and Sustainable Energy Reviews*, 80, 163-174.
- [2.5] Mohammed, J. A. K. (2016). Economical design of H-bridge multilevel inverter drive controlled by modified fast algorithm. *Microelectronics Reliability*, 65, 89-97.
- [2.6] Kangarlu, M.F. and Babaei, E. (2013). Cross-MLI: an innovative topology. *IET Power Electron.* 6, 642- 651.

- [2.7] Ye, M., Chen, L., Kang, L., Li, S., Zhang, J., & Wu, H. (2019). Hybrid multi-carrier PWM technique based on carrier reconstruction for cascaded H-bridge inverter. *IEEE Access*, 7, 53152-53162.
- [2.8] Laali, S., Abbaszadeh, K., & Lesani, H. (2010, October). Development of multi-carrier PWM technique for multilevel inverters. In *2010 International Conference on Electrical Machines and Systems* (pp. 77-81), Print ISBN:978-1-4244-7720-3, IEEE.
- [2.9] Ray, R. N., Chatterjee, D., & Goswami, S. K. (2010). Reduction of voltage harmonics using optimisation-based combined approach. *IET power electronics*, 3(3), 334-344.
- [2.10] Ray, R. N., Chatterjee, D., & Goswami, S. K. (2009). An application of PSO technique for harmonic elimination in a PWM inverter. *Applied soft computing*, 9(4), 1315-1320.
- [2.11] Mirjalili, S., Mirjalili, S. M., & Lewis, A. (2014). Grey wolf optimizer. *Advances in engineering software*, 69, 46-61.
- [2.12] Dzung, P. Q., Tien, N. T., Tuyen, N. D., & Lee, H. H. (2015, June). Selective harmonic elimination for cascaded multilevel inverters using grey wolf optimizer algorithm. In *2015 9th International Conference on Power Electronics and ECCE Asia (ICPE-ECCE Asia)* (pp. 2776-2781). IEEE, DOI: 10.1109/ICPE.2015.7168164.
- [2.13] Steczek, M., Chudzik, P., & Szeląg, A. (2017). Combination of SHE-and SHM-PWM techniques for VSI DC-link current harmonics control in railway applications. *IEEE Transactions on Industrial Electronics*, 64(10), 7666-7678.
- [2.14] Nalcaci, G., Yildirim, D., & Ermis, M. (2020, June). Selective harmonic elimination for light-rail transportation motor drives using Harris hawk's algorithm. In *2020 IEEE International Conference on Environment and Electrical Engineering and 2020 IEEE Industrial and Commercial Power Systems Europe (EEEIC/I&CPS Europe)* (pp. 1-6). IEEE, DOI: 10.1109/EEEIC/ICPSEurope49358.2020.9160694.
- [2.15] Wells, J. R., Geng, X., Chapman, P. L., Krein, P. T., & Nee, B. M. (2007). Modulation-based harmonic elimination. *IEEE Transactions on power electronics*, 22(1), 336-340.

2.3 POWER QUALITY ISSUES FOR PV INTEGRATED MICROGRID SYSTEM

2.3.1 INTRODUCTION

Power Quality (PQ) issue is one of the most serious issues for a microgrid system. The parameters that are responsible for a good PQ are frequency, voltage quality (interruptions, variations, unbalances, flicker, sags, and swells, transients), harmonics and power factor. It is drawing so much of attention due to the heavy penetration of power electronics-based loads in every walk of our lives [2.14]. The consumers seek

clean, high-quality power to operate their machinery at all levels. Poor PQ not only causes degradation and bad performance of electrical equipment but also system losses [2.15] - [2.17]. The regulatory intervention ensuring optimum PQ supply has been studied IEEE 1547, IEC, CIGRE WG 36-05 standards [2.22]- [2.24].

Solar energy is always a viable option for meeting power demands. Its clean and green features, easy accessibility, and cost-free nature have made it extremely popular [2.16]. Therefore, PV has been used as source to track the Maximum Power Point (MPP). There are numerous challenges, such as properly tracking MPP in non-uniform conditions and injecting harmonics-free voltage into the grid. To extract maximum power under uniform irradiance there are various traditional approaches such as Incremental Conductance (IC) [2.17], Hill Climbing (HC), Perturb and Observe (P&O) [2.18], etc. But in real time scenarios (under Partial Shading Conditions (PSC) these methods are incapable to perform as it gets trapped in the local maximum. Many metaheuristic strategies, including Slime Mould Algorithm (SMA) [2.19], Weighted Means of Vector Algorithms (INFO) [2.20] and others [2.21]- [2.26] have been studied.

2.3.2 EXISTING TOPOLOGIES AND ITS DRAWBACKS

For studying the PSC, the approaches such as Whale Optimization Algorithm (WOA) [2.21], Grey Wolf Optimization (GWO) [2.22], Colony Predation Algorithm (CPA) [2.23], Jaya Algorithm [2.24] and Jelly Search Algorithm (JSA) [2.25], [2.26] has been analysed. They have computational complexity for tracking Global Peak (GP) in (P-V) waveforms over the traditional methods. Additionally, it is not effective in controlling the duty cycles, thus, making the process lengthy. CPA suffers from a problem of slower tracking speed. Following that, it was determined that JSA has a good tracking speed over a wide exploration range but has higher implementation costs. It does not address the reinitialization of variables and dynamic shading pattern mentioned [2.25]. The techniques discussed exhibit higher computational demands on the processor, leading to lower efficiency in MPP tracking under PSC. The authors have not verified the robustness and consistency of the algorithm [2.26].

The choice of a proper converter is mandatory because it can reduce undesirable harmonics in order to deliver power efficiently to the grid. Voltage source inverters are commonly used with renewable energy sources. The Sinusoidal Pulse Width Modulation (SPWM) [2.27], conventional 180° and 120°, was used in a hybrid system with the Biogeography-Based Algorithm (BBO) and the Unified Power Quality Conditioner (UPQC) [2.28].

Power quality was improved using a Radial Basis Function Neural Network (RBFNN) integrated with a Proportional Integral (PI) controller [2.29]. A comparison of recent algorithms was done to selectively remove the harmonics [2.30]. For harmonic removal in multilevel inverters, a Modified Newton Raphson (MNR) and pattern recognition were utilised [2.31]. The SHEPWM and Selective Harmonic Mitigation

PWM (SHMPWM) based three-level NPC converters were employed, applying the harmonic suppression algorithm [2.32]. In [2.33], an Artificial Bee Colony (ABC) and filter compensation modules were used to minimise harmonics in microgrids.

A comparative analysis of various bionic algorithms was carried out [2.34], [2.35]. The typical SHE-PWM approach was found incapable of regulating the non-eliminated harmonics, resulting in higher values using a Harris Hawks Optimization (HHO).

The angles are obtained by using the set of transcendental equations in metaheuristic techniques [2.39]. This might seem to be easy but is quite tedious as it generates multiple solutions. As per the literature, direct solutions suffer from computational complexity and weaker convergence. Furthermore, a higher number of harmonics to be removed necessitates a large number of switching angles, which adds computational complexity and losses unnecessarily. These are the additional limitations of using the mentioned techniques. Most optimization techniques consider initial guesses to be sufficient for obtaining the solution. If a guess is not taken properly, then it might lead to an increase in iteration numbers, and there could be a chance of delay or no convergence at all. The 'n' no switching angles can eliminate the 'n-1' order harmonics, but higher orders are still present. There would be an increase in the switching per quarter cycle in order to get rid of them. Mostly, the causes of harmonics are inverter switching, MPP tracking, nonlinear loads, and others. To reduce the wide range of order harmonics, a large number of switching angles would be required, resulting in an increase in losses and making the system less efficient.

2.3.3 PROPOSED CONFIGURATION

2.3.3.1 Topology in detail

Due to PSC and variation in isolation, it is difficult to maintain the DC bus and output voltage using a single DC-DC boost converter. Various literature is cited in section 1.1 which implies difficult control methods, slower MPP tracking, and expensive implementation costs. Furthermore, if the input voltage is low, an additional Boost converter will be required to manage the entire power, increasing the overall cost and decreasing reliability. The presence of harmonics and wider voltage variations disrupting the power quality is also a major concern. Therefore, these issues have motivated the authors to design a prototype shown in Fig. 2.8, which is robust, non-bulky, low-cost, has a simple controller, and is easy to deploy.

The aforementioned concerns are addressed by a novel low-rated auxiliary unit integrated series compensation network on the ac side, which mitigates voltage demands and stabilizes the output ac voltage of the inverter. It also effectively eliminates harmonics with fewer switching angles and a single boost converter, addressing all of the aforementioned issues. The proposed prototype's layout is shown in Fig. 2.8. The primary PV panel is the supply panel, whereas the auxiliary panel is the compensatory panel. The primary PV panel is under partially shaded conditions. The auxiliary unit's ratings are 20% of the main units. The main PV panel is coupled to the DC-DC boost converter, which supplies the grid-synchronized

inverter. The proposed IJFA-PO technique computes the duty cycle for boost converter operation, which monitors the GMPP smoothly among all the local peaks at a quicker rate. The voltage is three times that of the PV voltage, making it ideal for grid synchronization but it has some limits. The greater ratio is attainable at the expense of decreased power output, which compromises the system's reliability.

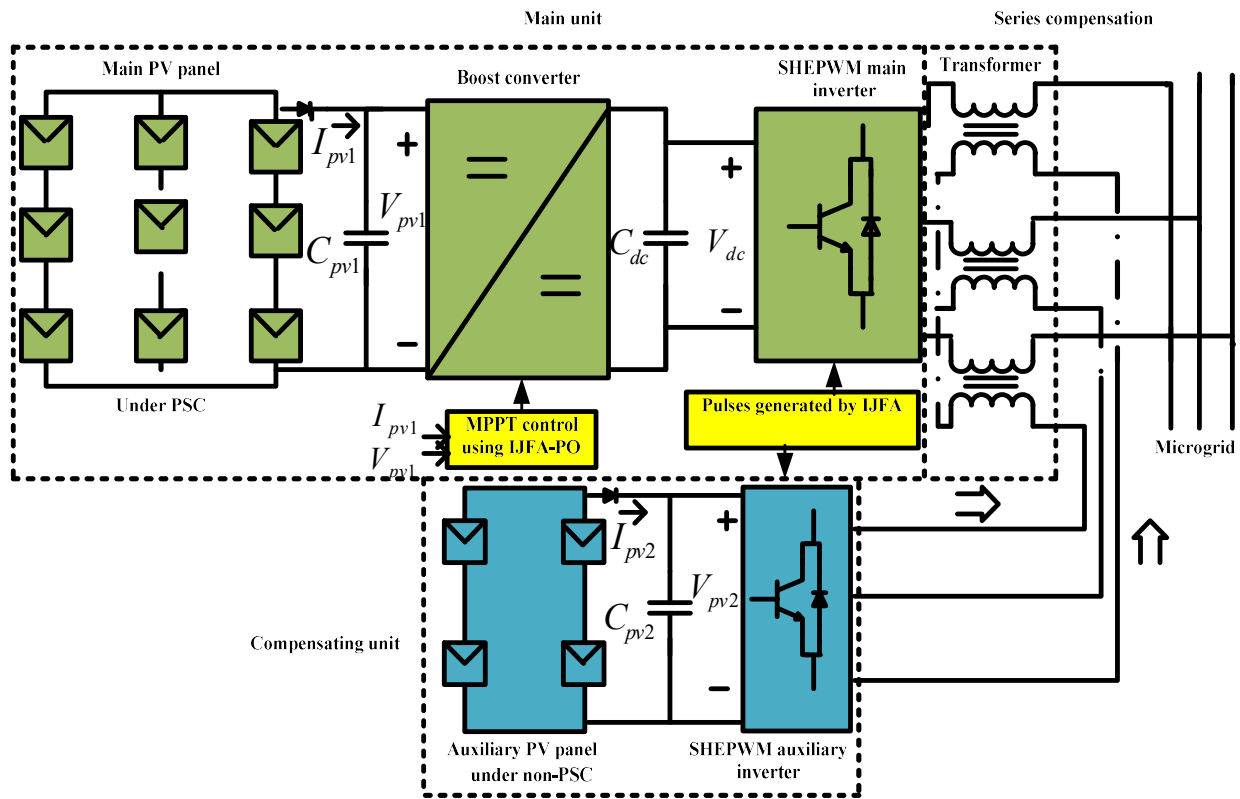


Fig. 2.8 Proposed prototype

As shown in Fig. 2.8, the auxiliary panel can directly feed the compensating inverter connected to the main inverter through a series compensating transformer. To identify the optimal performance for the proposed system, different switching strategies (180° conventional, IJFA implemented in 180°, 120° conventional, IJFA implemented in 120°, SPWM) were compared. It was found that IJFA based 120° produced improved results. These inverters were switched at a low frequency. The IJFA uses three switching angles for each inverter to drive them in the 120° SHE implemented mode. The performance of the optimized three switches per quarter cycle was better than the nine switching angles. As a result of this novel concept, switching losses are reduced, and the converter's life and efficiency are increased. The application of IJFA is not found in hybrid system fields. Its usage in the proposed scheme and the improved results obtained have contributed greatly. The main inverter has three switching angles that minimize harmonics (5th, 7th, 11th, 23rd), but other higher-order harmonics up to 29th will remain. In this chapter, harmonics up to the 29th order are considered. The auxiliary inverter deals with these harmonics in 180°

phase opposition, and the output voltage THD would be decreased greatly as a result. A piecewise mixed model was used in which the switching angles were stored offline for online implementation.

In a three-phase system, three switching angles can only reduce harmonics up to the 7th order, but higher orders still exist in a considerable number. The lower order harmonics were eliminated using the IJFA metaheuristic technique, and the higher orders were reduced or removed simultaneously using the auxiliary inverter in phase opposition. This significantly reduces the harmonics and improves the power quality, making it apt for grid synchronization. An auxiliary inverter also helped to regulate the voltage profile under wide voltage variations on the grid side. The setup is simple, cost-effective, and has easy application. It was found that the cost of using SHEPWM-based inverters is similar to that of other switching techniques. Thus, using an auxiliary converter does not make much of a difference in cost as it is effectively implementable with an already accessible drive compatible setup. It was considered for the unipolar pattern and harmonics up to the 29th order. The angles obtained were kept in the processor for an online implementation by applying a "piecewise mixed-model of approximation". This approach employs easier controlling techniques which occupies lesser memory storage as compared to other customary techniques. The THD achieved for the grid voltage and current is within the permissible limit prescribed by the IEEE-519 standard [2.36]- [2.39]. In the present work, the IJSA algorithm was tested under various characteristics such as steady-state weights, lower oscillations, speedy convergence for tracking MPP under PSC, and inverter switching. It causes drastic harmonic reduction, resulting in power quality enhancement. For inverter switching, the hypothesis proves that IJSA has superior performance in terms of rapid convergence, fewer tuning parameters, and lower computational effort. Various comparative plots and analysis shown later in the chapter highlight the capability of the present system to mitigate the issues identified earlier in the survey. The THD obtained by the proposed technique is the least of all. The proposed IJSA-based SHEPWM switching technique uses an objective function that generates switching angles of lower frequency for SHEPWM converters. The objective function converges to much lower values compared to other algorithms. It uses an auxiliary inverter for mitigating lower and higher order harmonics simultaneously and maintaining the wider voltage variation under PSC through series compensation. It would also meet grid demand and maintain voltage supply in the event of a wider voltage variation, dip or unbalance thus, improving or mitigating PQ issues.

2.3.4 EXISTING AND PROPOSED SWITCHING TECHNIQUES FOR HARMONIC ELIMINATION

2.3.4.1 Existing switching approaches

2.3.4.1.1 Sinusoidal Pulse Width Modulation Inverter (SPWM)

The two types of multilevel modulation methods are high switching frequency and fundamental switching control, in which SPWM and Space Vector PWM fall within the former. One of the primary

challenges with high-power applications such as SPWM inverters is power dissipation. If the output voltage levels are considered to be "n", then "n - 1" can be used to find the carrier waves. The output SPWM inverter in this chapter is developed for two levels, as illustrated in Fig. 2.9 (i). A Phase Lock Loop (PLL) was used for controlling purposes. The modulation index can be adjusted to modify the RMS value of the output voltage. If the value of MI is chosen carefully, it can reduce or eliminate harmonics to a great extent, which reduces the THD. Its switching pattern has been given in Fig. 2.2 (a).

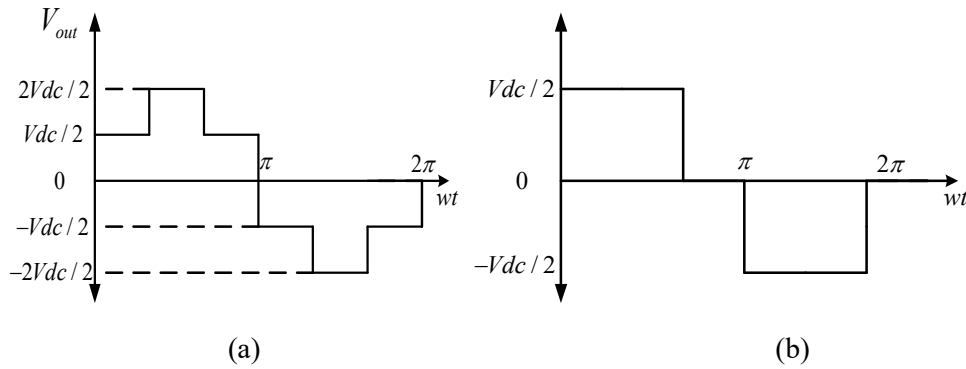


Fig. 2.9 (i) Pulse generation for a) 180° conventional b) 120° conventional

The output voltage in quasi sine wave form can be written in terms of Fourier series.

$$V_{an} = \frac{a_0}{2} + \sum_{n=1}^{\infty} (a_n \cos(nwt) + b_n \sin(nwt)) \quad (2.13)$$

As the waveform has symmetry of quarter-wave therefore, a_0 and $a_n = 0$ for all values of n , $b_n = 0$ for all even values of n ; n is the harmonic order, $\alpha_1 \dots \alpha_n$ are the switching angles. $f(wt)$ was taken from the waveform shown in Fig. 2.2 (i) (a).

2.3.4.1.2 Using the direct solution method for the conventional 180° switching strategy

$$b_n = \frac{4}{\pi} \left[\int_0^{\pi/2} f(wt) \sin(nwt) d(wt) \right] \quad (2.14)$$

$$b_n = \left(\frac{4}{\pi} \right) \left[\int_0^{\pi/3} \frac{V_{dc}}{3} \sin(nwt) d(wt) + \int_{\pi/3}^{\pi/2} \frac{2V_{dc}}{3} \sin(nwt) d(wt) \right] \text{ (delay of 0)} \quad (2.15)$$

$$b_n = \left(\frac{4V_{dc}}{3n\pi} \right) \left[[-\cos(nwt)]_0^{\pi/3} + 2[-\cos(nwt)]_{\pi/3}^{\pi/2} \right]$$

On solving,

$$b_n = \left(\frac{4V_{dc}}{3n\pi} \right) \left[1 + \cos\left(\frac{n\pi}{3}\right) \right] \quad (2.16)$$

$$V_{an} = \left(\frac{4V_{dc}}{3n\pi} \right) \left[1 + \cos\left(\frac{n\pi}{3}\right) \right] \sin(n\omega t) \quad (2.17)$$

with a phase of $\Phi_n = \tan^{-1}(a_n/b_n) = 0$

2.3.4.1.3 Using the direct solution method for the conventional 120° switching strategy

$$b_n = \frac{4}{\pi} \left[\int_{\pi/6}^{\pi/2} \frac{V_{dc}}{2} \sin(n\omega t) d(\omega t) \right] \quad (2.18)$$

It is obtained by using (2.13) and considering a delay of 30 in the limits

On solving,

$$b_n = \frac{2V_{dc}}{n\pi} \left[\cos(n\omega t) \right]_{\pi/2}^{\pi/6} \quad (2.19)$$

$$V_{an} = \frac{2V_{dc}}{n\pi} \sin\left(\frac{n\pi}{2}\right) \sin\left(\frac{n\pi}{3}\right) \sin(n\omega t) \quad (2.20)$$

at a phase angle of $\phi_n = \tan^{-1}\left(\frac{a_n}{b_n}\right)$

2.3.4.2 Proposed switching approaches

2.3.4.2.1 SHE implemented IJFA in a conventional 180° switching strategy

With a proper selection of three switching's per quarter cycle from the optimization technique, the harmonics up to 29th order were mitigated. $f(\alpha)$ was analyzed from the unipolar waveform shown in Fig. 2.10 (ii) (a).

$$b_n = \left(\frac{4}{\pi} \right) \int_0^{\pi/2} f(\alpha) \sin(n\alpha) (d\alpha) \quad (2.21)$$

The above equation has been obtained by using (2.1)

$$b_n = \left(\frac{4}{n\pi} \right) \left[\int_{\alpha_1}^{\alpha_2} \frac{V_{dc}}{3} \sin(n\alpha) (d\alpha) + \int_{\alpha_3}^{\alpha_4} \frac{V_{dc}}{3} \sin(n\alpha) (d\alpha) + \int_{\alpha_5}^{\pi/2} \frac{2V_{dc}}{3} \sin(n\alpha) (d\alpha) \right] \quad (2.22)$$

On solving,

$$b_n = \left(\frac{4V_{dc}}{3n\pi} \right) \left[\cos(n\alpha_1) - \cos(n\alpha_2) + \cos(n\alpha_3) - \cos(n\alpha_4) + 2\cos(n\alpha_5) \right]$$

$$b_n = \left(\frac{4V_{dc}}{3n\pi} \right) \left[-\sum_{k=1}^m (-1)^k \cos(n\alpha_k) - 2 \sum_{k=m+1}^m (-1)^k \cos(n\alpha_k) \right] \text{ where } 0 < \alpha_1 < \alpha_2 \dots < \alpha_5 < \frac{\pi}{2} \quad (2.23)$$

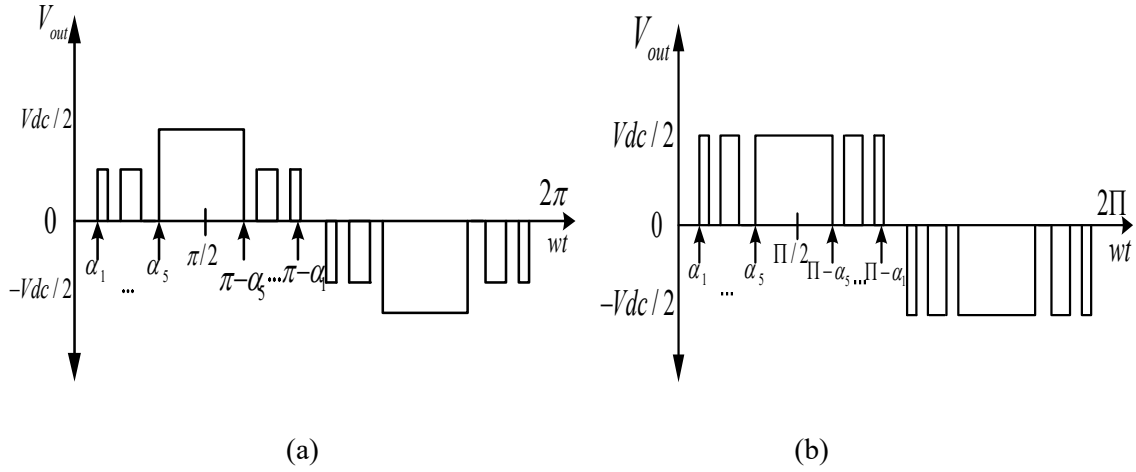


Fig. 2.10 (ii) Pulse generation for a) IJFA implemented in 180° b) IJFA implemented in 120°

2.3.4.2.2 SHE implemented IJFA in a conventional 120° switching strategy

$$b_n = \left(\frac{4}{\pi} \right) \int_x^{\pi/2} f(\alpha) \sin(n\alpha) (d\alpha) \quad (2.24)$$

Where, $x > 0$ is the delay according to the search-based SHE

$$b_n = \left(\frac{4}{\pi} \right) \left[\int_{\alpha_1}^{\alpha_2} \frac{V_{dc}}{2} \sin(n\alpha) (d\alpha) + \int_{\alpha_3}^{\alpha_4} \frac{V_{dc}}{2} \sin(n\alpha) (d\alpha) + \int_{\alpha_5}^{\pi/2} \frac{V_{dc}}{2} \sin(n\alpha) (d\alpha) \right] \quad (2.25)$$

On solving, it can be written as

$$b_n = -\frac{4}{n\pi} \sum_{k=1}^m (-1)^k \cos n\alpha_k \quad (2.26)$$

Where, $0 < \alpha_1 < \alpha_2 \dots < \alpha_5 < \frac{\pi}{2}$

Due to the symmetrical nature of unipolar line to line voltage, triplen harmonics are absent in a three-phase balanced system. The + and – signs of cos denote the rising and falling edges in the transition phases. The switching angles can be determined by expanding and equating voltage harmonics (2.26) to zero and setting the fundamental component to MI, where (MI < 1). The optimized angles with the lowest THD were chosen as they reduce harmonics introduced to the grid. The presence of trigonometric terms increases the complexity as it produces multiple or no solutions at all. To solve the non-linear equations acquired through direct solution or conventional technique, IJFA-based SHE comes into the picture. The existing solutions are discontinuous at some points, which requires an increased number of switching angles to

reduce harmonics. Lower switching rates are preferred since they result in fewer switching losses and higher efficiency. IJFA reduces overall THD by mitigating a wider spectrum of harmonics with only three optimum angles. These angles are calculated offline and stored in the lookup table memory of the Digital Signal Processor (DSP) for online use. The angles obtained for the lowest voltage THD to the closed point of MI are used to determine linearity. As a result, the SHE technique was used to overcome the problem of discontinuity.

2.3.5 Application of metaheuristic technique for angle generation and tracking of GMPP

2.3.5.1 Jelly Fish Algorithm (JFA) metaheuristic technique

Jui-Sheng Chou and Dinh-Nhat Truong developed JFA in 2021 which is inspired by jellyfish searching for food in the ocean. Three strategies are used by the jellyfish search optimizer. (i) Jellyfish move with the ocean current or within the group; (ii) Jellyfish are drawn to areas with more food; and (iii) the amount of food is assigned and the appropriate Fitness Function (FF) is computed. The heavy active and passive movements of the jellyfishes within the swarm cause a jellyfish bloom. When food sizes are compared, the optimum placements can be determined and the FF's best value may be evaluated. As a result, JFA can be modelled as

$$\vec{X}_{i+1} = \eta \vec{X}_i (1 - X_i), 0 \leq \vec{X}_0 \leq 1 \quad (2.27)$$

$$\vec{X}_i(t+1) = \vec{X}_i(t) + \vec{r} * (\vec{X}^* - \beta * r_1 * \mu) \quad (2.28)$$

Where the value for η is taken as 4; \vec{X}_i is a vector that contains the logistic chaotic values of the i^{th} jellyfish; \vec{X}_0 is an initial vector of jellyfish 0, generated randomly between [0, 1]; \vec{X}^* is the location with the most food; $*$ is the element-by-element vector multiplication; $\beta > 0$ is the distribution coefficient taken as $\beta = 3$; μ is the mean of the population and \vec{r}, r_1, r_2, r_3 is a random number between [0, 1]; $\vec{X}_i(t+1)$ is the ocean current in (2.28). The movements of jellyfish inside the swarm are controlled by passive and active motions. Jellyfish move about their positions in passive motion, and the fresh update of their positions is described by using (2.29). The active motion, on the other hand, is determined according to the formula shown in (2.30).

$$\vec{X}_i(t+1) = \vec{X}_i(t) + r_3 * \gamma * (U_b - L_b) \quad (2.29)$$

$$\vec{X}_i(t+1) = \vec{X}_i(t) + \vec{r} * \vec{D} \quad (2.30)$$

where $\gamma > 0$ indicates the length of the motion around the current location. U_b and L_b are the upper and the lower bound of the search space of the problem, respectively. is used to determine the direction of the

motion of the current jellyfish within the next generation. This motion corresponds to the tracking of the best food position and is expressed in (2.31). Where, j is the index of a jellyfish selected randomly.

$$\begin{aligned}\vec{D} &= \vec{X}_i(t) - \vec{X}_j(t); \text{if } FF(\vec{X}_i) < FF(\vec{X}_j) \\ \vec{D} &= \vec{X}_j(t) - \vec{X}_i(t); \text{otherwise}\end{aligned}\quad (2.31)$$

The $c(t)$ is used to switch between ocean currents, passive and active motions, all of which may be described mathematically in (2.32).

$$c(t) = \left(1 - \frac{t}{t_{\max}}\right) * (2 * r - 1) \quad (2.32)$$

where t is the current evaluation; t_{\max} is the maximum evaluation A jellyfish swarm is formed over time, and each jellyfish continues to migrate within the swarm to obtain a better position, using both active and passive motions, resulting in exploitation at this stage. Meanwhile, $c(t)$ switches between these motions. The user should choose between two control options i.e., population and t_{\max} . As per the latter, fewer settings are required, resulting in less labor and haphazard trials to fine-tune the JFA's performance.

2.3.5.1.1 Improved Jelly Fish Algorithm (IJFA) in detail and JFA limitations

The JFA algorithm's exploitation capability was found to be low due to the current jellyfish movement within the population. This slowed the convergence toward the best solution so far, resulting in a long time to find a better solution. Furthermore, local exploration capability searches multiple rounds within the regions where the swarm's presence is limited. As a result, looking for areas inside the swarm that haven't been investigated by any of the other jellyfish helped to fetch better results.

When the control variable r is small, the IJFA explores around the best-so-far solution, but when r is large, it improves exploration around the swarm for reaching other regions. As a result, the IJFA equation is as follows:

$$\vec{X}_i(t+1) = \vec{X}_i(t) + r * (\vec{X}_{r_1}(t) - \vec{X}_{r_2}(t)) + (1-r)(X^* - \vec{X}_{r_3}(t)) \quad (2.33)$$

where r_1, r_2 and r_3 are the indices of three solutions, whose values are between [0 1]; r is the control parameter which is used to control in moving of the current solution. If r is small, the current solution will be moved to a location located between the best-so-far and $\vec{X}_{r_3}(t)$ to accelerate convergence, if r is high, the current one is updated using two randomly chosen solutions from the population to improve the algorithm's ability to reach new regions. This method is then combined with the JS to modify its

performance to reach better solutions in fewer iterations. The IJFA approach in the proposed series compensation for the current scheme is given in the flowchart in Fig. 2.3.

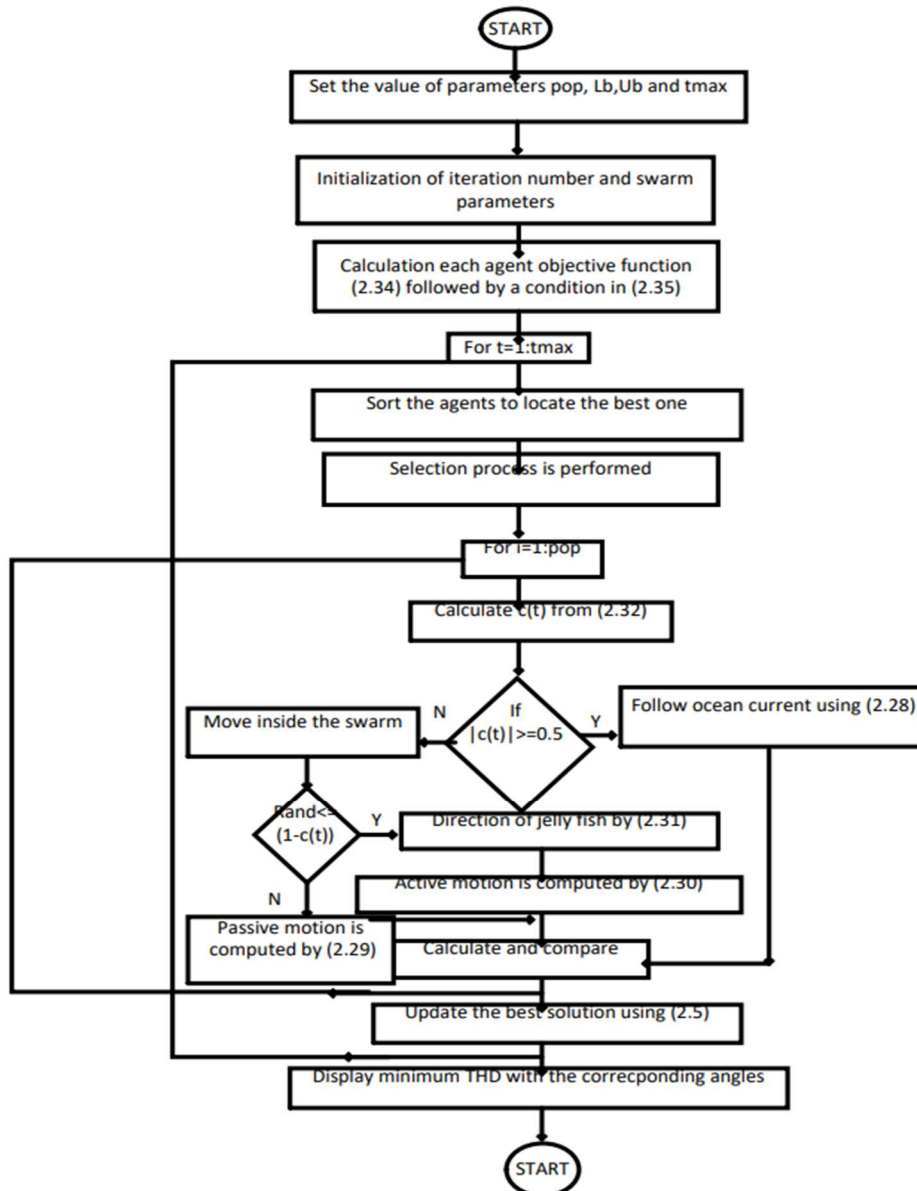


Fig. 2.11 Flowchart for the IJFA

2.3.5.1.2 Application of IJFA in proposed compensation technique

2.3.5.1.2.1 Angle obtained for the Main SHEPWM inverter in detail

The IJFA-based SHEPWM technique was used to determine the angle generation for the primary inverter. Three switching angles were found by equating the fundamental component to MI and the rest voltage harmonics to zero, as indicated earlier in (2.26). A search-based technique has been used to obtain angles and store them offline in the microcontroller memory. The three angles can attenuate harmonics up to the 5th, 7th, 11th, ... 23rd order, but higher-order harmonics such as the 25th, ... 29th, and so on will still

exist. As a result, an auxiliary inverter was used to implement novel series compensation to attenuate existing higher-order harmonics.

2.3.5.1.2.2 Angle calculation for Auxiliary SHEPWM inverter to suppress higher orders in detail

As SHEPWM involves trigonometric concepts, it has limits in terms of displaying many solutions. Therefore, to achieve convergence variables must be chosen at the exact point. To avoid the difficulty of finding a solution to a non-linear equation, the problem was changed to an optimization function $t_1(\alpha)$. The THD obtained should be a minimum (2.34) and the corresponding angles are to be considered further. The objective function used to produce the angles for the auxiliary inverter for decreasing the existing dominating harmonics

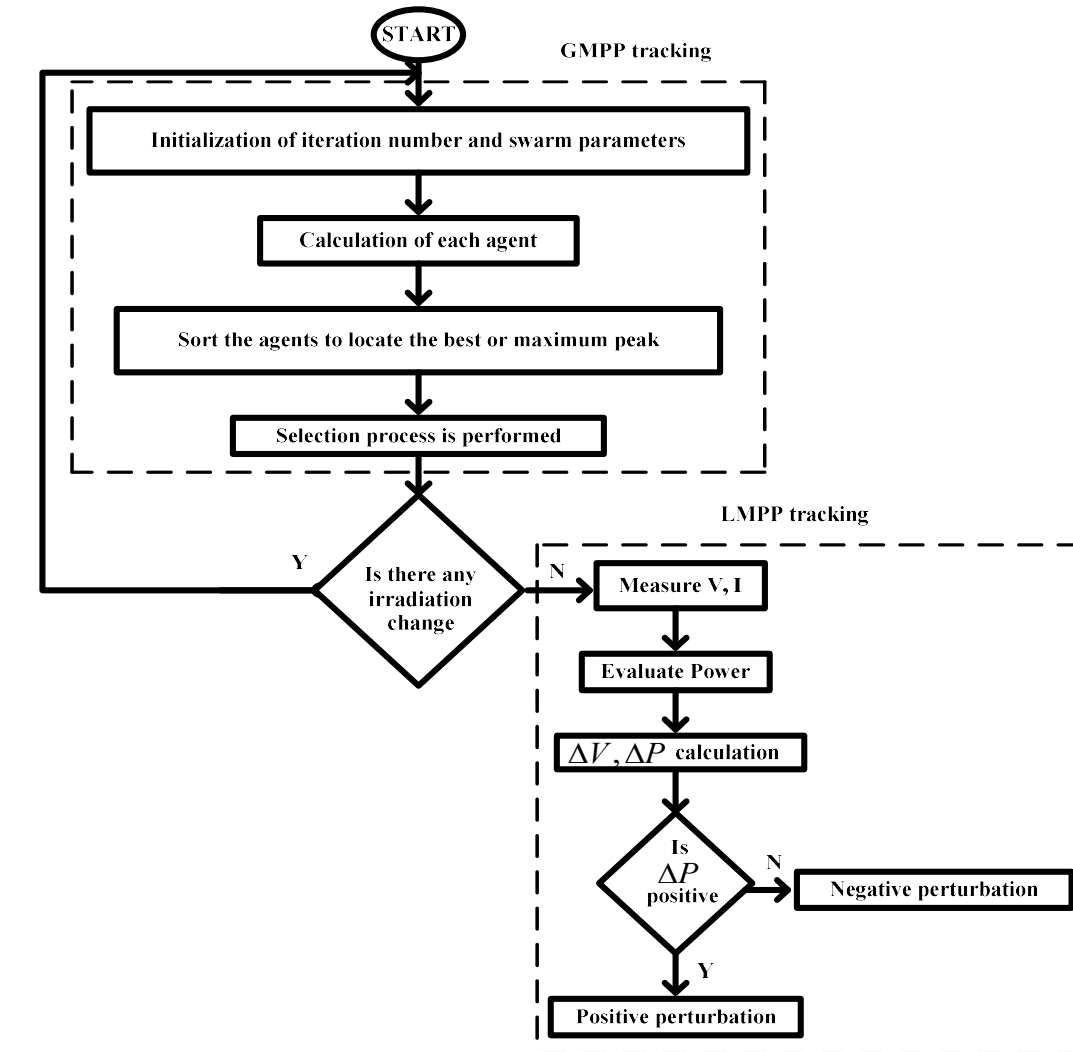
$$t(\alpha) = K_1 * (b_1 - M)^2 + K_5 * \varepsilon_2^2 + \dots + K_n * \varepsilon_n^2 \quad (2.34)$$

Subjected to
$$0 < \alpha_1 < \alpha_2 \dots < \alpha_m < \pi/2 \quad (2.35)$$

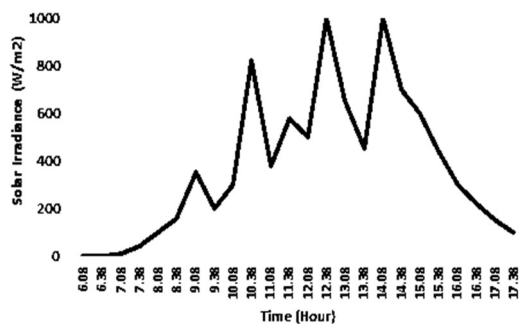
where, $K_1 \dots K_n$ are the weights that are applied to the harmonics to be minimized priority-wise, $\varepsilon_1 \dots \varepsilon_n$ are the values that are set according to the magnitude of the respective harmonic that is to be reduced. Normally, it is set to zero but here it is taken according to the amount in which the higher-order harmonics are to be reduced. The values of $K_1 \dots K_n$ in (2.34) have to be selected wisely to reduce the magnitude of the harmonics with $\varepsilon_1 \dots \varepsilon_n$ amount respectively. As an example, suppose the harmonic amplitudes of the 25th and 29th harmonics are 23% and 14%, respectively. For reducing the amplitude of the harmonics, the weights must be used in order of priority, with the 25th priority being given first, followed by the 29th. To cancel out the 25th harmonic, it must be set to a value of 23% but in the opposite phase. This also applies to any harmonic order of any amplitude. The IJFA algorithm includes the objective function (2.34) for reducing existing dominating harmonics in particular. The technique was repeated until the desired outcome and convergence were achieved. The angles obtained in the IJFA-based SHEPWM approach (2.34) should strictly follow the criteria illustrated in (2.35). As indicated in Figure 1, the three angles achieved are sent to the auxiliary inverter, which undergoes series compensation with the main unit. For a three-phase system, IJFA mitigates a wider range of harmonics 5th, ... 23rd with only three optimum angles, while others up to 29th are minimized by employing (2.34) and (2.35) in IJFA and series compensation technique, thus lowering overall THD. These angles are calculated offline and stored in the lookup table memory of the DSP for online use. The objective function (2.22) was used to minimize the three-phase output voltage THD (2.5).

2.3.5.2 Partial Shading Condition (PSC): concern for PQ issues

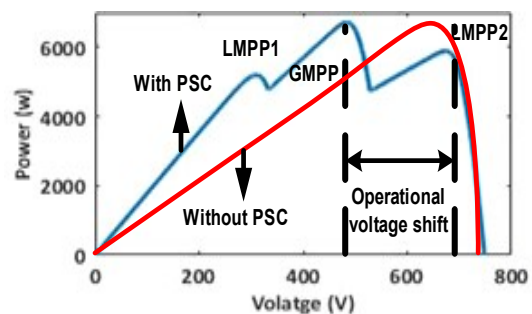
PSC is caused by passing clouds, building shadows, neighboring trees, bird excreta, and other factors. The efficiency of PV is affected by many peaks and non-convex features. The array consists of modules with solar irradiation of 250 (shaded), 1000 (non-shaded), 800, 1000 W/m² at a module temperature of 25°C. Under uniform irradiation, simple P&O is effective. However, under non-uniform irradiance, it is unable to track the GMPP among the numerous LMPPs, and the speed drops.



(a)



(b)



(c)

Fig. 2.12 For tracking power (a) Flowchart of the IJFA-PO (b) Solar irradiance at various times of the day, c) PV curve with Partial Shading conditions (PSC) and uniform isolation in a general scenario

The challenges have been discussed in section 2.9 and the ways to overcome it has been detailed in section 2.10.1. As a result, integration of IJFA and P&O is carried out to address these PSC scenarios, as presented in Fig. 2.12 (a). Figs. 2.12 (b) and (c), respectively, show a pictorial representation of a general scenario of irradiance variation at different hours of the day and the power vs. voltage curve under PSC and non-PSC aspects. The optimization technique helped to understand the MPPT performance with the continuous variation of environmental conditions. Multiple peaks can be observed under the PSC case with a target set that MPPs should follow GMPP.

2.3.6 IMPLEMENTATION OF THE CONTROL TECHNIQUE

Piecewise mix model equations have been used to store the set of switching angles produced by IJFA. This control method makes use of a set of linear and nonlinear equations that were computed offline using the IJFA and then stored in the processor memory for online usage (2.37). When compared to other existing strategies, this processor takes little memory space and has a lower computational complexity. Fig. 2.5 depicts the fluctuation of triggering angles with various modulation indices in this method.

For, $0.5 \leq MI \leq 0.7$

$$\begin{aligned}\alpha_1 &= -110MI + 95.33, \\ \alpha_2 &= -140MI + 117.33, \\ \alpha_3 &= -160MI + 136, \\ \alpha_4 &= -150MI + 133.67, \\ \alpha_5 &= -190MI + 162.67\end{aligned}\quad (2.36)$$

For, $0.71 \leq MI \leq 0.9$

$$\begin{aligned}\alpha_1 &= 500MI^2 - 880MI + 389, \\ \alpha_2 &= 450MI^2 - 815MI + 370, \\ \alpha_3 &= -100MI^2 - 50MI + 38 \\ \alpha_4 &= 150MI^2 - 350MI + 201.5 \\ \alpha_5 &= 438MI^2 - 784.3MI + 362.39\end{aligned}\quad (2.37)$$

Fig. 2.13 depicts the control system in which the SHEPWM main inverter's three-phase voltage is compared to an appropriate reference output voltage. The error is processed by the PI controller that has been set up to generate MI. The set of triggering angles in the form of equations is stored for different values of MI, and the SHEPWM inverters are triggered by the pulses generated by the driver circuit using that set of equations.

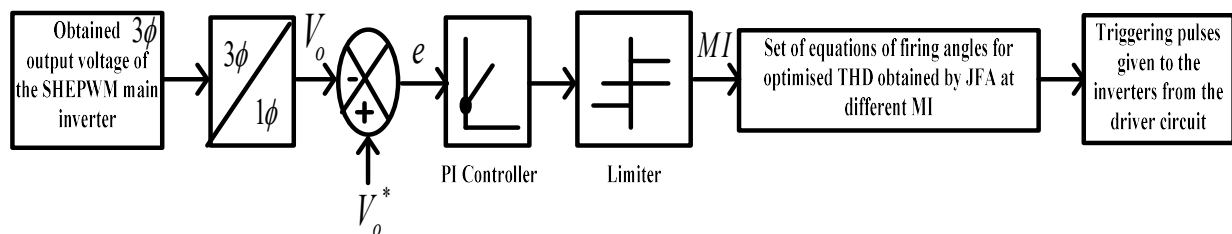


Fig. 2.13 Control unit

2.3.7 RESULTS

2.3.7.1 Simulation results

The model was developed in the MATLAB/Simulink 2016b environment. Fig. 2.14 (a) depicts MPP tracking under partially shaded conditions. The grid voltage is depicted in Fig. 2.14 (b). It was found that the corresponding algorithm has fewer tuning variables and is easier to implement with a tracking time of 0.01sec.

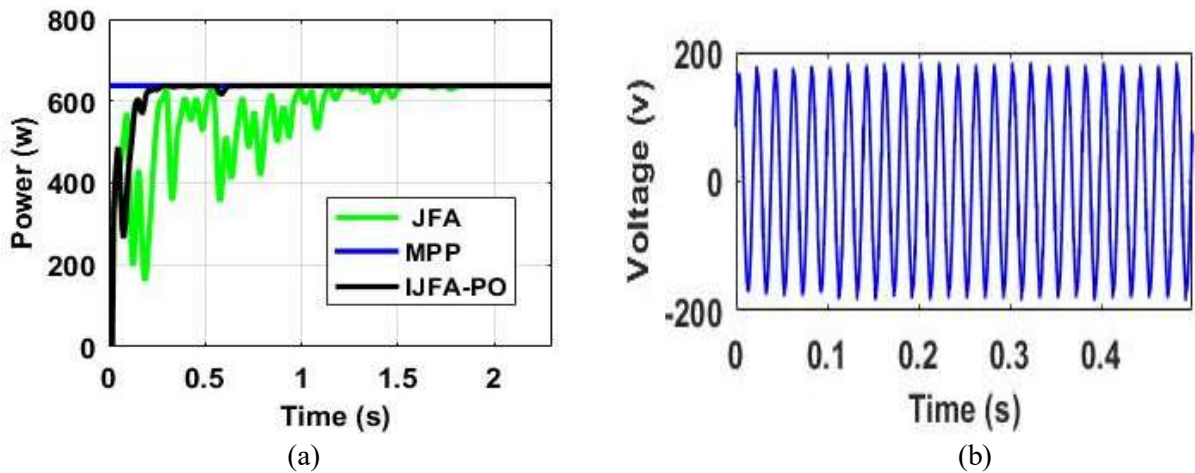
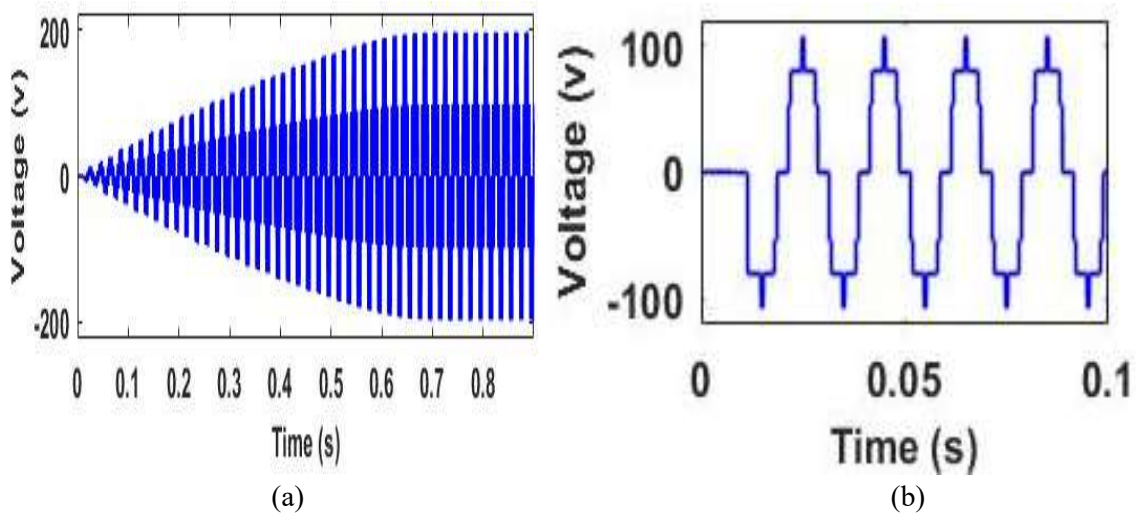


Fig. 2.14 (a) PSC power curve versus time; (b) System voltage at the grid side

Fig. 2.15 shows the output waveform of voltage at the main inverter side using the SPWM, conventional 180°, IJFA implemented in 180°, conventional 120°, IJFA implemented in 120°. Initially, some transients can be observed in Fig 2.15, but with an increase in time, the output voltage becomes much steadier. Three switching angles were generated by the IJFA based SHEPWM technique, used for the main and compensating SHEPWM inverters at a modulation index of 0.85, as indicated in Table 2.3.



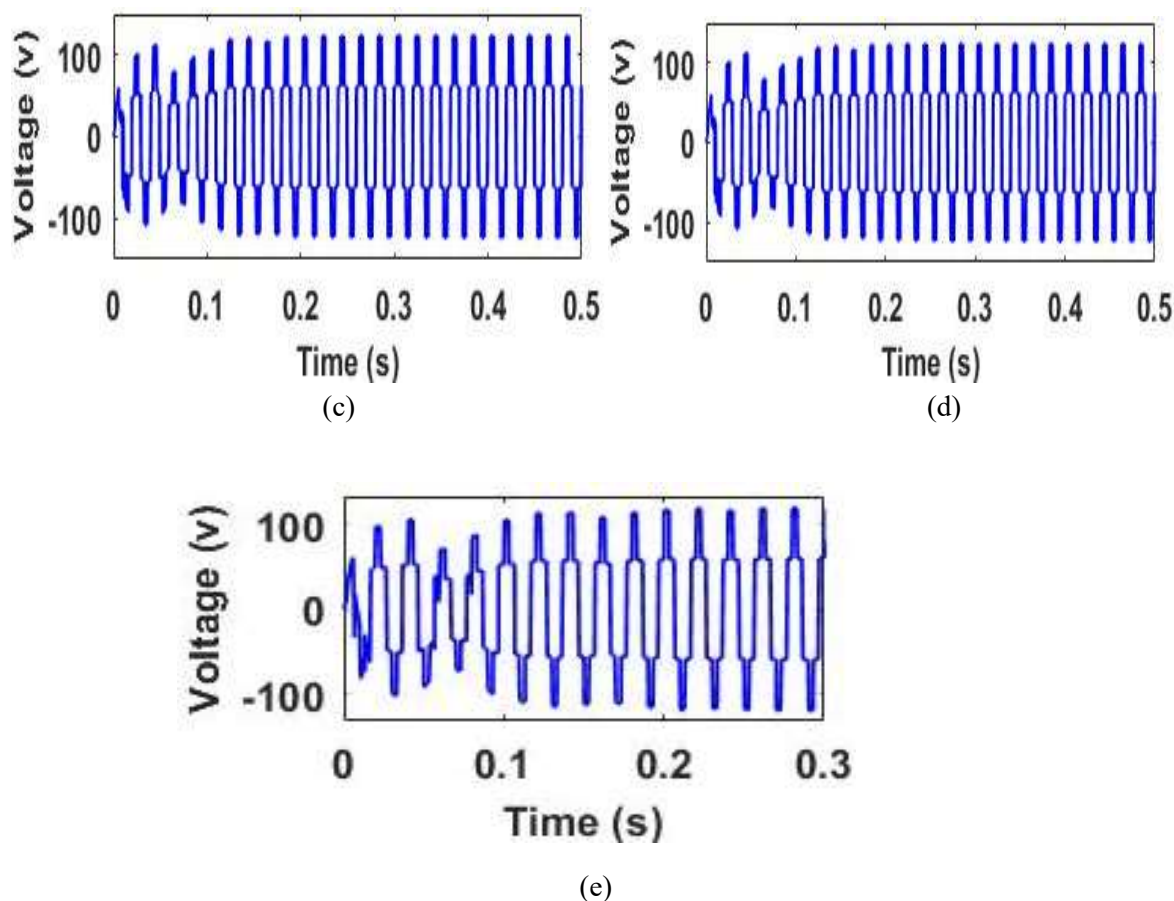


Fig. 2.15 Voltage waveform for unipolar switching at the main inverter side a) SPWM b) 180° conventional c) IJFA implemented in 180° d) 120° conventional e) IJFA implemented in 120°

Table 2.3 Switching angles obtained for different values of firing angles

N	α_1	α_2	α_3	α_4	α_5	α_6	α_7	α_8
3	18.67	23.98						
5	10.45	16.32	22.3	26.56				
7	4.32	8.12	19.67	26.54	30.43	32.85		
9	17.89	25.7	33.62	35.47	39.9	42.2	48.39	52.52

2.3.7.2 Experimental setup

A per phase system test setup was used to verify the modelling results of the proposed method shown in Fig. 2.16. The solar panels used have a 260-watt capacity, a 35.24-volt open circuit voltage, and an 8.57-amp short circuit current rating. PV panels were used to power both the main and auxiliary inverters at the same time under two separate situations. In the test room, incandescent bulbs were used to create an artificial isolation for consistent irradiance. The PSC was created by adjusting the intense light intensity of 1000 W and covering 20% of it with cardboard, as illustrated in Fig. 2.16. For temperature and irradiation sensing, the LM35 and Pyranometer were used respectively. These signals were amplified

using a PIC 18F452 controller in a computer interface environment. To trigger the MOSFET of the boost converter, the pulse is amplified using a voltage optocoupler from the (TLP-250H of 1636 series) driver. To drive both inverters, SHEPWM pulses were created using the IJFA algorithm and stored in the PIC18F452 microcontroller. The results were seen in a Digital Storage Oscilloscope (DSO) using a transformer with a rating of 230/48V, 2A and a load of 1A, 0.8 power factor.

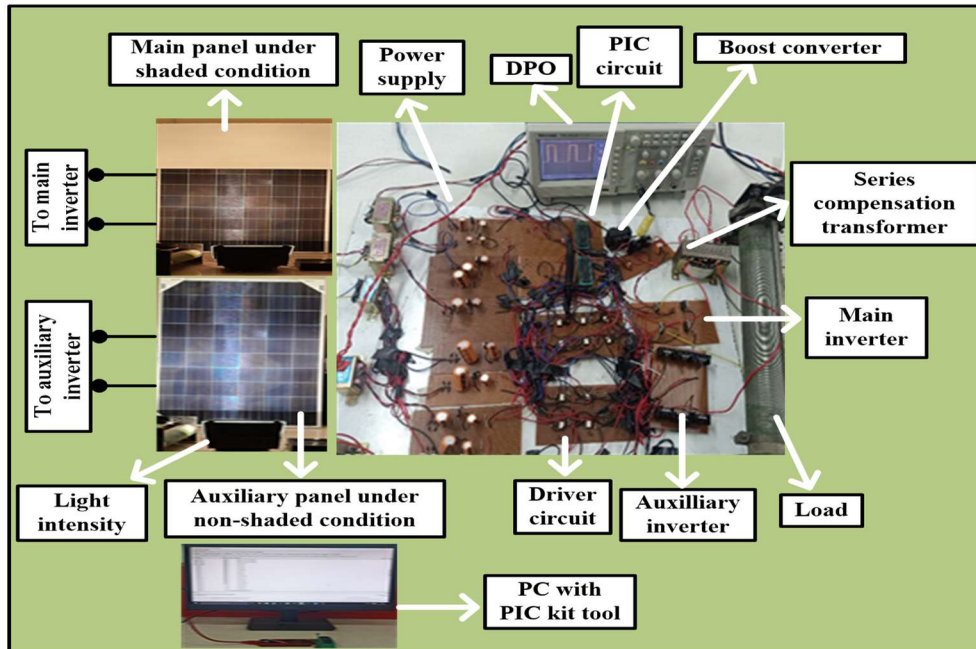


Fig. 2.16 Experimental setup

Figs. 2.17 (a) and (b) show the gate pulses delivered to switches in the main and compensating inverters using IJFA-based 120° conduction. As the results for the IJFA-based 120° are found to be the best, therefore, its firing pulses have been implemented for the hardware setup. Three switching pulses per quarter cycle have been used for the inverter separately.

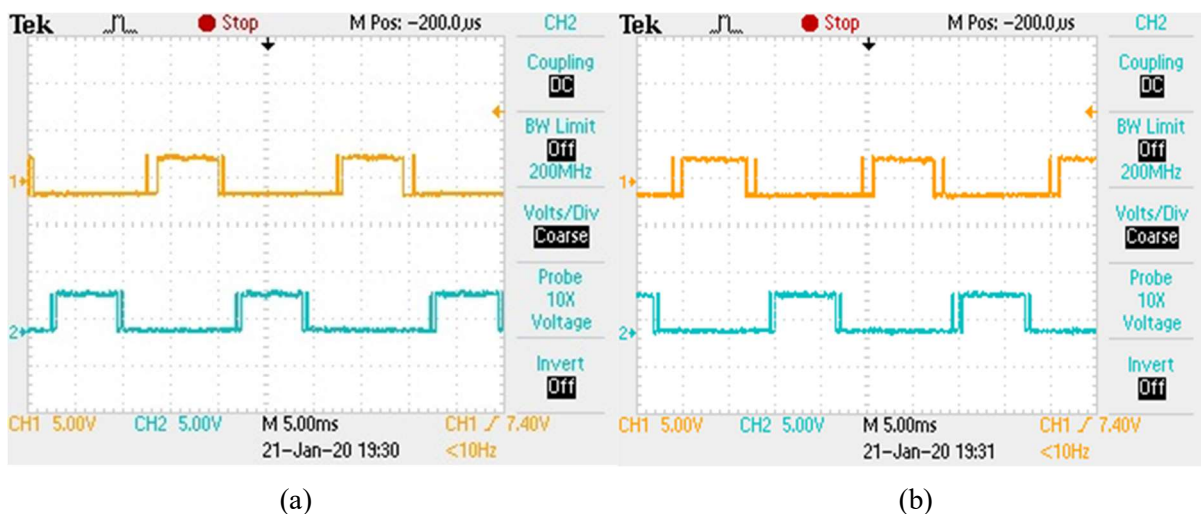
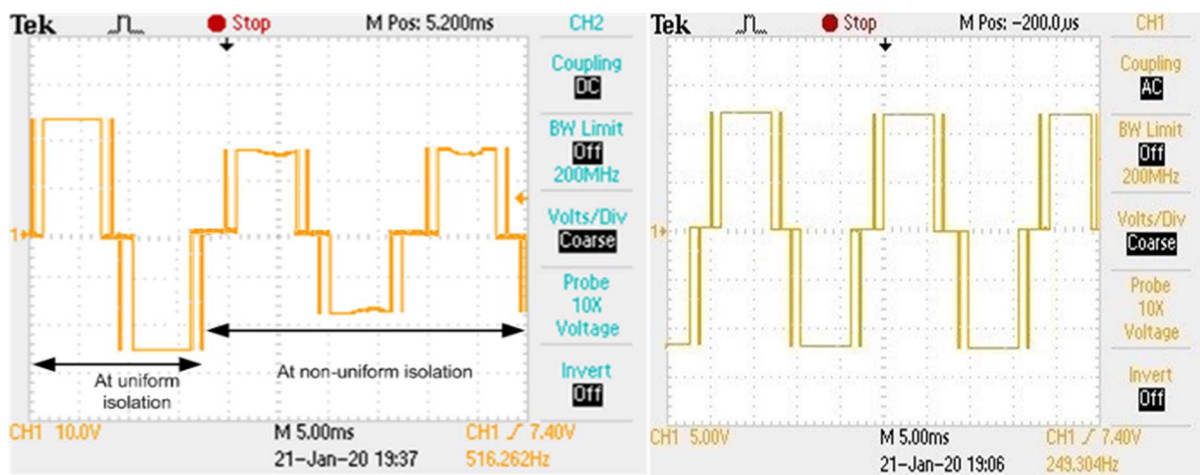


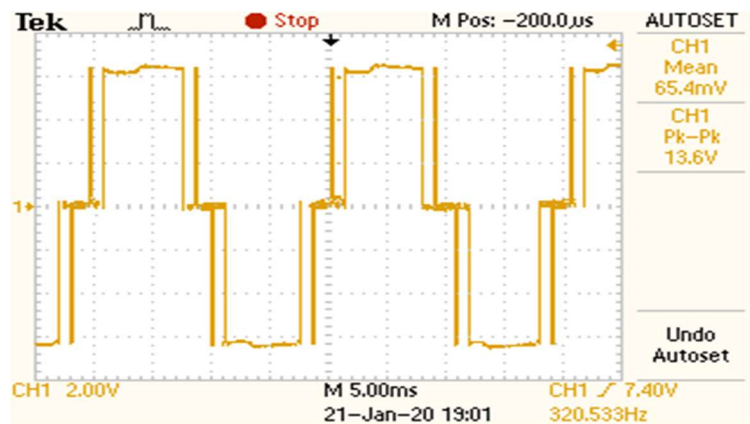
Fig. 2.17 Gate pulses of switches a) SHEPWM-based 120° conduction in the main inverter (scale: CH1: Y-axis: 5V/div.) b) SHEPWM-based 120° conduction in the auxiliary inverter (scale: CH1: Y-axis: 5V/div.)

The output waveforms of the main and auxiliary voltages are shown in Figs. 2.18 (a), (b). In Fig. 2.18 (a), voltage variation can be seen for both uniform and non-uniform isolation. Fig. 2.18 (c) shows the output after series compensation, similar to before PSC. Due to the change in irradiance, voltage variation causes a change in the dc bus which was overcome by an auxiliary inverter. FFT analysis has been shown to manifest a higher number of harmonics present than the latter at an MI of 0.5. Fig. 2.19 (c) shows the FFT analysis at an MI of 0.8. The after-compensation results were improved for MI at 0.8. The amplitude of the targeted harmonics has been lowered by a significant amount. Due to the fact that the experimental setup is in phase, triple-n harmonics are also present. The harmonic order was focused up to the 29th order, as anything beyond that was insignificant due to easier filtration. The IJFA, implemented in 120°, eliminates the maximum order of harmonics. For the three-phase system, the THD attained by simulation results was only 1.32%, as shown in Fig. 2.20 (b) and Table 2.4. The THD for the per phase laboratory experimental prototype was found to be 2.58%, as shown in Fig. 2.19 (c). Fig. 2.19 (d) and (e), respectively shows the output current and MPP tracking under uniform irradiation and PSC for the proposed system. It was observed that the simulated results of Fig. 2.14 (b) corroborates with Fig. 2.19 (d). As a result, it was determined that the simulated and experimental results were completely in accord.



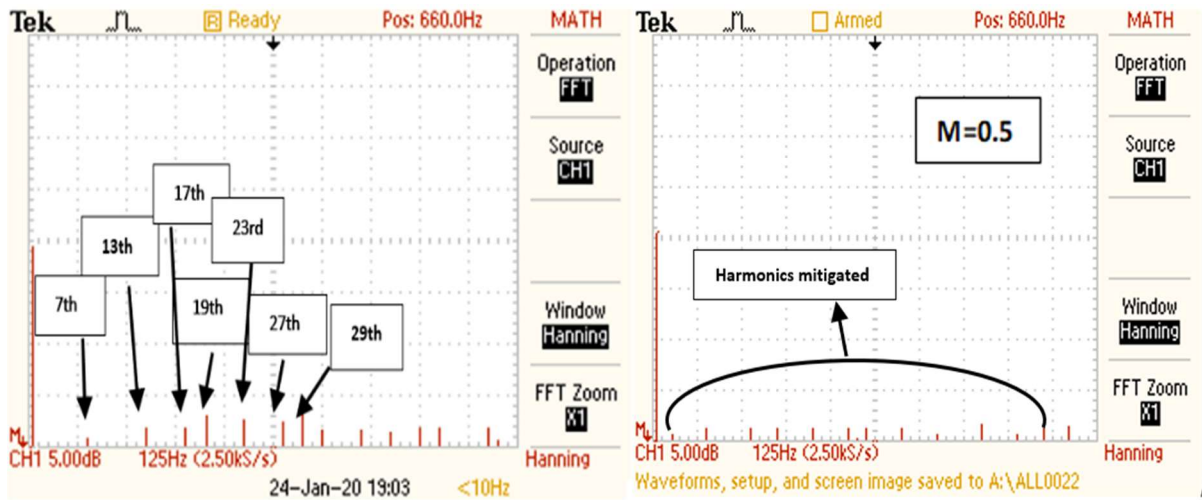
(a)

(b)



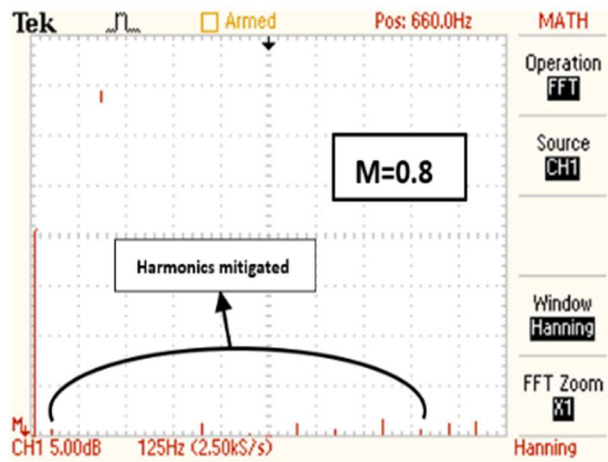
(c)

Fig. 2.18 Output voltage waveform a) SHEPWM based 120° conduction in main inverter (scale: CH1: Y-axis: 60V/div.) b) SHEPWM based 120° conduction in auxiliary inverter (scale: CH1: Y-axis: 12V/div.) c) at the grid side after series compensation (scale: CH1: Y-axis: 120V/div.)

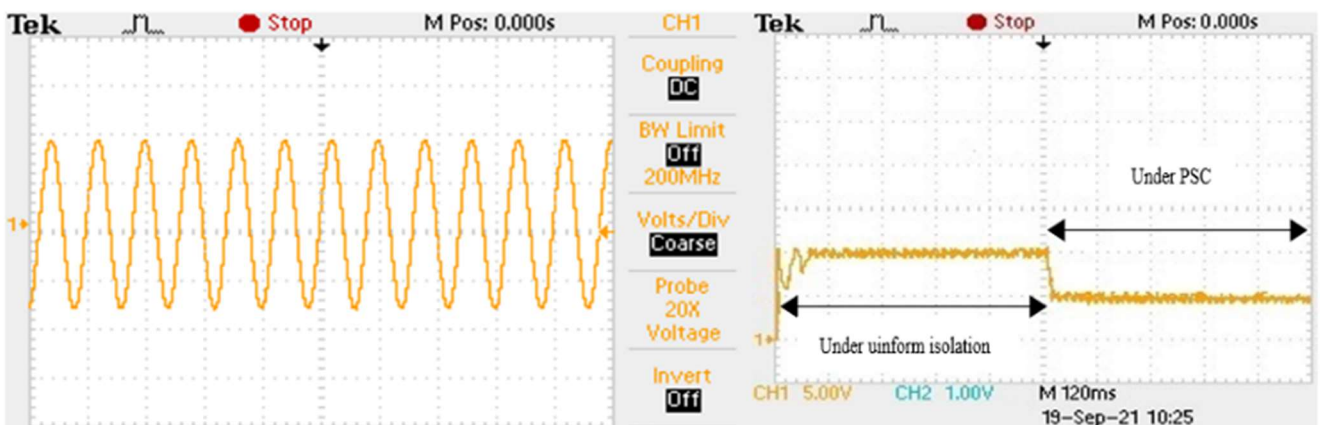


(a)

(b)



(c)



(d)

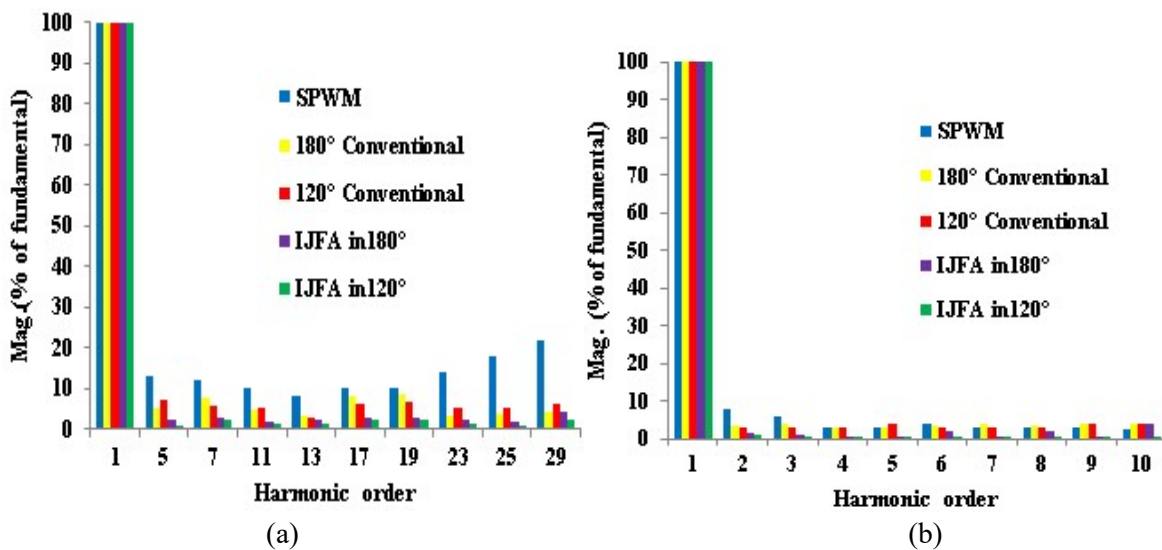
(e)

Fig. 2.19 Voltage harmonics spectra up to the 29th harmonic order a) before series compensation (scale: CH1: Y-axis: 60V/div; X-axis: 250Hz/div) b) after series compensation (scale: CH1: Y-axis: 120V/div; X-axis: 250Hz/div) at MI=0.5 c) at MI=0.8, after series compensation (scale: CH1: Y-axis: 120V/div; X-axis: 250Hz/div)

d) The output current waveform (scale: CH1: Y-axis: 1A /div.; X-axis: 250 ms/div), e) MPP tracking (scale: CH1: Y-axis: 212W /div.; X-axis: 50 ms/div)

2.3.7.3 Comparison with the existing and the proposed scheme

Fig. 2.20 (a) shows the FFT analysis for each output voltage before compensation. Fig. 2.20 (b) shows the FFT analysis after compensation. It was found that the IJFA, implemented in 120° conduction, has given superior results. The values are obtained by using (2.22) in opposition to cancelling out the existing dominant harmonics. Three switching angles were generated by the IJFA based SHEPWM technique, used for the main and compensating SHEPWM inverters at a modulation index of 0.85, as indicated in Table 2.3. The comparison of various bio-inspired algorithms has been done in Fig. 2.20 (c), in which IJFA has given better results for the given plot. The behavior of triggering pulses over MI has been given in Fig. 2.20 (d). The optimized pulses give better results than the conventional ones. The comparison of various bio-inspired algorithms has been done in Fig. 2.20 (c), in which IJFA has given better results for the given plot. The behavior of triggering pulses over MI has been given in Figure 2.20 (d). The optimized pulses give better results than the conventional ones. The convergence time for IJFA is 0.10 sec respectively, as shown in Fig. 2.20 (e), for 50 iterations with a population size of 100 at 0.85 MI. Run time versus population size has been studied in Fig. 2.20 (f). It was found that IJFA outperforms with existing GWO, WOA, and JAYA in terms of obtaining optimized THD and its corresponding angles. It has faster, easier implementation and more accurate convergence with a smaller number of tuning parameters. It attains convergence much more accurately and at a faster rate than others. On an Intel® Core™ i5, 2.30 GHz processor with 4.00 GB of installed memory, all stages of programming are coded in MATLAB. Thus, IJFA has superior performance over others in giving optimized THD and its corresponding angles.



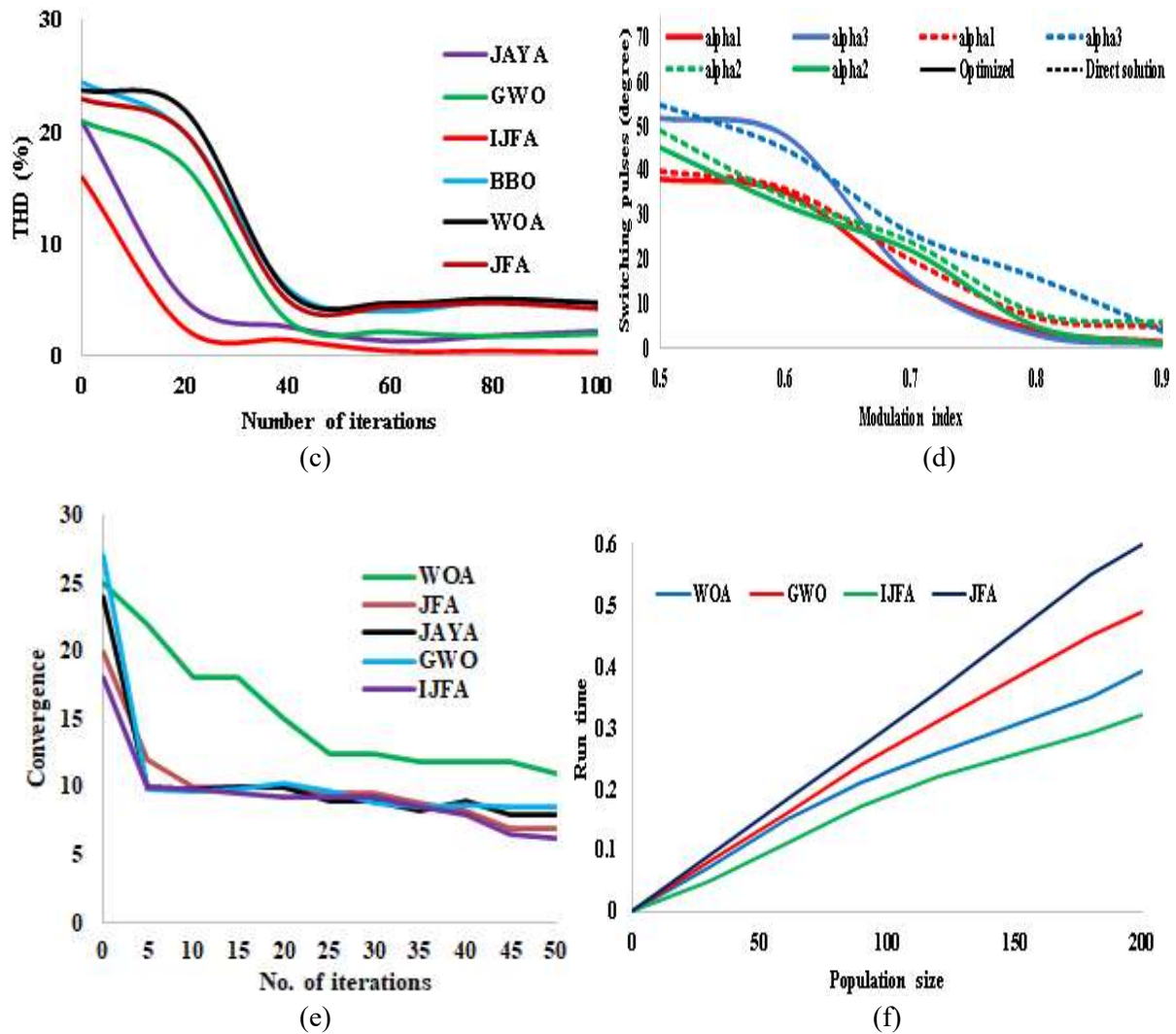


Fig. 2.20 Analysis of system output a) FFT analysis of the main SHEPWM inverter b) FFT analysis at the grid side c) voltage THD variation over iterations for various metaheuristic techniques d) Switching angle behaviour vs. MI for conventional and optimised pulses (e) Convergence vs. number of iterations plot (f) Run time vs. population size plot

The previously mentioned metaheuristic techniques [2.19]– [2.26] for PSC tracking has certain limitations mentioned. To address those problem, a hybrid IJFA-PO method was proposed, which combines the benefits of both traditional and innovative methods. It outperformed others in terms of faster and more accurate convergence with a smaller number of tuning parameters. It converges to much lower values compared to other algorithms. Table 2.4 shows the results of a comparative analysis of various MPPT approaches.

Table 2.4 Comparison of the proposed MPPT techniques with the existing MPPT techniques

MPPT	Complexity	Tracking under PSC	Dynamic performance	Tracking Speed	Accuracy
Modified traditional methods [2-3]	Easy	No	Poor	Low	Less

Hybrid MPPT techniques ^[4-11]	Easy	Yes	Moderate	Moderate	Moderate
Integration of metaheuristic with traditional (IJFA-PO)	Moderate	Yes	Excellent	High	High

The behavior of three switching angles per quarter cycle was equal to that of nine switching angles, as shown in Fig. 2.21. Three switching angles are the ideal option for the proposed model. It eliminates the greatest number of harmonics possible, resulting in a THD of only 1.32%. When MI is low, higher-order harmonics have more amplitude than lower-order harmonics and vice versa happens for higher values of MI.

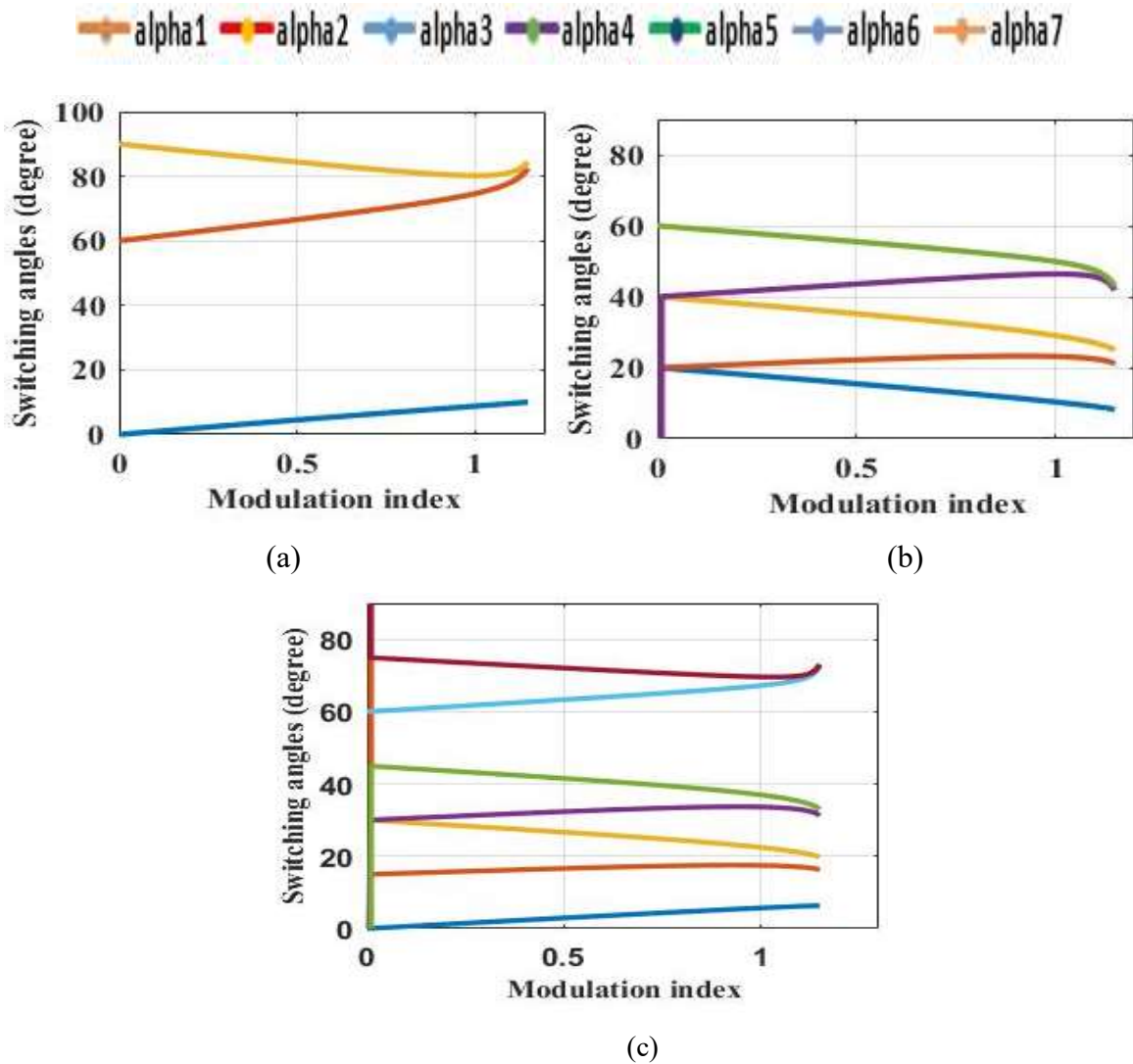


Fig. 2.21 Behavior of switching angles vs. modulation index a) for three switching angles b) for five switching angles c) for seven switching angles

A comparative analysis based on précised tracking in the lowest time, computational complexity, robustness, stability, cheaper real-time implementation without any processing units, etc. was carried out. Table 2.5 shows the results of a comparative analysis of several optimization approaches.

Table 2.5 Comparison of different evolutionary techniques

PSO [21]		WOA [6]		GWO [21]		BBO [13]		JFA [11]		IJFA	
Weight (w)	0.4	Population size	10*5	Population matrix	10*5	Population size	50	Population size	100	Population size	100
Balance factors c_1, c_2, c_3, c_4	1.3, 0.6, 1.9, 1.7					Genes in each population	5				
Random variable: r_1, r_2	0.6, 0.5	Random variable r_1, r_2	0.7, 0.6	Random variable r_1, r_2	0.7, 0.6	Elitism value	2	Random variable r_1, r_2, r_3, r_4	0.5, 0.9, 0.1, 0.4	Random variable r_1, r_2, r_3	0.8, 0.6, 0.3
No. of equations	Low	No. of equations	Low	No. of equations	Low	No. of equations	High	No. of equations	Medium	No. of equations	Medium
Complexity	Easy	Complexity	Easy	Complexity	Easy	Complexity	Moderate	Complexity	Moderate	Complexity	Moderate
Elapse time (s)	0.43	Elapse time (s)	0.22	Elapse time (s)	0.26	Elapse time (s)	0.34	Elapse Time (s)	0.26	Elapse time (s)	0.19
THD (%)	2.5	THD (%)	2.98	THD (%)	3.5	THD (%)	3.8	THD (%)	2.48	THD (%)	1.32

Figs. 2.21 (a) and (b) show the behavior of three switching angles to the modulation index every quarter cycle for an evolutionary algorithm. The switching angles are inversely proportional to the modulation index, and there has been a moderate movement to the origin, as shown in the graph. These angles satisfy the criteria in (2.34) while also controlling the fundamental component and suppressing harmonics in the output voltage. Both inverters function well in the 0.8-0.87 modulation index region, which explains the choice of three switching angles over others. The comparative plot in Fig. 2.21 (c) depicts the change in THD for different switching strategies at different modulation indices. The amplitudes of voltage harmonics were compared to the standards indicated in Table 2.6. This chapter undergoes comparative analysis of several switching techniques to get a better picture.

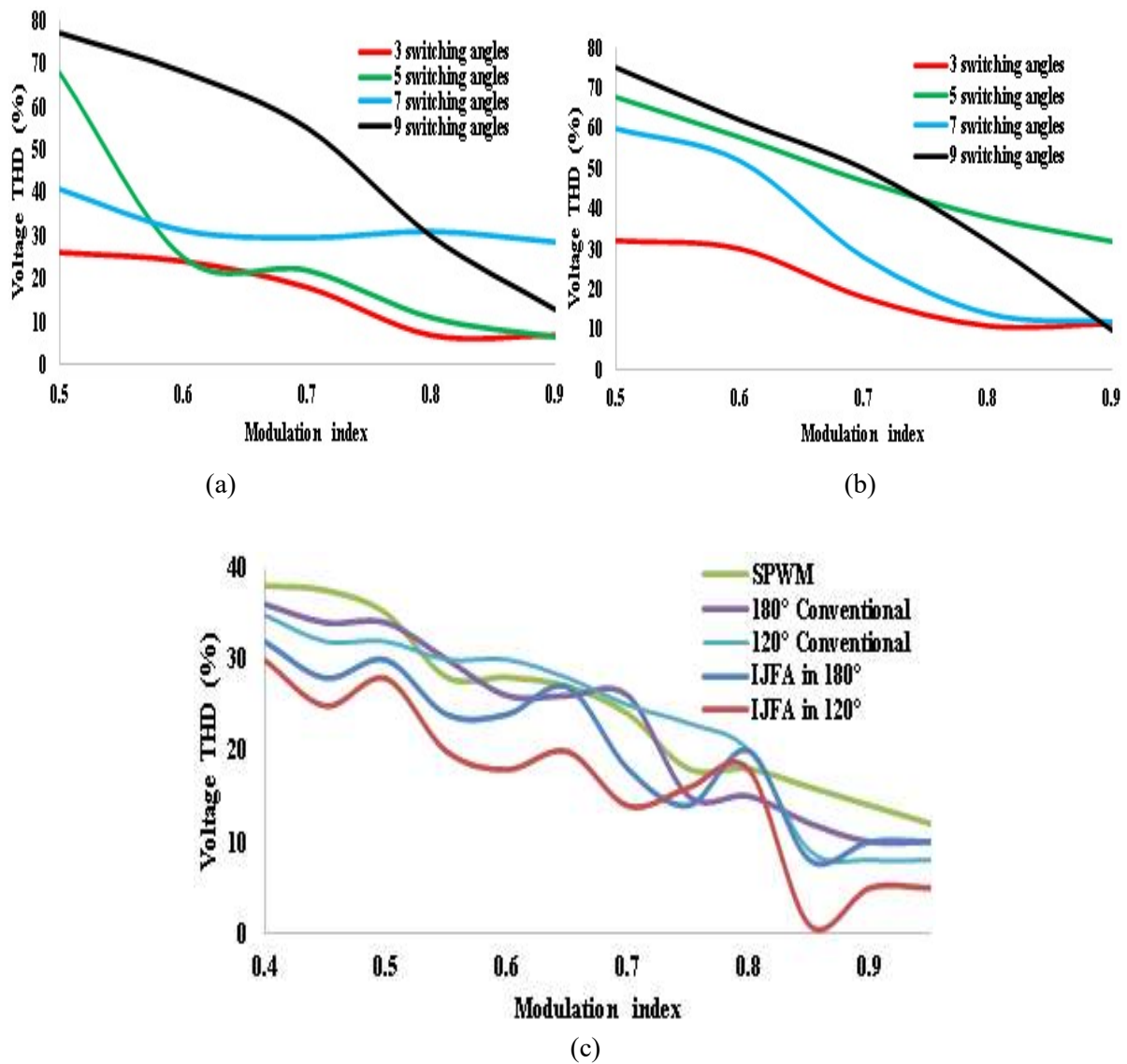


Fig. 2.21 Voltage output analysis for the variation of THD vs. MI a) IJFA implemented in 180° b) IJFA implemented in 120° c) characteristics of different metaheuristic techniques

Table 2.6 Comparison of voltage harmonic amplitudes of standards with the proposed techniques

Voltage harmonics amplitude on grid synchronization	b_5	b_7	b_{11}	b_{13}	b_{17}	b_{19}	b_{23}	b_{25}	b_{29}	THD (%)
IEC [2,23]	5	4	3	2.5	1.6	1.2	1.2	1.2	1.06	6.5
CIGRE WG 36-05 [2,25]	6	5	3.5	3	2	1.5	1.5	1.5	--	8
IEEE-1547 and 2030 [2,22], [2,24]	-----									5
	Proposed Technique used									
Voltage harmonics amplitude after series compensation (%)	b_5	b_7	b_{11}	b_{13}	b_{17}	b_{19}	b_{23}	b_{25}	b_{29}	THD (%)
Values for SPWM switching mode	2.4	3.6	2.3	1.9	2.2	4	2	1.8	3.2	6.1
Values for 180° conventional	2.7	3.27	0.17	3.35	0.5	0.9	4.17	0.08	2.05	5.1

Values for 120° conventional	1.12	2.5	1.25	1.1	0.22	1.8	1.8	1.12	2.08	4.3
Values for JFA in 180°	2.5	2.2	0.15	1.7	0.32	0.31	1.5	0.47	1.9	3.2
Values for JFA in 120°	1.5	1.29	2.3	0.8	0.32	0.78	0.89	0.70	0.77	2.5
Values for IJFA in 180°	1.56	1.2	0.45	0.7	0.8	0.43	1.3	0.11	1.9	2.5
Values for IJFA in 120°	0.49	0.27	0.17	0.15	0.5	0.9	0.57	0.28	0.55	1.32

Table 2.7 shows the results of a comparison of existing and proposed designs. It was inferred that the present proposed scheme works better due to the inclusion of novel series compensation, appropriate for industrial and domestic applications.

Table 2.7 Comparative analysis of existing and proposed schemes

Parameters	Ref [12]	Ref [14]	Ref [15]	Ref [16]	Ref [17]	Ref [18]	Ref [19]	Proposed
Technique used	UPQC	RBFNN-PI	FPGA	MNR with pattern recognition	Homotopy algorithm	ABC	Filter compensation module	IJFA
Voltage THD (%)	3.71	2.72	16.54	7.25	33.94	3.1	5.1	1.32

2.3.8 CONCLUSION

With the use of series compensation under PSC, it was possible to eliminate harmonics while also improving the voltage profile for the PV integrated grid system. During wider voltage variations, the compensating inverter fulfils the voltage demand on the grid side. The overall THD of the output voltage was reduced to 1.32%, which is well within the specifications of IEEE 1547, IEC, and CIGRE WG 36-05. In comparison to existing approaches with changing loads, the IJFA based SHE using proposed series compensation gives improved results. The experimental results of the prototype have also been presented in support of the simulated outputs. The three switching angles performance was equivalent to nine switching angles per quarter cycle in reducing harmonics, resulting in lower losses and improved system efficiency. A piecewise mixed-model approach has been used to store angles offline in the micro-controller for the online applications. It can be concluded that the current proposed system produces superior results when compared to other existing algorithms and meets all of the scheme's objectives. The same topology can be applied to large power plants for effective control of output voltage as well as output harmonics. This research can be extended to faulty conditions on the main unit side also. Then, in this case, the auxiliary unit undergoing series compensation would maintain an uninterrupted power supply,

maintain the output voltage, and control the harmonics with the specified values. This PV-wind hybrid generation scheme can be operated in standalone mode in remote areas where the grid supply to the consumers is not available. The proposed schemes improve the power quality obtained from the units installed and, thus, can have a very positive impact on improving the quality of life in the remote grid-secluded regions.

Publication

- ❖ Suman, S., Chatterjee, D., & Mohanty, R. A novel approach for mitigating power quality issues in a PV integrated microgrid system using an improved jelly fish algorithm. *Journal of Bionic Engg.*, DOI: 10.1007/s42235-022-00252-7. [SCIE, Q2, Impact factor: 2.68]

References

- [2.16] Choudhary, P., & Srivastava, R. K. (2019). Sustainability perspectives-a review for solar photovoltaic trends and growth opportunities. *Journal of Cleaner Production*, 227, 589-612.
- [2.17] Alsumiri, M. (2019). Residual incremental conductance based nonparametric MPPT control for solar photovoltaic energy conversion system. *IEEE Access*, 7, 87901-87906.
- [2.18] Sarvi, M., & Azadian, A. (2021). A comprehensive review and classified comparison of MPPT algorithms in pv systems. *Energy Systems*, 1-40, 281–320, DOI: <https://doi.org/10.1007/s12667-021-00427-x>.
- [2.19] Mirza, A. F., Mansoor, M., Zhan, K., & Ling, Q. (2021). High-efficiency swarm intelligent maximum power point tracking control techniques for varying temperature and irradiance. *Energy*, 228, 120602.
- [2.20] Hassan, A. Y., Ismaeel, A. A., Said, M., Ghoniem, R. M., Deb, S., & Elsayed, A. G. (2022). Evaluation of Weighted Mean of Vectors Algorithm for Identification of Solar Cell Parameters. *Processes*, 10(6), 1072.
- [2.21] Chakraborty, S., Saha, A. K., Chakraborty, R., & Saha, M. (2021). An enhanced whale optimization algorithm for large scale optimization problems. *Knowledge-Based Systems*, 233, 107543.
- [2.22] Eltamaly, A. M., & Farh, H. M. (2019). Dynamic global maximum power point tracking of the PV systems under variant partial shading using hybrid GWO-FLC. *Solar Energy*, 177, 306-316.
- [2.23] Tu, J., Chen, H., Wang, M., & Gandomi, A. H. (2021). The colony predation algorithm. *Journal of Bionic Engineering*, 18(3), 674-710.

- [2.24] Zhang, Y., Ma, M., & Jin, Z. (2020). Comprehensive learning Jaya algorithm for parameter extraction of photovoltaic models. *Energy*, 211, 118644.
- [2.25] Abdel-Basset, M., Mohamed, R., Chakraborty, R. K., Ryan, M. J., & El-Fergany, A. (2021). An improved artificial jellyfish search optimizer for parameter identification of photovoltaic models. *Energies*, 14(7), 1867.
- [2.26] Chou, J. S., & Truong, D. N. (2021). A novel metaheuristic optimizer inspired by behavior of jellyfish in ocean. *Applied Mathematics and Computation*, 389, 125535.
- [2.27] Santhoshi, B. K., Mohanasundaram, K., Kaliappan, V. K., & Sathyamurthy, R. (2022). Sinusoidal pulse width modulation for a photovoltaic-based single-stage inverter. *Environmental Science and Pollution Research*, 29, 29830–29840, DOI: <https://doi.org/10.1007/s11356-021-18422-1>.
- [2.28] Sarker, K., Chatterjee, D., & Goswami, S. K. (2018). Modified harmonic minimisation technique for doubly fed induction generators with solar-wind hybrid system using biogeography-based optimisation. *IET Power Electronics*, 11(10), 1640-1651.
- [2.29] Sujatha, B. G., & Anitha, G. S. (2018). Enhancement of PQ in grid connected PV system using hybrid technique. *Ain Shams Engineering Journal*, 9(4), 869-881.
- [2.30] Peraza-Vázquez, H., Peña-Delgado, A., Ranjan, P., Barde, C., Choubey, A., & Morales-Cepeda, A. B. (2021). A bio-inspired method for mathematical optimization inspired by arachnida salticidade. *Mathematics*, 10(1), 102.
- [2.31] Al-Hitmi, M., Ahmad, S., Iqbal, A., Padmanaban, S., & Ashraf, I. (2018). Selective harmonic elimination in a wide modulation range using modified Newton–Raphson and pattern generation methods for a multilevel inverter. *Energies*, 11(2), 458.
- [2.32] Ning, L., Tong, G., Hui, Z., & Ping, Y. (2019). Comparative research of harmonic suppression algorithm of the three-level NPC converter. *The Journal of Engineering*, (16), 1271-1274.
- [2.33] Ramesh, A., & Sait, H. H. (2020). An approach towards selective harmonic elimination switching pattern of cascade switched capacitor twenty nine-level inverter using artificial bee colony algorithm. *Microprocessors and Microsystems*, 79, 103292.
- [2.34] Nalcaci, G., Yildirim, D., & Ermis, M. Selective harmonic elimination for light-rail transportation motor drives using Harris hawk’s algorithm. In *2020 IEEE International Conference on Environment and Electrical Engineering and 2020 IEEE Industrial and Commercial Power Systems*

Europe (EEEIC/I&CPS Europe), Madrid, Spain, 2020, 1-6, DOI: 10.1109/EEEIC/ICPSEurope49358.2020.9160694.

[2.35] Memon, M. A., Mekhilef, S., Mubin, M., & Aamir, M. (2018). Selective harmonic elimination in inverters using bio-inspired intelligent algorithms for renewable energy conversion applications: A review. *Renewable and Sustainable Energy Reviews*, 82, 2235-2253.

[2.36] Cleveland, F. M. IEC 61850-7-420 communications standard for distributed energy resources (DER). In *2008 IEEE Power and Energy Society General Meeting-Conversion and Delivery of Electrical Energy in the 21st Century*, Pittsburgh, Pennsylvania, USA, 2008, 1-4.

[2.37] Blooming, T. M., & Carnovale, D. J. Application of IEEE Std 519-1992 harmonic limits. In *Conference Record of 2006 Annual Pulp and Paper Industry Technical Conference*, Appleton, Wisconsin, USA, 2006, 1-9, DOI: 10.1109/PAPCON.2006.1673767.

[2.38] Basso, T. *IEEE 1547 and 2030 standards for distributed energy resources interconnection and interoperability with the electricity grid* (No. NREL/TP-5D00-63157), National Renewable Energy Lab. (NREL), Golden, CO (United States), 2014, DOI: <https://doi.org/10.2172/1166677>.

[2.39] Beaulieu, G., Bollen, M. H., Malgarotti, S., & Ball, R. Power quality indices and objectives. Ongoing activities in CIGRE WG 36-07. In *IEEE Power Engineering Society Summer Meeting*, National Renewable Energy Lab. (NREL), Golden, CO (United States), 2002, 2, 789-794.

[2.40] Chatterjee, D. (2011). A novel magnetizing-curve identification and computer storage technique for induction machines suitable for online application. *IEEE Transactions on Industrial Electronics*, 58(12), 5336-5343.

MITIGATING POWER QUALITY ISSUES FOR THE PV-WIND HYBRID SYSTEM**3.1 INTRODUCTION**

In recent years, renewable sources of electricity have been gaining increased importance. The clean and green features are what are making these resources popular. Solar and wind power have additional advantages in that they are both readily available and free [3.1].

The choice of a proper converter is necessarily important for feeding the power grid. Multilevel converters can efficiently convert DC to AC [3.2]. There are many PWM techniques adopted, such as Sinusoidal Pulse Width Modulation (SPWM), Space Vector PWM (SVPWM), and SHEPWM for the same. It has been reported that the Total Harmonic Distortion (THD) of SPWM, was approximately 40%, which is considered significant in terms of maintaining power quality. Power quality was maintained by using a static VAR compensator [3.3]. To improve power quality detailed discussion have been carried out in the present chapter.

3.2 POWER QUALITY IMPROVEMENT FOR THE MICROGRID CONNECTED PV-WIND HYBRID GENERATION SCHEME WITHOUT SERIES COMPENSATION**3.2.1 Existing Schemes**

Several articles discuss the attractive features of the SHEPWM inverter. It has decreased switching and conversion losses, better electromagnetic interference (EMI), etc. Therefore, SHEPWM is considered a good option in terms of higher power applications and has also been used in the present chapter. It eliminates "d-1" of lower order harmonics with "d" of triggering angles [3.4]. To achieve this, the solving of non-linear equations was difficult using the Gauss-Newton Raphson method [3.5]. To solve a higher degree polynomial equation, this method would increase the computation time and complexity and decrease the convergence speed.

There are many optimization techniques adopted to solve the problems. These evolutionary techniques are appropriately suited depending upon the problem statement. A detailed discussion of the wind-penetrated microgrid system has been discussed [3.6]. DFIG operations at sub and super synchronous speeds and their control have been discussed in detail [3.7]- [3.9]. A control technique using a piecewise-mixed model for storing angles offline has been described [3.19].

BBO based SHEPWM technique, [3.10] in a DFIG connected microgrid system. A comparison with several other search-based algorithms such as Particle Swarm Optimization (PSO), Cuckoo Search Algorithm (CSA), etc., has been performed in which BBO performed better. In [3.11], the Grey Wolf Optimization (GWO) technique is used in the hybrid system to solve the real and reactive power problems.

A modified grey wolf optimization technique has been used in the hybrid cascaded multilevel inverter for harmonic reduction [3.12]. MPP was tracked using the bacterial foraging method [3.13]. WOA has been thoroughly discussed in [3.14], [3.15] for a variety of engineering field applications. A comparative analysis of different optimization algorithms has been executed in standalone systems [3.16]. Later, [3.17] introduced a modified whale optimization technique for solar parameter identification. [3.18] has used an adaptive genetic algorithm technique to track the MPPT in a PV system.

3.2.2 PROPOSED TOPOLOGY

3.2.2.1 Its features in detail

The proposed model is illustrated in Fig. 3.1. Generally, the microgrid is powered by a distributed storage system or generators. Contrary to that, a hybrid source of PV and wind has been introduced here. The stator is coupled with the microgrid at a frequency of 50 Hz. The direction of the wind tends to rotate the wind turbine. The turbine is accountable for the pitch angle control, which adjusts the speed for the blade's protection. The induction generator is directly coupled to the gearbox.

As shown in Fig. 3.1, there are two types of converters used in the process: rotor-side converters (RSC) and grid-side converters (GSC). RSC is directly connected to the IG rotor, whereas GSC, as the name says, is connected to the grid. When the wind speed is high, the DFIG will operate in a super-synchronous mode, and when the wind speed is low, it will operate in a sub-synchronous mode. In the latter part, active power is given to the rotor from the DC bus and vice-versa. At the time of sub-synchronous mode, PV with a DC-DC boost converter supports and helps to maintain the voltage dip. The MPPT controller helps track the maximum power. Perturb and Observe (P & O) has been used in this regard. Conventional control strategies, converters, and non-linear loads all produce harmonics, thus leading to major power quality issues. This leads to an extensive need for harmonic compensation. The back-to-back converters use an optimized SHEPWM technique that helps to deal with the harmonics. It works at a low frequency to avoid switching losses, thus making the system more competent. The SHEPWM technique uses the Modified Whale Optimization application (MWOA) technique.

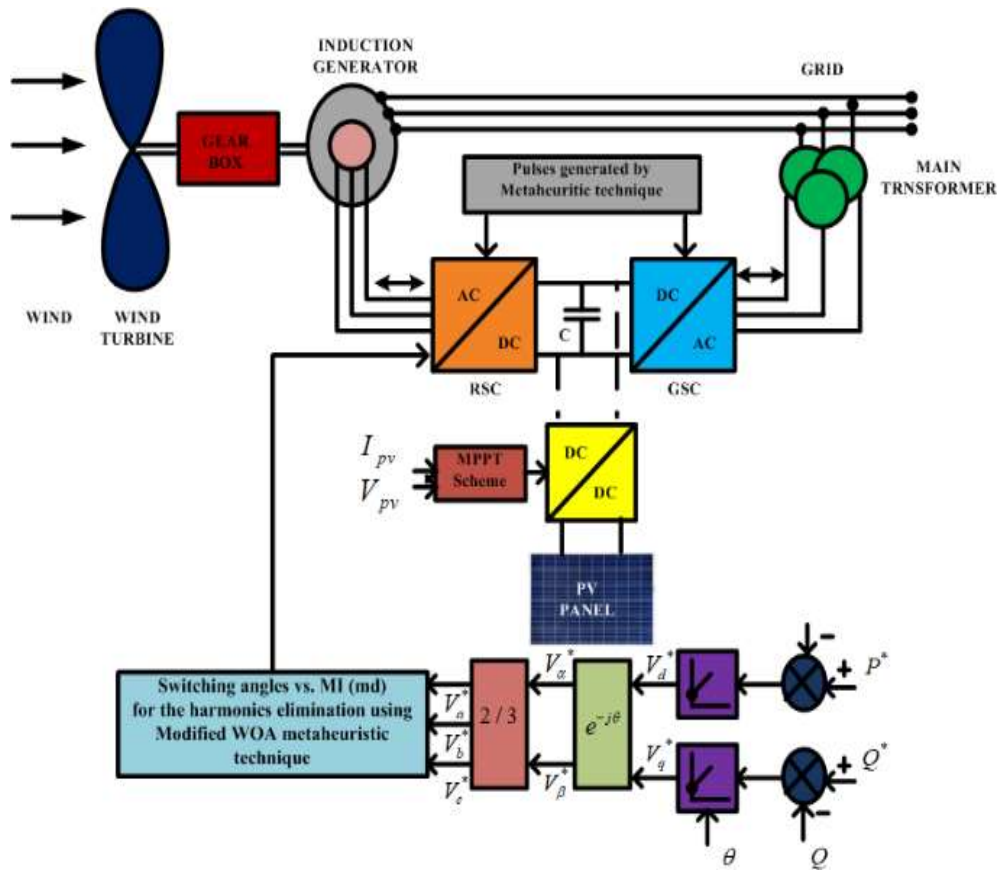


Fig. 3.1 Proposed model

The angles found are given to the lookup table for offline usage. The five switching angles produce equivalently good results as seven switches, but with fewer switching losses, thus improving the system efficiency. A comparison with other search-based techniques was carried out, but MWOA solves the purpose more efficiently and gives a satisfactory result.

A modified whale optimization technique has been used in the present technique as its usage for harmonic reduction is not noted much in the literature for hybrid systems. The MWOA is superior when compared to PSO, GWO, and BBO. The use of objective functions in the MWOA easily reduces both higher and lower order harmonics, which was a limitation in the simple SHEPWM technique. The adopted modified WOA-based optimized SHEPWM control technique has easier implementation and faster convergence in the hybrid microgrid connected system, which marks the novelty of the chapter. Standard reports have been used for comparison [3.20], [3.21] in the present chapter. The hardware results are also included to justify their applications in the practical scenario.

3.2.3 SHEPWM APPLICATION IN CONVERTERS FOR HARMONIC ANALYSIS

This has been detailed in section 2.4.3.

3.2.4 APPLICATION OF METAHEURISTIC TECHNIQUE IN SHEPWM BASED INVERTER

3.2.4.1 Whale Optimization Algorithm (WOA)

WOA is a swarm-based optimizing technique that is motivated by how the whale hunts. Its implementation is easier and it has superior performance over many other complex evolutionary techniques. It has only one controlling parameter, i.e., the time, which is to be tuned finely. Humpback whales search for their food in a multidimensional search space. The algorithm is very similar to grey wolf optimization (GWO). The location of these whales is considered a decision, whereas the distance between the whales and the food can be denoted as an objective function.

3.2.4.1.1 Steps for WOA for food hunt

➤ Encircling the prey

The whales forage for and surround their prey. Initially, the optimal design is unknown, so the current best solution is considered the target prey or close to the optimum solution. Meanwhile, the search for the supreme search agent continues so that the other search agents update their positions near to it. It can be expressed by equations:

$$\vec{D} = \left| \vec{C} \cdot \vec{X}^*(t) - \vec{X}(t) \right| \quad (3.1)$$

$$\vec{X}(t+1) = \vec{X}^*(t) - \vec{A} \cdot \vec{D} \quad (3.2)$$

$$\vec{A} = 2\vec{a} \cdot \vec{r}_1 - \vec{a} \quad (3.3)$$

$$\vec{C} = 2\vec{r}_2 \quad (3.4)$$

Where, \vec{A} and \vec{C} coefficient vectors, t refers to the present iteration, \vec{X}^* is the position of the prey, and \vec{X} is the position of the whale. ‘.’ is the element-by-element multiplication and $\|$ is the absolute value, \vec{a} decreases from 2 to 0 in each iteration, \vec{r}_1 and \vec{r}_2 are taken as random vectors in $[0, 1]$.

➤ Bubble-Net attacking Method (Exploitation phase)

It is bifurcated into two steps:

➤ Shrinkage of the encircling mechanism

This is accomplished by lowering the value of \vec{a} . The updated current position was achieved by the previous position and obtained the best position.

➤ Spiral updating position

When whales approach their prey, they produce bubbles in a spiral pattern. They do this to compute the distance between them and the prey, which forms a spiral shape which is denoted as \bar{D}' .

$$\bar{X}(t+1) = \bar{D}' \cdot e^{bl} \cdot \cos(2\Pi l) + \bar{X}^*(t) \quad (3.5)$$

$$\bar{X}(t+1) = \bar{X}^*(t) - \bar{A} \cdot \bar{D} \quad \text{if } p < 0.5 \quad (3.6)$$

$$\bar{X}(t+1) = \bar{D}' \cdot e^{bl} \cdot \cos(2\Pi l) + \bar{X}^*(t) \quad \text{if } p \geq 0.5 \quad (3.7)$$

Where, l is the arbitrary value between $[-1,1]$, b is the fix coefficient of the spiral shape, and p is the probability parameter.

➤ Searching for prey (Exploration phase)

\bar{A} is considered responsible for the exploration of the search for the prey and \bar{X}_{rand} is the current spot of the whale arbitrarily taken from the whale population. If $|\bar{A}| \leq 1$ the whales will approach the prey (exploitation) and if $|\bar{A}| > 1$ the whales will not update their position based on the best solution but will choose a random whale as the best position (exploitation). It is given in the equations below:

$$\bar{D} = |\bar{C} \cdot \bar{X}_{rand} - \bar{X}| \quad (3.8)$$

$$\bar{X}(t+1) = \bar{X}_{rand} - \bar{X} \cdot \bar{D} \quad (3.9)$$

3.2.4.1.2 Limitation of WOA and implementation of MWOA

Some of the limitations of WOA have compelled the authors to develop MWOA. For the exploration and exploitation phases, mostly the values are based on randomization, which would increase the computational complexity and time for the complex problems. As it has been mentioned earlier, it depends on one parameter i.e., \bar{a} , which decreases the convergence speed. Some of the limitations of WOA have compelled the authors to develop MWOA. For the exploration and exploitation phases, mostly the values are based on randomization, which would increase the computational complexity and time for the complex problems. As it has been mentioned earlier, it depends on one parameter i.e., \bar{a} , which decreases the convergence speed. There is a lack of proper balance between exploration and exploitation phases. As the location of the best search is not considered a priority, therefore, it cannot jump out of the local optima, which represents a decline in performance.

If the vector position changes during the process, it might result in a larger step calculation and the search space not being explored properly. Correction factors Cf_1 and Cf_2 are introduced to minimize the change in vector position.

3.2.4.1.3 MGWO application to the proposed compensation technique

The modified equations of WOA can be written as:

$$\bar{D} = |\bar{C} \cdot \bar{X}_{rand} - \bar{X}| / Cf_1 \quad (3.10 \text{ (a)})$$

$$\bar{X}(t+1) = \bar{X}_{rand} - \bar{X} \cdot \bar{D} / Cf_1 \quad (3.11 \text{ (a)})$$

The equation (3.10 (a)) helps the whale survey the space of search efficiently in small steps and approach the prey. By modifying equation (3.10 (a)), whales are made to swim in the shrunk space to catch their prey, thus enhancing the exploitation of the search space efficiently.

$$\bar{X}(t+1) = \bar{D}' \cdot e^{bl} \cdot \cos(2\pi l) + \bar{X}^*(t) / Cf_2 \quad (3.12 \text{ (a)})$$

The exploration phase is also modified by the Cf_2 amount to limit the random movement of the whales. The values of Cf_1 and Cf_2 are 2.3 and 1.9, respectively. It was found that the whales reach the optimal solution in a search space efficiently and speedily compared to WOA. The steps followed to achieve the results are given as follows:

The Pseudocode for MWOA

1. Whales' population was initialized using \bar{X}_i where, $(i = 1, 2, 3, \dots, n)$.
2. The values were updated for each search agent a , A , C , l , and p by using the condition $(t < \text{maximum iteration})$.
3. For $(p < 0.5)$, if $(|A| < 1)$, present search agent was updated using equation (3.6).
4. If $(|A| \geq 1)$, \bar{X}_{rand} was selected and the present search agent was updated using equations (3.10 (a)) and (3.11(a)).
5. For $(p \geq 0.5)$, the location of the present search agent was updated using equation (3.12 (a)).
6. If any search agent goes beyond the search space, then the process restarts from step 2.
7. The fitness of each search agent and upgraded \bar{X}^* was computed. If the termination criteria are met, optimal solution (switching angles with the minimum corresponding THD) would be displayed otherwise process restarts from step 3.

3.2.5 WIND CHARECTARSTICS EQUATIONS

3.2.5.1 Wind turbine characteristics

A wind turbine consists of blades that are fixed to the shaft through the gearbox and rotor hub. It transforms the kinetic energy to mechanical energy which is further converted to electrical energy by the shaft. The output mechanical power (P_m) achieved can be expressed as

$$P_m = \frac{1}{2} \rho A v^3 C_p(\lambda, \beta) \quad (3.13)$$

Where, ρ is the air density, v is the wind speed, A is the swept area of the turbine, C_p is the coefficient which judges the performance and also which is a non-linear function of Tip Speed Ratio (TSR), (λ) and pitch angle (β). TSR can be written as

$$\lambda = \frac{wR}{v} \quad (3.14)$$

Where, w is the speed of the turbine, R =radius of the blade.

$$C_p(\lambda, \beta) = C_1(C_2 / \lambda_i - C_3\beta - C_4)e^{-C_5/\lambda} \quad (3.15)$$

The value of (C_1 , C_2 , C_3 , and C_4) can be computed by estimating from the non-linear function or by the lookup table [3.6].

$$\lambda_i = \left[\frac{1}{\lambda + .089} - \frac{0.035}{\beta^3 + 1} \right]^{-1} \quad (3.16)$$

The aim was to keep tracking the rotor speed with the changing wind velocity so that C_p is set to the maximum value. To achieve maximum power from IG, C_p should remain set to the highest value as shown in Fig. 3.2.

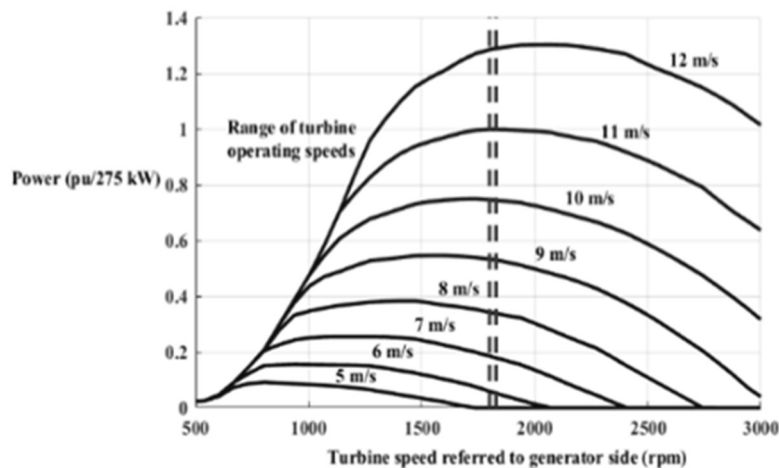


Fig.3.2 Turbine power output versus speed of the shaft

3.2.5.2 Mathematical modeling of DFIG

There are two categories of generators, comprising an induction generator and a synchronous generator. The present chapter deals with the induction generator, which has three types: squirrel cage induction

generator (SCIG), wound rotor induction generator (WRIG), and doubly fed induction generator (DFIG). Amongst all, DFIG is the most popular because of its simple pitch control, which deals with both active and reactive power. Besides this, it can work at variable speed, sub or synchronous speed to obtain maximum power as well. Power converters are much cheaper, lighter, and have less power loss as their ratings are only 30% of the power rating.

Equations (3.15)– (3.27) show the conventional equations for DFIG in a synchronous rotating frame. The equivalent circuit can be seen in the d and q axis frames in Fig. 3.3 and Fig. 3.4.

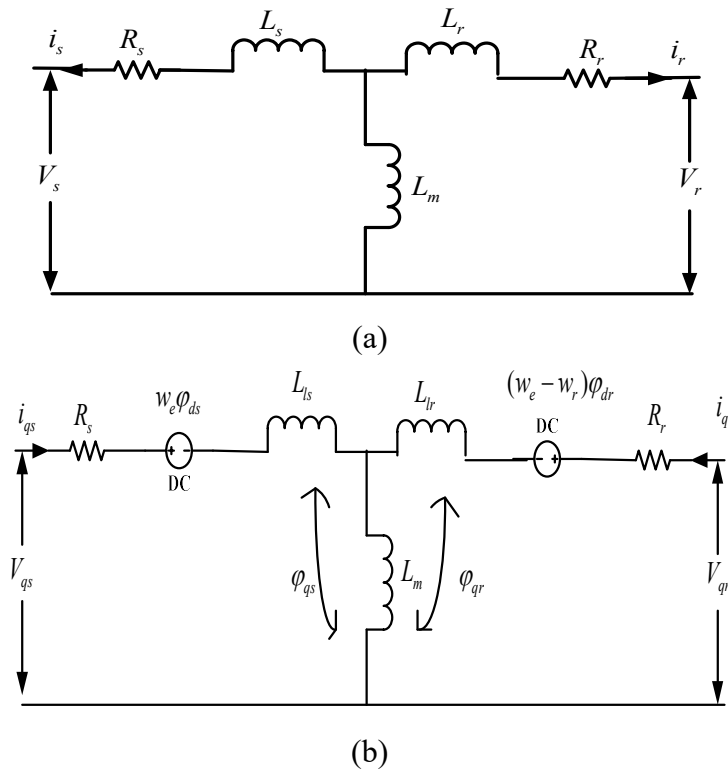


Fig. 3.3 DFIG (a) Equivalent circuit (b) Dynamic equivalent circuit in q axis frame

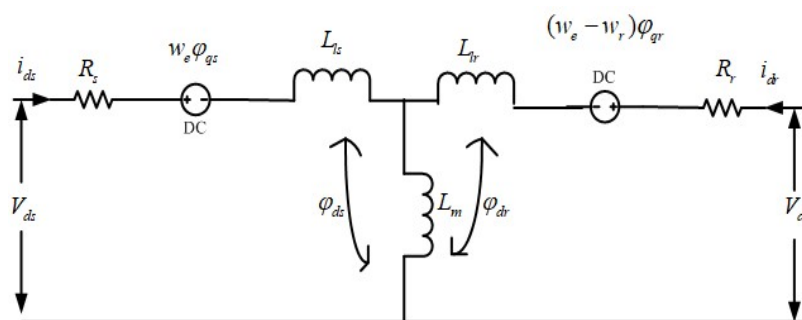


Fig. 3.4 Dynamic equivalent circuit in d axis frame

The d-q frame stator and rotor equations are given below.

$$V_{qs} = R_s i_{qs} + \frac{d}{dt} \phi_{qs} + w_e \phi_{ds} \quad (3.17)$$

$$V_{ds} = R_s i_{ds} + \frac{d}{dt} \phi_{ds} + w_e \phi_{qs} \quad (3.18)$$

$$V_{qr} = R_r i_{qr} + \frac{d}{dt} \phi_{qr} + (w_e - w_r) \phi_{dr} \quad (3.19)$$

$$V_{dr} = R_r i_{dr} + \frac{d}{dt} \phi_{dr} + (w_e - w_r) \phi_{qr} \quad (3.20)$$

Flux linkage equations can be written as

$$\phi_{qs} = L_{ls} i_{qs} + L_m (i_{qs} + i_{qr}) \quad (3.21)$$

$$\phi_{ds} = L_{ls} i_{ds} + L_m (i_{ds} + i_{dr}) \quad (3.22)$$

$$\phi_{qr} = L_{lr} i_{qr} + L_m (i_{qs} + i_{qr}) \quad (3.23)$$

$$\phi_{dr} = L_{lr} i_{dr} + L_m (i_{ds} + i_{dr}) \quad (3.24)$$

where, $V_{ds}, V_{qs}, V_{qr}, V_{dr}, \phi_{ds}, \phi_{qs}, \phi_{dr}, \phi_{qr}, i_{ds}, i_{dr}, i_{qs}, i_{qr}, L_{ls}, L_{lr}, R_s, R_r$ are the stator and rotor voltage, current, flux, difference of self-inductance and the mutual inductance and the resistance respectively, L_m is the mutual inductance, w_e, w_r are the angular and the rotor speed respectively. The active and reactive power of stator and rotor P_s, Q_s, P_r, Q_r respectively can be written as:

$$P_s = \frac{3}{2} (V_{ds} i_{ds} + V_{qs} i_{qs}) \quad (3.25)$$

$$Q_s = \frac{3}{2} (V_{qs} i_{ds} - V_{ds} i_{qs}) \quad (3.26)$$

$$P_r = \frac{3}{2} (V_{dr} i_{dr} + V_{qr} i_{qr}) \quad (3.27)$$

$$Q_r = \frac{3}{2} (V_{qr} i_{dr} - V_{dr} i_{qr}) \quad (3.28)$$

By (3.31) electromagnetic torque (T_{em}) can be determined.

$$T_{em} = p(\phi_{ds} i_{qs} - \phi_{qs} i_{ds}) \quad (3.29)$$

Where, p is no of pole pairs.

3.2.5.3 Reactive power compensation

Reactive power is an essential component of an electric power systems: without it, rotating machines could not rotate, and transmission lines could not transmit active power. Reactive compensation is the process of injecting positive and/or negative Var's to a power system to essentially attain voltage control.

Depending upon the application, reactive compensation can be achieved passively with capacitors and reactors or actively with power electronic solutions e.g., FACTS such as STATCOMS, capacitor banks. It has several advantages such as reducing power losses, increased utilization of machineries, power factor control and voltage control.

RSC extracts the optimum power from the variable-speed wind turbines and regulates the DFIG terminal voltage. The stator Flux-Oriented Control (SFOC) performs the control of RSC. Therefore, the stator active power (P_s) and the electromagnetic torque (T_e) can be controlled through (i_{qr}), whereas the stator reactive power (Q_s) can be adjusted by the (i_{dr}) as follows:

$$P_s = \frac{3}{2} [-i_{qs} V_{qs}] = \frac{3L_m}{2L_s} [i_{qr} \omega_e \Phi_{ds}] \quad (3.25a)$$

$$Q_s = \frac{3}{2} [i_{ds} V_{qs}] = \frac{3\omega_e}{2} [i_{ds} \Phi_{ds}] \quad (3.26a)$$

$$T_{em} = \frac{3PL_m}{2 \times 2L_s} [-i_{qr} \Phi_{ds}] \quad (3.29a)$$

The q-axis component is utilized for the extraction of the peak power from the variable-speed wind turbines during the wind speed variation. Hence, the PI controller is used to find the error between the rotational speed of the DFIG rotor that compared with the actual rotational speed (ω_r) in order to generate the reference q-axis component of the rotor current (i_{qr-ref}).

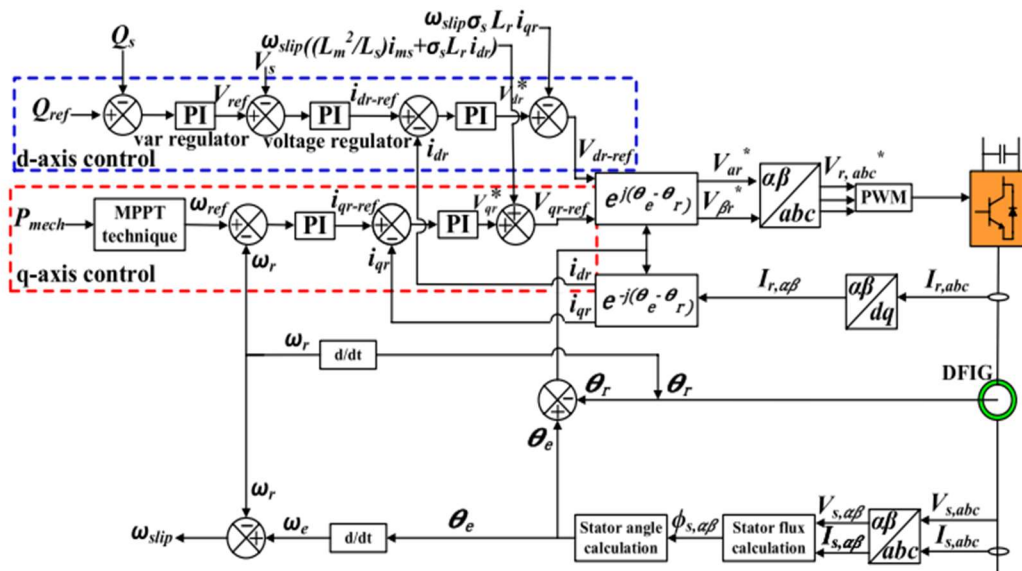


Fig 3.1(a) RSC controller

The d-axis component is utilized for regulation the DFIG stator voltage and also injects voltage at the time of sag, (Q_{ref}) is taken as zero in order to maintain the unity power factor at the stator terminals of the DFIG. The mathematical equation can be expressed as

$$V_{dr_ref} = V_{dr}^* - (w_e - w_r)\sigma_s L_r i_{qr} \quad (3.30)$$

$$V_{qr_ref} = V_{qr}^* + (w_e - w_r) \left(\sigma_s L_r i_{dr} + \frac{L_m^2}{L_s} i_{ms} \right) \quad (3.31)$$

The GSC controller maintains the DC-bus voltage (V_{dc}) constant irrespective of magnitude and direction of rotor power flow and regulate the reactive power exchanged with the grid. Voltage-Oriented Control (VOC) system is used to carry out the control strategy of the GSC. Hence, the injected active power from the GSC (P_c) and the DC-bus voltage (V_{dc2}) is adjusted through (i_{dg}), while the injected reactive power from the GSC (Q_c) is controlled by the (i_{qg}) as follows:

$$P_c = \frac{3}{2} (V_d i_{dg}) \quad (3.32)$$

$$Q_c = -\frac{3}{2} (V_d i_{qg}) \quad (3.33)$$

Therefore, the reference d-axis component of the GSC current (i_{dg-ref}) is generated from comparing the reference DC-bus voltage ($V_{dc2-ref}$) with the measured value (V_{dc}) and applying the difference to PI-controller. On the other hand, the q-axis component (i_{qg}) is employed to control the exchanged reactive power with the electrical grid.

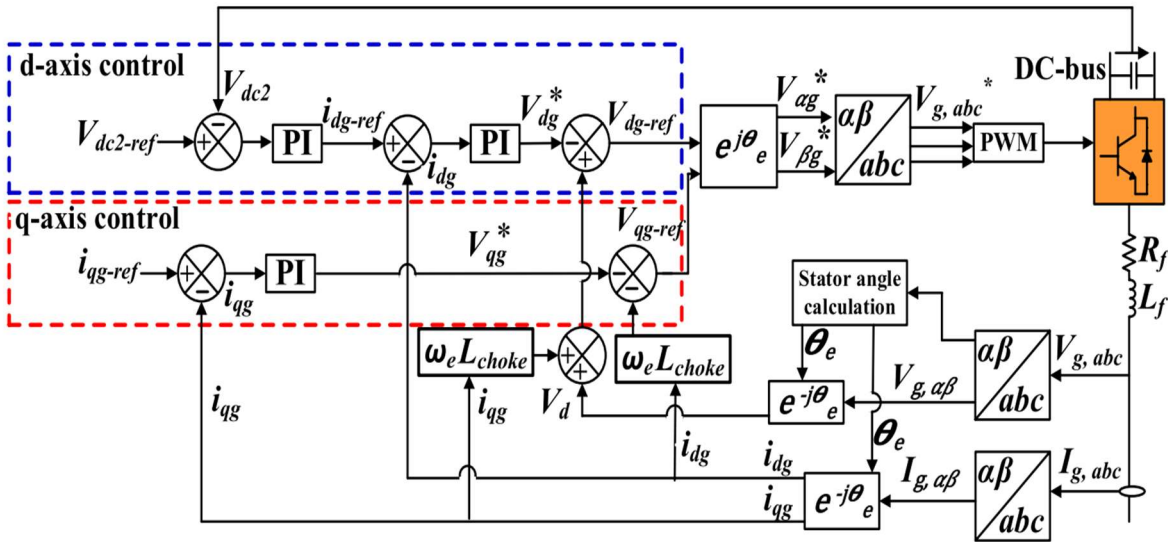


Fig. 3.1(b) GSC controller

During the normal operation conditions, the reference q-axis component of the GSC current (i_{qg-r}) is determined at zero value to maintain the wind farm at unity power factor. Then, the (i_{dg-re}) and the (i_{qg-r}) are compared with the d-q axis components of measured GSC current (i_{dg}, i_{qg}) and the

differences are applied to PI controllers to create the reference d–q axis components of GSC voltage (V_{dg-r} , V_{qg-ref}) that can be described as:

$$V_{dg-r} = -V_{dg}^* + w_e L_{chok} i_{qg} + V_d \quad (3.34)$$

$$V_{qg-ref} = -V_{qg}^* + w_e L_{choke} i_{dg} \quad (3.35)$$

3.2.6 RESULT ANALYSIS

3.2.6.1 MATLAB Simulation discussion

The proposed model has been carried out in MATLAB 2016b. The angles for the inverters were found by the WOA. The five switching angles obtained for both the converters are $\alpha_1 = 10.33^\circ$, $\alpha_2 = 18.16^\circ$, $\alpha_3 = 24.33^\circ$, $\alpha_4 = 25.07^\circ$, $\alpha_5 = 27.50^\circ$; $\alpha_1 = 16.33^\circ$, $\alpha_2 = 22.45^\circ$, $\alpha_3 = 23.45^\circ$, $\alpha_4 = 28^\circ$, $\alpha_5 = 32.47^\circ$ respectively for reducing the lower and higher-order harmonics. These angles were stored in the lookup table offline for use later for online applications. The proposed control strategy has been used to get the outputs shown in Figs. 3.5 and 3.6. The voltage waveforms at the stator and rotor sides are taken at a speed of 1450 rpm under both with and without harmonic elimination conditions.

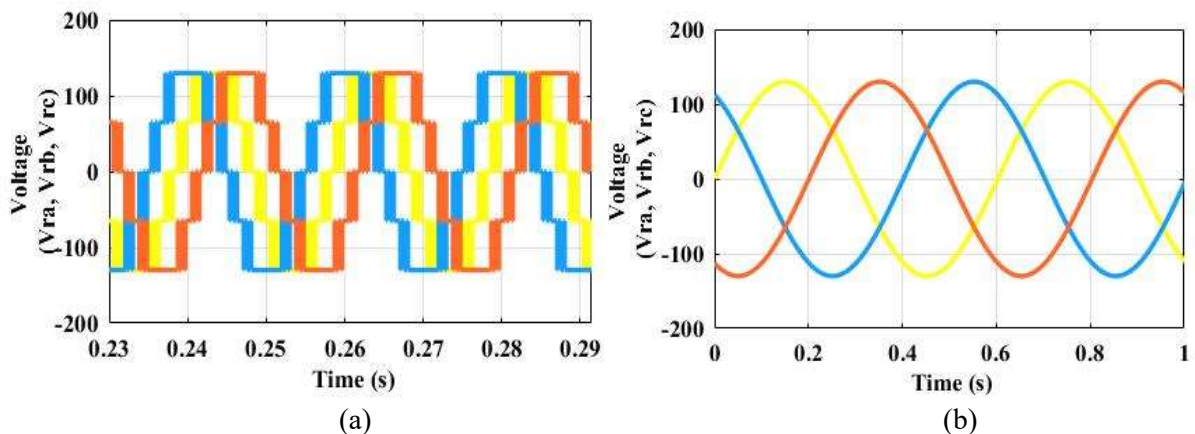


Fig. 3.5 System output at 1450 rpm (a) rotor voltage output without harmonic elimination (b) rotor voltage output with harmonic elimination

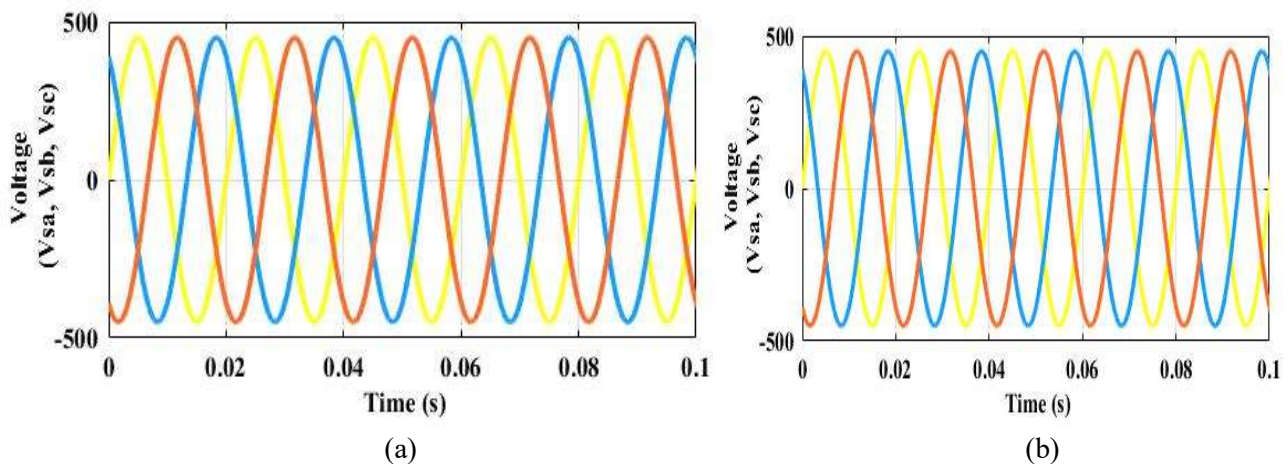


Fig. 3.6 System output at 1450 rpm (a) stator output voltage without harmonic elimination (b) stator output voltage with harmonic elimination

3.2.6.2 Comparison with the existing schemes

A comparative analysis has been shown in In Table 3.2. The values of voltage harmonics deduced by b_5 , $b_7...$ of the standard reports are compared with the proposed technique. By using the SHEPWM based MWOA control strategy, the pulses were generated at a modulation index of 0.85. The objective function (2.3) was used to get the optimized switching angles. Fig. 3.7 shows the different numbers of switching angles for $n = 3, 5,$ and $7,$ over the range of modulation index. It was considered for up to twenty-nine harmonics. Higher orders can also be taken for testing the present system. For the computation of five switching angles, the 5th, 7th, 11th, 13th harmonics, and fundamental were set to zero and the desired value, respectively. It was found that with just five switching angles, an equivalently good result was achieved with seven triggering pulses, keeping the system efficiency intact as well as keeping the switching losses low, as shown in Figure 3.7. This means that with seven switching angles, the 5th, 7th, 11th, 13th, and 17th can be controlled, but by using five triggering pulses, these lower orders can be controlled along with the higher orders like the 19th, 23rd, 25th, and 29th... etc.

Table 3.1 Comparison of voltage harmonic amplitudes of literature survey with the proposed technique

Standard Reports used											
Voltage harmonics amplitude on grid synchronization	b_5	b_7	b_{11}	b_{13}	b_{17}	b_{19}	b_{23}	b_{25}	b_{29}	THD (%)	
IEC 1996	5	4	3	2.5	1.6	1.2	1.2	1.2	1.06	6.5	
CIGRE 2004	6	5	3.5	3	2	1.5	1.5	1.5	--	8	
Proposed Technique used											
Voltage harmonics amplitude on grid synchronization	b_5	b_7	b_{11}	b_{13}	b_{17}	b_{19}	b_{23}	b_{25}	b_{29}	THD (%)	
Values	0.89	0.27	0.17	0.35	0.5	0.9	0.17	0.08	0.05	1.6	

Fig. 3.7 (a) shows the THD variation over the modulation index for the different switching angles. The THD found by using different optimization algorithms at varying iterations is shown in Fig. 3.7 (b). It was discovered that using MWOA produces better results than other evolutionary techniques. The angles found when applying MWOA to the SHEPWM inverters are equally efficient in working as the seven switching angles, hence with reduced switching losses. The details of the parameters for different metaheuristic

techniques used have been given in Table 3.2. Harmonic spectra for various switching angles ($n = 3, 5, 7$) at the rotor and stator side under with and without harmonics conditions have been shown in Fig. 3.8.

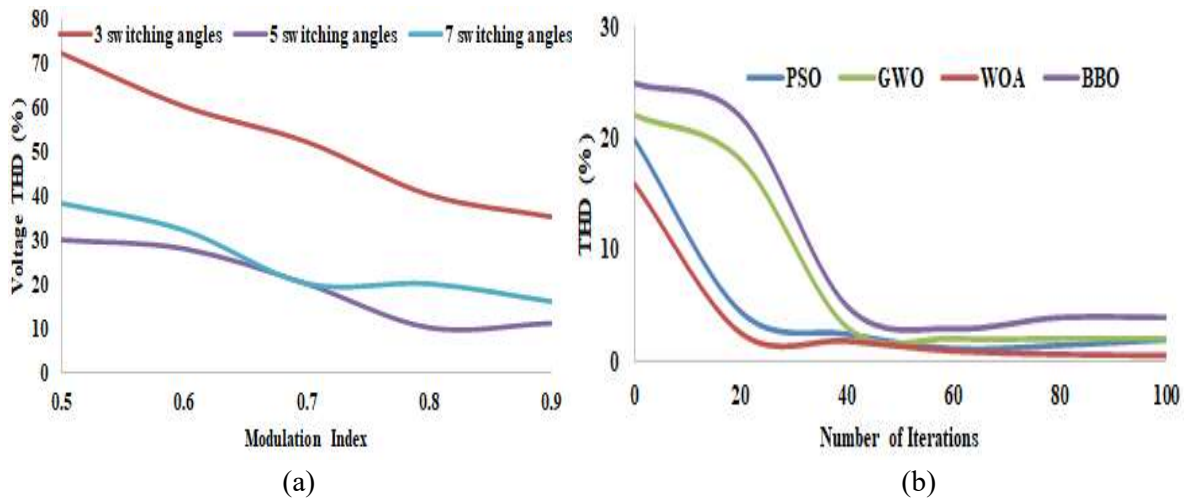
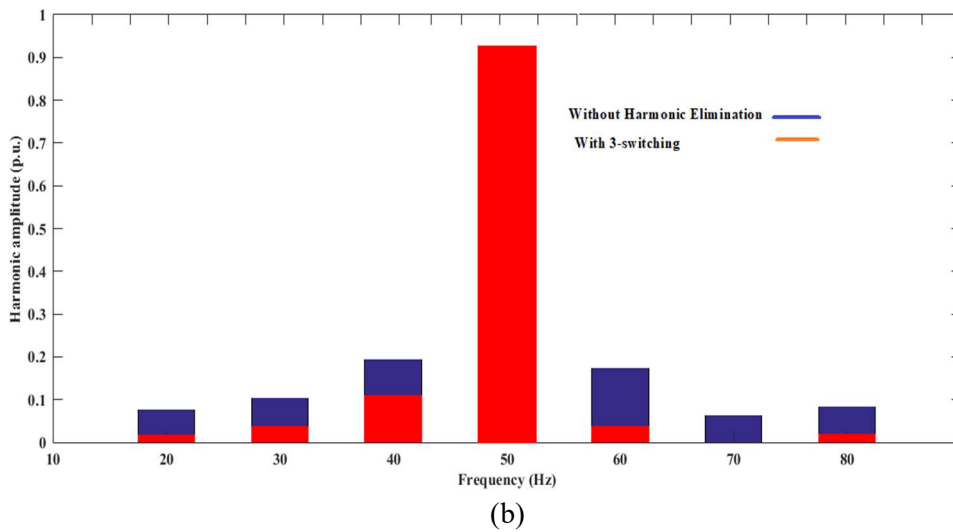
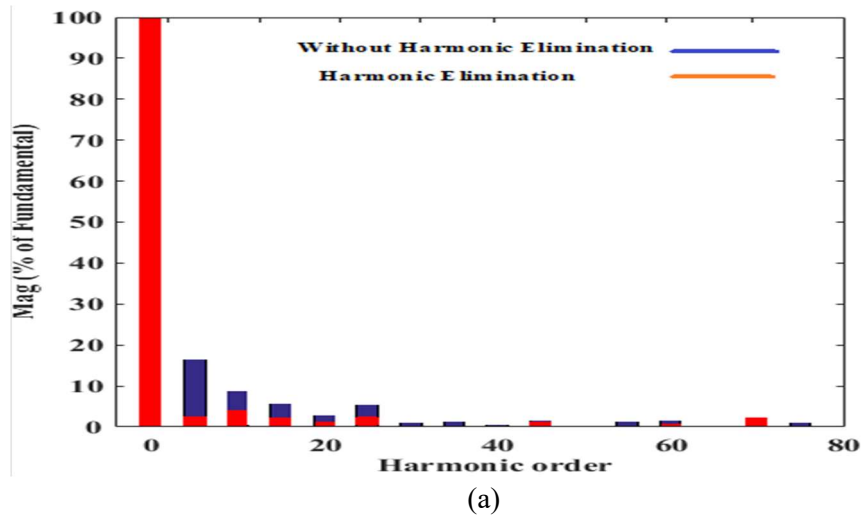
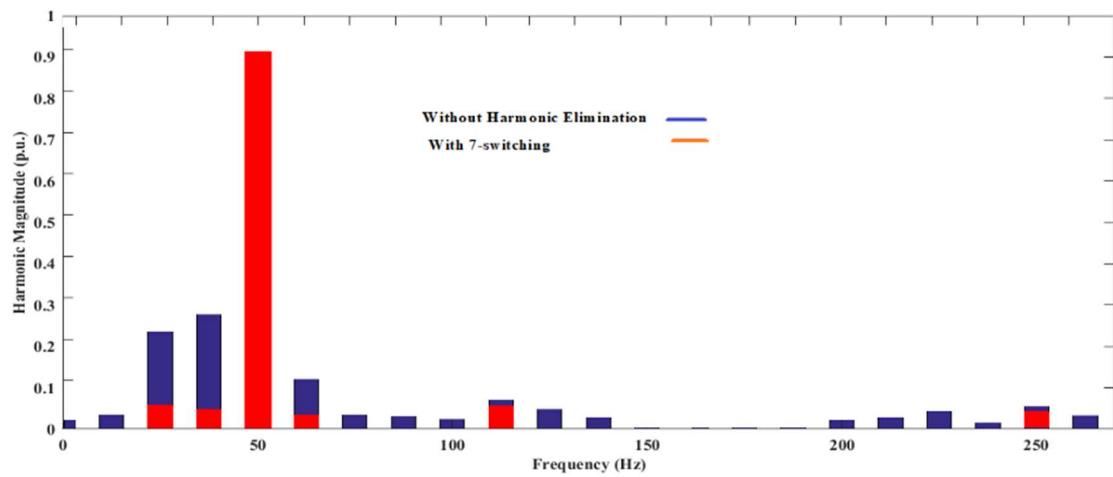


Fig. 3.7 Characteristics behavior (a) THD vs. modulation index for various switching angles (b) THD vs. no. of iterations for various algorithms used





(c)

Fig. 3.8 DFIG harmonic spectra with and without harmonic (a) at rotor side (b) for three switching angles at stator side (c) for seven switching angles at stator side

Table 3.2 Comparison of metaheuristic techniques with the proposed technique

PSO		MWOA		GWO		BBO	
Weight (w)	0.4	Population matrix	10*5	Population matrix	10*5	Population size	50
Balance factors c_1, c_2, c_3, c_4	1.3, 0.6, 1.9, 1.7					Genes in each population	5
Random variable: r_1, r_2	0.6, 0.5	Random variable r_1, r_2	0.7, 0.6	Random variable r_1, r_2	0.7, 0.6	Elitism value	2
No. of equations	Low	No. of equations	Low	No. of equations	Low	No. of equations	High
Complexity	Easy	Complexity	Easy	Complexity	Easy	Complexity	Moderate
CPU time (s)	0.43	CPU time (s)	0.22	CPU time (s)	0.26	CPU time (s)	0.34
THD (%)	2.8	THD (%)	1.6	THD (%)	2.2	THD (%)	2.5

3.2.7 CONCLUSION

In the present chapter, MWOA, BBO, PSO, and GWO-based inverters were used to reduce the lower and higher-order harmonics obtained at the stator and rotor side of the DFIG system. The best performance of all was that of MWOA, considering factors such as convergence time, minimum THD possible, etc. The angles obtained from the evolutionary techniques were stored offline in the microcontroller memory for online usage. Thus, with five switching angles, they achieve equivalently good results as seven switches.

Thus, with fewer switching losses, system efficiency is maintained. Various characteristic curves such as THD vs. iterations, THD vs. modulation index, etc. were carried out to justify the same. Thus, the proposed method achieves the desired purpose, and the simulation results justify that it can be used for practical scenarios.

Publication

- ❖ Suman, S., Chatterjee, D., Anand, M., Mohanty, R., & Bhattacharya, A (2022). An Improved Harmonic Reduction Technique for the PV-Wind Hybrid Generation Scheme using Modified Whale Optimization Algorithm (MWOA). *U.P.B. Sci. Bull.*, Series C, 84(1), ISSN 2286-3540. [Scopus, Q3, Impact Factor: 0.49]

References

- [3.1] Choudhary, P., and Srivastava, R. K. (2019) ‘Sustainability perspectives-a review for solar photovoltaic trends and growth opportunities’, *Journal of Cleaner Production*, 227, pp: 589-612.
- [3.2] Ray, R. N., Chatterjee, D., & Goswami, S. K. (2009) ‘Harmonics elimination in a multilevel inverter using the particle swarm optimisation technique’, *IET Power Electronics*, 2(6), pp. 646-652.
- [3.3] Elena, D. F., (2021) ‘The impact of SVC device on the voltage and power quality in the electrical transmission network’, *U.P.B. Sci. Bull., series c*, 83(1), pp. 53-64, ISSN 2286-3540.
- [3.4] Ray, R.N., Chatterjee, D. and Goswami, S.K. (2010) ‘A PSO based optimal switching technique for voltage harmonic reduction of multilevel inverter’, *Expert Syst. with Appl.*, 37(12), pp.7796–7801.
- [3.5] Tang, T., Han, J., & Tan, X. (2006) ‘Selective harmonic elimination for a cascade multilevel inverter’ In *2006 IEEE international symposium on industrial electronics*, 2, pp. 977-981).
- [3.6] Mahela, O. P., & Shaik, A. G. (2016) ‘Comprehensive overview of grid interfaced wind energy generation systems’ *Renewable and Sustainable Energy Reviews*, 57, pp. 260-281.
- [3.7] Dris, Y., Benhabib, M.C., Meliani, S.M. & Dumbrava, V. (2021) ‘Performance analysis of a hybrid farm (photovoltaic system wind turbine) connected to the grid using nine- switches converter’, *U.P.B. Sci. Bull., series c*, 83(3), pp. 53-64, ISSN 2286-3540.
- [3.8] Bellabas, B., Denai, M. & Allaoui, T., (2020) ‘A hierarchical control scheme to improve the stability and energy quality of a hybrid wind/photovoltaic system connected to the electricity grid’, *U.P.B. Sci. Bull., series c*, 82(2), pp. 307-323, ISSN 2286-3540.
- [3.9] Gao, K., Wang, T., Han, C., Xie, J., Ma, Y., & Peng, R. (2021) ‘A Review of Optimization of Microgrid Operation’, *Energies*, 14(10), pp. 28-42.
- [3.10] Sarker, K., Chatterjee, D., & Goswami, S. K. (2018) ‘Modified harmonic minimisation technique for doubly fed induction generators with solar-wind hybrid system using biogeography-

based optimisation, *IET Power Electronics*, 11(10), pp. 1640-1651.

[3.11] Goud, B. S., & Rao, B. L. (2020) 'Power quality improvement in hybrid renewable energy source grid-connected system with grey wolf optimization, *International Journal of Renewable Energy Research (IJRER)*, 10(3), pp.1264-1276.

[3.12] Routray, A., Singh, R. K., & Mahanty, R. (2019) 'Harmonic reduction in hybrid cascaded multilevel inverter using modified grey wolf optimization' *IEEE Transactions on Industry Applications*, 56(2), pp.1827-1838.

[3.13] Wei, L., Li, K. & Wu, Y. (2021) 'Research on photovoltaic systems maximum power point tracking based on improved automatic Bacterial Foraging method', *U.P.B. Sci. Bull.*, series C, 83(3), ISSN 2286-3540.

[3.14] Rana, N., Abd Latiff, M. S., & Chiroma, H. (2020) 'Whale optimization algorithm: a systematic review of contemporary applications, modifications and developments' *Neural Computing and Applications*, 32,16245-16277.

[3.15] Mohammed, H. M., Umar, S. U., & Rashid, T. A. (2019) 'A systematic and meta-analysis survey of whale optimization algorithm' *Computational intelligence and neuroscience*, 2019, Article ID 8718571, 25 pages, 2019, DOI: <https://doi.org/10.1155/2019/8718571>.

[3.16] Diab, A. A. Z., Sultan, H. M., Mohamed, I. S., Kuznetsov, O. N., & Do, T. D. (2019) 'Application of different optimization algorithms for optimal sizing of PV/wind/diesel/battery storage stand-alone hybrid microgrid', *IEEE Access*, 7, pp. 119223-119245.

[3.17] Ye, X., Liu, W., Li, H., Wang, M., Chi, C., Liang, G., ... & Huang, H. (2021) 'Modified Whale Optimization Algorithm for Solar Cell and PV Module Parameter Identification', *Complexity*, 2021.

[3.18] Youche L. & Huaizhong C. (2019) 'Optimization design for photovoltaic generation mppt based on improved adaptive genetic algorithm', *U.P.B. Sci. Bull.*, series C, 81(3).

[3.19] Chatterjee, D. (2011) 'A novel magnetizing-curve identification and computer storage technique for induction machines suitable for online application', *IEEE Transactions on Industrial Electronics*, 58(12), pp. 5336-5343.

[3.20] CIGRE, J. W. (2004) C3. 07/CIRED 'Power quality indices and objectives', *Final WG Report*.

[3.21] International Electro-technical Commission. (1996) 'Assessment of emission limits for distorting loads in MV and HV power systems', *IEC technical report*, 61000, pp. 3-6.

3.3 POWER QUALITY ISSUES FOR PV-WIND HYBRID DISTRIBUTED GENERATOR WITH SERIES COMPENSATION INTEGRATED TO MICROGRID

3.3.1 INTRODUCTION

The development of renewable energy sources (RES) based on PV-wind is becoming the centre of attraction due to the rise in economic and environmental issues [3.22]. Wind turbines using doubly fed induction generator (DFIG) are becoming popular over other induction generators (IG) due to several benefits, such as wide speed operation, separate active and reactive power control, and low-rated converters [3.23], [3.24]. In DFIG systems, the back-to-back converters are responsible for active and reactive power control. A review study done by [3.25] on the mitigation of power quality issues (voltage sag, voltage swell, voltage and current harmonics, system unbalances, and fluctuations), especially super harmonics, to ensure high-quality microgrid output power. Similarly, series compensation has been carried out to deal with the issues of power quality detailed in this chapter.

3.3.2 EXISTING TOPOLOGIES

The authors in [3.25] present a study in which a thermal exchange optimization (TEO) algorithm is used to optimise direct power control and DC-link voltage dynamics in the DFIG systems. The tuning of the PI controller for this application was found to be tedious, time-consuming, and non-systematic. Several filter devices were used for harmonic compensation, and the controlling parameters were optimised using evolutionary techniques detailed in [3.26]. An analytical study on harmonics has been carried out in [3.27], [3.28]. An intelligent control strategy for Optimum Power Quality Enhancement (OPQE) unified Power Quality Conditioner with Active and Reactive Power (UPQC-PQ) for grid-connected hybrid power systems is stated by [3.29]. An Atom Search Optimization (ASO) based Fractional-order Proportional Integral Derivative (FOPID) controller was used to regulate voltage while reducing power loss and total harmonic distortion (THD). Salp Swarm algorithm (SSA) has been used to calculate the size of distributed generators (DG) in order to optimise the voltage profile and reduce the lack of generation given in [3.30]. The Active Power Filter (APF) has been used for power quality (PQ) improvement, where the controller for APF has been designed to improve the voltage profile and compensate for reactive power and harmonics. [3.31] propose a scheme that can be used for both balanced and unbalanced grid conditions. It uses a reference current generator (RCG) applied to a fractional order proportional integral (FOPI) based power management strategy to control a three-phase inverter and manage power flow to the grid, loads, etc. It injects maximum active power and minimum reactive power into the electric grid and loads it at inverter power capacity under grid faults. For harmonic compensation, a Lyapunov-based algorithm [3.32], [3.34]- [3.35] was used, and its integration with PI was used for charging shunt active power filter (SAPF) for electric vehicle applications. A literature survey by [3.36]– [3.38], on inverter topologies have

been discussed for harmonic elimination using the selective harmonic elimination (SHE) technique in RES. The conventional method of control, such as vector control, is simple and popular, but the use of PI controllers makes the tuning complex due to time delays and nonlinearity [3.39]. Therefore, researchers have shifted to optimization-based control tuning. [3.40] uses Biogeography Based Optimisation (BBO) based harmonic compensation, which is found to be complex and lengthy given in [3.40]. In [3.41], for a standalone DFIG system, Grey Wolf Optimiser (GWO) and Artificial Bee Colony (ABC) have been used for tuning PI for controlling the stator voltage and current. The complex control strategy and large battery storage system in [3.41], [3.42] will affect the cost of the overall system.

3.3.3 PROPOSED SCHEME

3.3.3.1 Configuration description

For the existing DFIG wind energy conversion schemes, when wind velocity varies widely, both the DC bus voltage and the output voltage can be affected. Although various literature is available for this purpose, they lack the desired results for the wider wind speed variation. The reason for stator harmonics is the switching at the rotor side, which is dependent on rotor speed. The proposed architecture shown in Fig. 3.9 addresses both these problems, along with power quality, i.e., harmonically related issues, and copes with the wider voltage variation by supplying additional voltage. As it can be observed that the stator is directly connected to the grid, whose frequency is similar to the grid, DFIG, coupled with the wind turbine through the gearbox, has to control the pitch angle for speed control. DFIG operation is carried out under two modes, i.e., sub-synchronous and super-synchronous modes of operation. The former occurs under low wind speeds where the active power is extracted from the DC bus and disbursed to the rotor, whereas vice-versa happens in the latter case to supply the grid. The advantage of this IG, in particular, is that the extension of the speed range is possible. In the proposed scheme, the number of converters used are three in numbers that are RSC, GSC, and lastly, the CC. The inverters are operated at a low switching frequency. The RSC is responsible for active reactive power control and harmonic reduction injected by the rotor. GSC deals with the grid injected harmonics and maintains the DC bus constant. Lastly, CC controls the grid's injected harmonics and compensates for low generated voltage. The combined operation of GSC and CC contributes to reactive power compensation under the Unified Power Factor Control (UPFC) mode. At high wind speeds, RSC and GSC provide continuous power supply to the grid. The collective operation of GSC and CC under the Dynamic Voltage Restorer (DVR) model helps in voltage dip mitigation, or maintaining the voltage demands on the grid side under wide voltage variations, thus improving power quality. DVR is a method of overcoming voltage sags and swells that occur in electrical power distribution. It injects voltage of certain amplitude and frequency as required at the load side, even when the source voltage is unbalanced or distorted. The PV-based DC-DC boost converter feeds power to the rotor, CC, at low wind speed to maintain an uninterrupted power supply. The

maximum power is extracted from the PV arrays through the Maximum Power Point (MPPT) controller using the Hill climbing algorithm. The ratings of GSC and RSC are higher compared to CC. Series compensation controls the harmonics and injects the required voltage when needed, which is purely novel. Also, the present scheme uses a recently developed SAR-based SHEPWM technique to achieve the desired objective and overcome the problems highlighted in the aforesaid literature. The application of SAR in hybrid problem formulation is not marked yet.

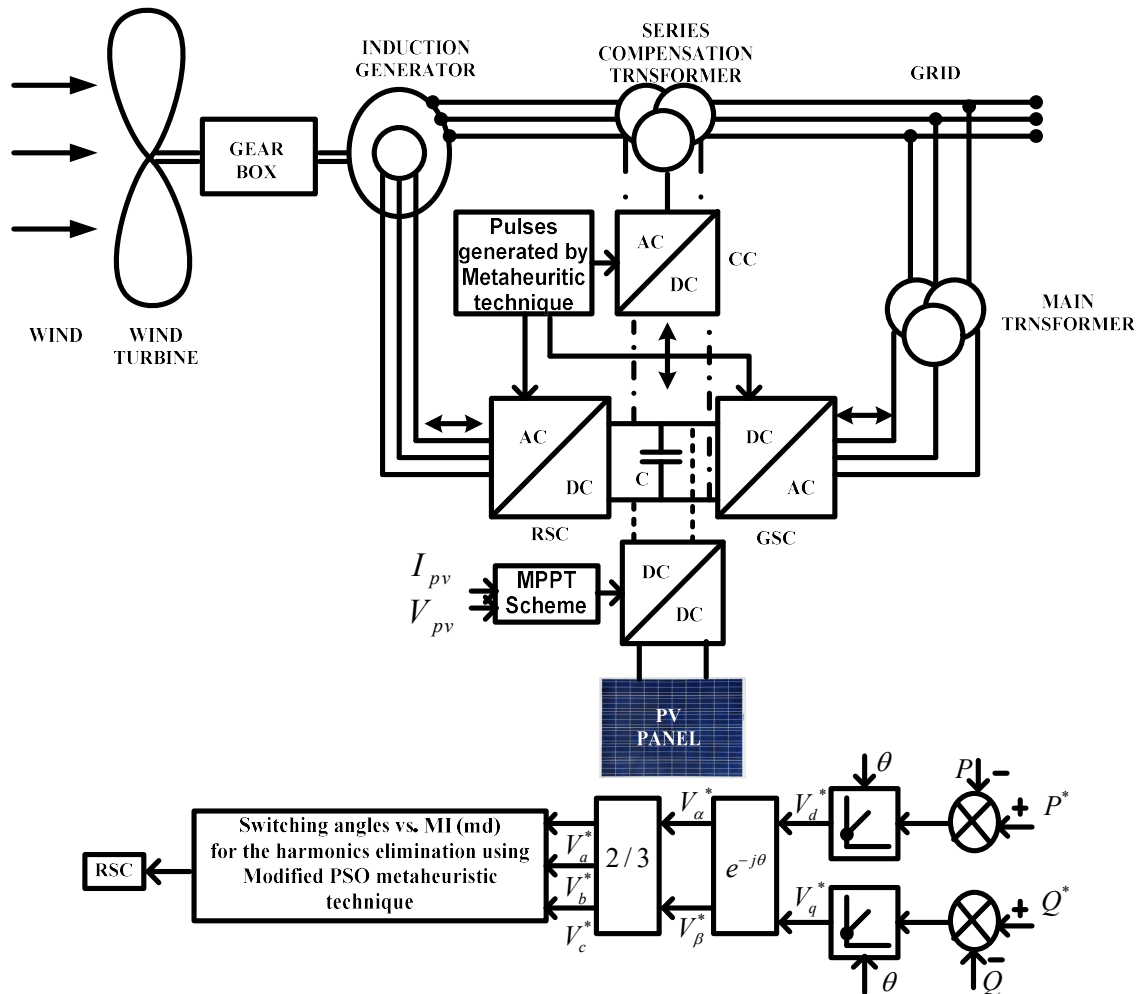


Fig. 3.9 Proposed Scheme with the control unit

The inverters feeding high current to the rotors develop stress in the device due to continuous conduction and switching. Conduction is uncontrollable because it is load dependent, but switching losses have to be looked after. Since these inverters are dealing with high power ratings, it would be beneficial if the switching were minimized, as that would reduce the switching losses. As this has higher frequency impacts on converter life, cost, and efficiency. So, the SHEPWM technique has been utilised to control these harmonics using the least number of switches per cycle. Besides, just three switching angles are used, which gives equivalently good results as seven switches, which tends to decrease the losses and

increase system utility. In the present approach, various metaheuristic techniques were compared to calculate the minimum THD, in which the SAR algorithm has so far given the minimal possible THD whose particular set of switching angles were considered. The angles for different MI were stored offline in the signal processor memory for online practice. In this model, the optimised switching angles for RSC, GSC, and Compensating Converter (CC) giving the minimum possible THD are generated by the SAR-based SHEPWM technique using proposed series compensation. In the present work, the objective function is framed in such a way that it eliminates lower order harmonics and controls the higher ones through the SAR algorithm and series compensation (phase opposition) provided by the compensating converter. It uses only three switching angles instead of higher switching numbers, which contributes fewer losses and increases system utility. The three switching angles eliminate the lower-order harmonics and optimise the other higher-order harmonics. Also, at low wind speeds and wide voltage variations, it supplies voltage to cater to the demand on the grid. The harmonic behaviour has been analysed under a wide range of modulation indices (MI). Besides, the comparison of different metaheuristic techniques has been done, and it was found that SAR suits best for the present model, shown later. This realistic approach has been successfully implemented and has superior performance over the existing techniques.

Application of the Search and Rescue (SAR) based search technique in [3.44], is completely new in hybrid system field and has been implemented here to test the feasibility of the system. A piecewise mixed model concept given in [3.45] has been used for control purposes. The control technique is apt for the present scheme as it is simpler yet more effective than used in [3.26], [3.27], and [3.28]. The THD obtained was compared with several standard reports of IEC, IEEE-519, and CIGRE WG 36-05 [3.41]–[3.49], and it was found that it was within the permissible limit.

3.3.4 HARMONICS INVESTIGATION IN A DFIG SYSTEMS

The mathematical description of the DFIG system under linear and non-linear load conditions has been included. Rotor current contains positive and negative sequence harmonics of order $(6n + 1)$ and $(6n - 1)$, respectively, where $n=1, 2, \dots$ multiplied with the synchronous frequency [3.28]. It has been mentioned in detail below.

For positive sequence harmonic order,

$$N = 1, \omega_s = \omega_e, \text{slip} = s, \quad (3.36)$$

For negative sequence harmonic order,

$$N = -1, \omega_s = -\omega_e, \text{slip} = 2 - s, \quad (3.37)$$

For $(6n + 1)$ sequence harmonic injected in rotor,

$$N = 1, w_s = (6n+1)w_r + w_m, slip = \frac{(6n+1)w_r}{(6n+1)w_r - w_m}, \quad (3.36a)$$

For $(6n-1)$ sequence harmonic injected in rotor,

$$N = -1, w_s = (6n-1)w_r - w_m, slip = \frac{(6n-1)w_r}{(6n-1)w_r - w_m}. \quad (3.37a)$$

Where, w_s is the synchronous speed, s is slip, w_m = mechanical frequency, w_r = rotor injected frequency. Positive sequence set can be defined as $(6n+1)$, and positive sequence frequency as $(6n+1)W$ i.e., 7 W, 13 W, etc. Negative sequence set is defined as $(6n-1)$, where $n=1, 2, \dots, 15$, and negative sequence frequency is defined as $(6n-1)W$, i.e., 5 W, 11 W, and so on. Therefore, the harmonics in the current at the stator side can be considered as $f_r + f_m, -5f_r + f_m, 7f_r + f_m$, etc.

The rotor speed causes rotor flux harmonics and fundamental flux interactions, which lead to subharmonics in the stator side voltage and current. So, these unwanted harmonics have to be removed from the DFIG system to give it a wider speed range. The converter on the rotor side should guarantee sinusoidal input at a slip frequency with the stator frequency maintained at 50 Hz. Since then, RSC has used a six-step switching method, which causes ripples in the output. For nearly sinusoidal output, a high switching frequency is required, which causes higher losses in the converters. In the case of quasi-sine wave switching, the positive and negative sequence rotor current is produced by harmonics. Therefore, the rotor voltages for both cases are given as follows:

For the case of positive sequence,

$$\begin{aligned} V_{an} &= \text{Im}((k/(6n+1))e^{j(6n+1)wt}), \\ V_{bn} &= \text{Im}((k/(6n+1))e^{j(6n+1)wt} e^{j(2\pi/3)}), \\ V_{cn} &= \text{Im}((k/(6n+1))e^{j(6n+1)wt} e^{-j(2\pi/3)}). \end{aligned} \quad (3.38)$$

For the case of negative sequence,

$$\begin{aligned} V_{an} &= \text{Im}((k/(6n-1))e^{j(6n-1)wt}), \\ V_{bn} &= \text{Im}((k/(6n-1))e^{j(6n-1)wt} e^{j(2\pi/3)}), \\ V_{cn} &= \text{Im}((k/(6n-1))e^{j(6n-1)wt} e^{-j(2\pi/3)}). \end{aligned} \quad \text{Where, } k = 2V_{dc}/\Pi. \quad (3.39)$$

3.3.4.1 Generation of stator harmonics by rotor speed

It was found that the reason for stator harmonics is the six-stepped switching at the rotor side, which is dependent on rotor speed. The frequency on the stator side (f_s) should be maintained at 50 Hz irrespective of rotor speed. The rotational injection frequency was regulated to keep the stator frequency constant. Rotor speed and mechanical frequency (f_m) are dependent on wind speed. Also, a compensating converter (CC) has been used to deal with the harmonics injected by RSC. The stator frequencies for positive and negative sequences are $(6n+1)*(f_r + f_m)$ and $(6n-1)*(f_r - f_m)$, respectively. The fundamental

component can be calculated by $f_r + f_m$. Rotor frequency can be calculated by $f_r = sf_s$ where $s = N_s - N_r/N_s$ and $f_m = PN_r/120$ where, P denotes the pole and rotor speed (N_r).

Table 3.3 Stator harmonics generation for a wide range of rotor speed due to the rotor harmonics presence

Harmonic order at the rotor side	Rotor speed (rpm)					Generated stator harmonic order
	1000	1250	1500	1750	2000	
5th	-1 ⁿ	0	1	2	3	
7th	3	2	1	0	-1 ⁿ	
11th	-3 ⁿ	-1 ⁿ	1	3	5	
13th	5	3	1	-1 ⁿ	-3 ⁿ	
17th	-5 ⁿ	-2 ⁿ	1	4	7	
19th	7	4	1	-2 ⁿ	-5 ⁿ	
23rd	-7 ⁿ	-3 ⁿ	1	5	9	
25th	11	5	1	-3 ⁿ	-7 ⁿ	
29th	-11 ⁿ	-4 ⁿ	1	6	11	

ⁿ the opposite sequence of generated stator harmonic order is denoted by a negative sign

For the present scheme, DFIG of 2.8 kW, 4 poles were used at a synchronous speed of 1500 rpm. A speed range of 1000 to 2000 rpm was chosen by considering an operating slip of 30%. For 2000 rpm, the rotor frequency (f_r) and rotor mechanical frequency (f_m) were found to be -16.66 Hz (the "-" sign shows reverse sequence) and 66.66 Hz, respectively. On calculating the rotor injected for the 7th order, the generated stator frequency was found to be 50 Hz, i.e., a fundamental harmonic component in the reverse direction. Hence, the 25th order rotor injected frequency gives a stator frequency of 350 Hz, which is the 7th order harmonic in the reverse direction. In the case of 1500 rpm, the rotor injected frequency was calculated to be 0 Hz, and the mechanical frequency was found to be 50 Hz. Therefore, the stator frequency was found to be 50 Hz, i.e., fundamental in the forward direction. Thus, it was found that the stator frequency was the same for higher and lower rotor injected harmonic orders. Similarly, at 1750 Hz, the rotor injected frequency and mechanical frequency were determined to be 8.33 Hz and 58.33 Hz, respectively. So, for 7th order rotor frequency, the stator frequency was found to be 0 Hz, which signifies number of harmonics to the stator, i.e., the DC component which has been shown in Table 3.3. If the stator should have no harmonics, then it is highly required that the rotor should eliminate or lower the harmonics produced in the output voltage and current at various speeds. Hence, a metaheuristic technique has been developed to look after such problems.

As observed in Table 3.3, the harmonics on the stator side will depend mostly on the rotor speed, and accordingly, the switching per quarter cycle will be decided. In the present technique, the minimum

number of switches is three, which is used to mitigate the harmonics, and the three numbers of switches are equivalently good at mitigating harmonics as seven. RSC switching is the reason for the injection of rotor harmonics, which can be either six-step or PWM.

3.3.5 COMPARISON OF CONVENTIONAL AND PROPOSED IMPROVED SWITCHING STRATEGIES FOR INVERTERS

To avoid switching losses generally, a quasi-sine wave is generated at the output of the rotor voltage for a DFIG system. The inverters can be switched using 180° and SHE modes of conduction, which would introduce $(6k \pm 1)$ harmonics where $k=1,2, \dots$ in the voltage output. These conduction modes are improved to reduce the harmonics produced, as shown in Fig 3.10.

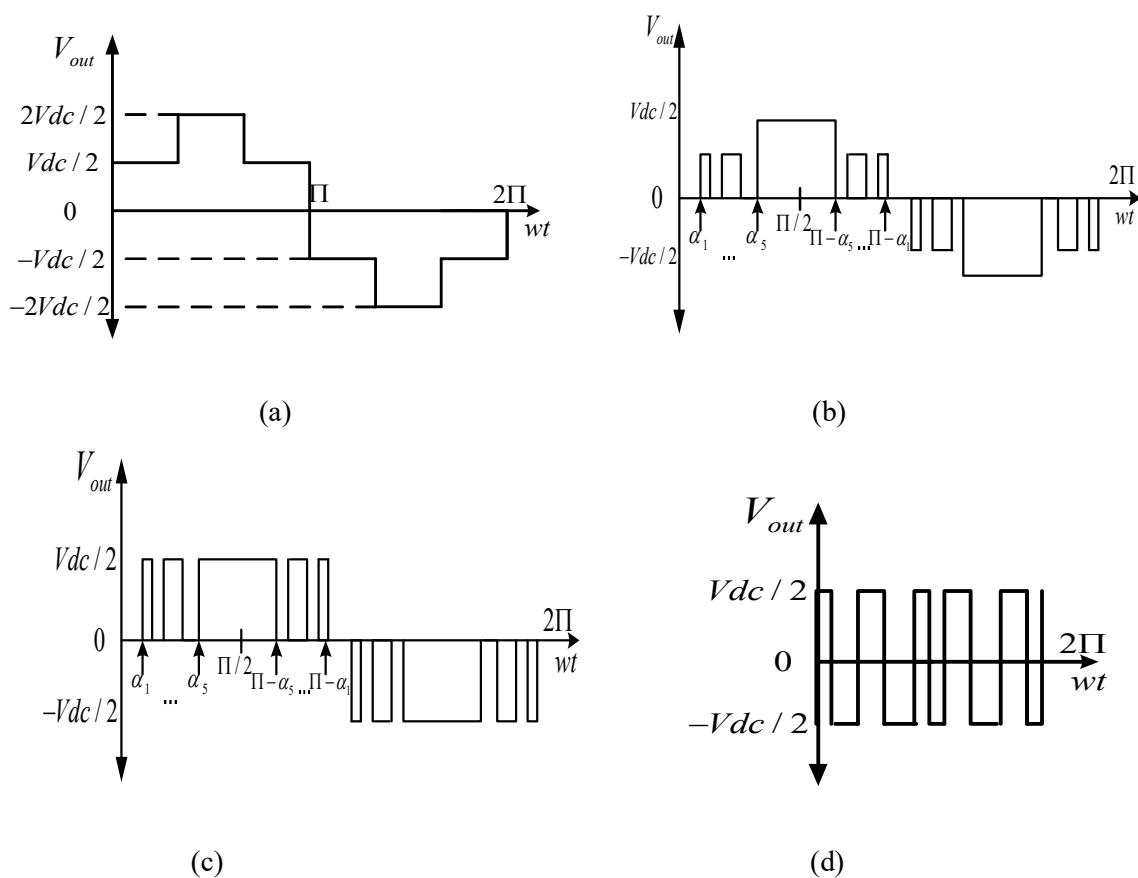


Fig. 3.10 Switching techniques used a) 180° conventional b) SHE in 180° c) SHE for unipolar d) SHE for bipolar

3.3.5.1 Traditional method

3.3.5.1.1 In the case of 180° switching strategy

The output voltage in quasi sine wave form can be written in terms of Fourier series [3.37] and [3.38].

$$V_{an} = \frac{a_0}{2} + \sum_{n=1}^{\infty} (a_n \cos(nwt) + b_n \sin(nwt)), \quad (3.40)$$

The value of a_0 and $a_n=0$ for all values of n , $b_n=0$ for all values of n due to quarter wave symmetry. $f(\omega t)$ was taken from the waveform shown in Fig. 3.10 (a).

3.3.5.1.2 In the case of SHEPWM switching strategy

Considering the basic Fourier equation (3.40) of voltage waveform the equation is symmetrical for the quarter, i.e., even, harmonics are zero and only odd harmonics are present

$$[f(\omega t) = f(\Pi - \omega t)].$$

$$b_n = \frac{4}{\Pi} \left[\int_x^{\Pi/2} f(\omega t) \sin(n\omega t) d(\omega t) \right], \quad \text{On solving, } (x > 0), \quad (3.41)$$

$$b_n = -\frac{4}{n\pi} \sum_{k=1}^m (-1)^k \cos n\alpha_k, \quad (3.42)$$

$$\text{Following } 0 < \alpha_1 < \alpha_2 \dots < \alpha_5 < \Pi/2. \quad (3.43)$$

3.3.5.2 Improved approach

3.3.5.2.1 In the case of 180° switching strategy

The standard voltage equation (3.34) was taken, as per the values mentioned for a_0, a_n and b_n for quarter wave. To remove the $(n-1)$ number of harmonics at the output side, ‘ n ’ no switching angles are required. But a higher number of switching angles would increase the inverter switching loss due to higher switching frequency. If the switching frequency is not high enough, then the lower order harmonics can be controlled. Therefore, fewer switches were used to cater to the higher number of harmonics. The bio-inspired algorithms were used to generate the three switching per quarter cycle to mitigate up to 29th order harmonics. $f(\alpha)$ was analyzed from the waveform shown in Fig. 3.10 (b).

$$b_n = \left(\frac{4}{\Pi} \right) \int_0^{\Pi/2} f(\alpha) \sin(n\alpha) (d\alpha),$$

$$b_n = \left(\frac{4}{n\Pi} \right) \left[\int_{\alpha_1}^{\alpha_2} \frac{V_{dc}}{3} \sin(n\alpha) (d\alpha) + \int_{\alpha_3}^{\alpha_4} \frac{V_{dc}}{3} \sin(n\alpha) (d\alpha) + \int_{\alpha_5}^{\Pi/2} \frac{2V_{dc}}{3} \sin(n\alpha) (d\alpha) \right],$$

On solving the above expression in general terms, it can be given for the n th term

$$b_n = \left(\frac{4V_{dc}}{3n\Pi} \right) \left[-\sum_{k=1}^m (-1)^k \cos(n\alpha_k) - 2 \sum_{k=m+1}^m (-1)^k \cos(n\alpha_k) \right]. \quad (3.40a)$$

The + and – signs of $\cos \alpha$ denotes rising and falling edges, respectively, in the transition states while switching. For line-to-line voltage, triplen harmonics are absent due to their symmetrical nature in the case of a three-phase balanced system. But harmonics for $n = 1, 5, 7, \dots$ etc. or for $n = (6k \pm 1)$ harmonics where

$k=1, 2, \dots$ are present and are chosen for elimination. By expanding (3.40), setting the fundamental component to MI , where ($MI < 1$) and other voltage harmonics equating to zero, angles can be calculated which mitigate harmonics. Proper selection of the angles was carried out, which gives a minimum THD that could decrease harmonics introduced to the grid as far as possible.

3.3.5.2.2 In the case of the SHEPWM switching strategy

The SHEPEM technique for harmonic elimination was carried out by considering two different cases.

3.3.5.2.2.1 SHE implemented SAR in unipolar case

As per Fig. 3.10 (c), the output voltage waveform (b_n) can be written as

$$b_n = \left(\frac{4}{\Pi}\right) \int_x^{\Pi/2} f(\alpha) \sin(n\alpha)(d\alpha), \text{ (where, } x > 0), \quad (3.41a)$$

$$b_n = \left(\frac{4}{\Pi}\right) \left[\int_{\alpha_1}^{\alpha_2} \frac{V_{dc}}{2} \sin(n\alpha)(d\alpha) + \int_{\alpha_3}^{\alpha_4} \frac{V_{dc}}{2} \sin(n\alpha)(d\alpha) + \int_{\alpha_5}^{\Pi/2} \frac{V_{dc}}{2} \sin(n\alpha)(d\alpha) \right],$$

On calculation,

$$b_n = -\frac{4}{n\pi} \sum_{k=1}^m (-1)^k \cos n\alpha_k. \quad (3.42b)$$

3.3.5.2.2.2 SHE implemented SAR in bipolar case

Similarly, for the bipolar case (3.45) can be written by referring to Fig. 3.10 (d).

$$b_n = \left(\frac{4}{\Pi}\right) \int_0^{\Pi/2} f(\alpha) \sin(n\alpha)(d\alpha), \text{ (where, } x > 0), \quad (3.44)$$

$$b_n = \left(\frac{4}{\Pi}\right) \left[\int_0^{\alpha_1} \frac{V_{dc}}{2} \sin(n\alpha)(d\alpha) - \int_{\alpha_1}^{\alpha_2} \frac{V_{dc}}{2} \sin(n\alpha)(d\alpha) + \int_{\alpha_2}^{\alpha_3} \frac{V_{dc}}{2} \sin(n\alpha)(d\alpha) - \int_{\alpha_3}^{\alpha_4} \frac{V_{dc}}{2} \sin(n\alpha)(d\alpha) + \int_{\alpha_4}^{\Pi/2} \frac{V_{dc}}{2} \sin(n\alpha)(d\alpha) \right], \quad (3.45)$$

$$b_n = \left(\frac{2V_{dc}}{n\Pi}\right) \left[[-\cos(n\alpha)]_0^{\alpha_1} + [\cos(n\alpha)]_{\alpha_1}^{\alpha_2} + [\cos(n\alpha)]_{\alpha_3}^{\alpha_2} + [\cos(n\alpha)]_{\alpha_3}^{\alpha_4} + [\cos(n\alpha)]_{\Pi/2}^{\alpha_4} \right],$$

$$b_n = \left(\frac{2V_{dc}}{n\Pi}\right) [-2 \cos(n\alpha_1) + 1 + 2 \cos(n\alpha_2) - 2 \cos(n\alpha_3) + 2 \cos(n\alpha_4)], \quad (3.46)$$

$$b_n = \left(\frac{2V_{dc}}{n\Pi}\right) \left[1 + 2 \sum_{k=1}^m (-1)^k \cos(n\alpha_k) \right]. \quad (3.47)$$

The angles for the unipolar and bipolar were calculated by expanding (3.43) and (3.47) to zero with the fundamental equated to M . The presence of trigonometric terms, which have a transcendental nature, adds to the complexity caused by numerous or no results. In order to resolve the issue of non-linear equations obtained through the direct solution or traditional method, SAR comes into the picture. Also, to

reduce the wider range of harmonics, existing methods are confined to discontinuity at certain points or require a higher number of gating pulses. Lower switching is desirable due to lower switching losses and effective efficiency. SAR helps to mitigate a wider range of harmonics with only fewer optimized angles. It also reduces the harmonics in the stator side voltage of the DFIG, thus reducing the overall THD. These angles are determined offline and put into the Digital Signal Processor (DSP) lookup table memory for online usage. The angles achieved for the minimum voltage THD with respect to the closed point of M are taken for the consideration of linearity. Thus, the problem of discontinuity was solved by using the SHE technique.

3.3.6 APPLICATION OF OPTIMIZATION TECHNIQUE FOR HARMONIC MITIGATION

Optimization technique has been used to extract angles so that the minimum possible THD can be calculated to get the optimized result. To calculate the angles for RSC, GSC and CC SAR based SHE was used.

3.3.6.1 SEARCH AND RESCUE OPTIMIZATION ALGORITHM IN DETAIL

This algorithm is based on search and rescue operations for various aims, such as searching for food sources, lost people, or hunting strategies, etc. Codes for training are provided by institutes such as the American Society for Testing and Materials (ASTM) and the National Fire Protection Association (NFPA). The training is helpful in indicating the probability of the presence or locating an object by clues and traces [3.44]. The clues are classified into two.

1. Hold a clue- At the initial stage, wherever a clue is found, it is set aside.
2. Abandoned clue- The clue found by humans is set aside in the search for better clues.

The hold and abandoned clues are stored in matrices such as X (for locating humans) and M (memory matrices) respectively. The N , D , and C represent the number of humans, the dimension of the problem, and the clue matrix, respectively. So, humans search for clues or in the direction in which the clue points. This can be classified into two categories.

$$C = \begin{bmatrix} X \\ M \end{bmatrix} = \begin{bmatrix} X_{11} \dots X_{1D} \\ \vdots \\ X_{N1} \dots X_{ND} \\ M_{11} \dots M_{1D} \\ \vdots \\ M_{N1} \dots M_{ND} \end{bmatrix}, \quad (3.48)$$

3.3.6.1.1 Phases of the SAR

- **Social phase**

They connect the found clues together and search in that particular direction. Initially, for every human, a clue is selected arbitrarily from the matrix C . The search direction is given below:

$$SD_i = (X_i - C_k), k \neq i, \quad (3.49)$$

Where X_i , C_k , and SD_i are the i^{th} human location, for locating k^{th} clue, in i^{th} human direction, respectively. K is the arbitrary integer ranging within $[1, 2N]$. As, $k \neq i$, the probability of searching the lost person increases, and search is done around the position that has better clues. For maximization problems, ($X_i > C_k$), X_i is selected to search and vice versa. Furthermore, the humans try to explore a certain location only one time in search and rescue operations. Hence, movements of humans toward each other should be limited [3.44]. This limitation is imposed by the binomial crossover operator. The updated i^{th} human in all dimensions is given by

$$X'_{i,j} = \begin{cases} \begin{cases} C_{k,j} + r_1 * SD_{i,j}, & \text{if } f(C_k) > f(X_i) \\ X_{i,j} + r_1 * SD_{i,j}, & \text{otherwise} \end{cases} & \text{if } r_2 < SE \text{ or } j = j_{rand} \\ X_{i,j}, & \text{otherwise,} \end{cases} \quad (j = 1, \dots, D), \quad (3.50)$$

Where $X'_{i,j}$ is the upgraded location of the j^{th} dimension for the i^{th} human, $C_{k,j}$ is the location of the j^{th} dimension for the stored clue k^{th} , $f(C_k)$ and $f(X_i)$ are the objective function for C_k and X_i solution respectively. r_1 and r_2 is considered randomly within $[-1, 1]$, $[0,1]$ respectively, where r_1 values are constant for each dimension and r_2 varies. j_{rand} is considered randomly within $[1, D]$ which ensures that at least one dimension of $X'_{i,j}$ is different from $X_{i,j}$. A social effect (SE) is an algorithm parameter ranging between 0 and 1. In the social phase, SE is used to control the group member's effect.

➤ Individual Phase

It is focused on the search based on or around the current positions, regardless of the position and number of clues found by others. The idea of connecting different clues is used for this phase. The updated location of the i^{th} human is calculated as the following equation:

$$X'_i = X_i + r_3(C_k - C_m), i \neq k \neq m, \quad (3.51)$$

Where, k and m are random integers from the range $[1, 2N]$. r_3 is a random number ranging within $[0, 1]$. For each human search phase matrix, C is upgraded.

➤ Boundary Control

The social and individual phase solutions should be located in the solution space, and if they are absent, they should be updated. The updated i^{th} human position is given by (3.52).

$$X'_{i,j} = \left\{ \begin{array}{l} (X_{i,j} + X_j^{\max})/2, \text{ if } X'_{i,j} > X_j^{\max} \\ (X_{i,j} + X_j^{\min})/2, \text{ if } X'_{i,j} < X_j^{\min} \end{array} \right\} \quad (j = 1, \dots, D), \quad (3.52)$$

Where, X_j^{\max} and X_j^{\min} indicate the maximum and minimum of the j^{th} dimension respectively.

➤ Upgrading Information and Positions

For maximization problems for condition mentioned in (3.53), the old position (X_i) will be stored randomly in memory matrix (M) which is the new position, or else this position is discarded and the memory contains the old value. It can be given as

$$M_n = \left\{ \begin{array}{l} X_i, \text{ if } f(X'_i) > f(X_i), \\ M_n, \text{ otherwise,} \end{array} \right. \quad (3.53)$$

$$X_i = \left\{ \begin{array}{l} X'_i, \text{ if } f(X'_i) > f(X_i), \\ X_i, \text{ otherwise,} \end{array} \right.$$

Where M_n is the position of the n^{th} stored clue in the matrix (M). n is chosen at random from the range $[1, N]$.

➤ Abandon Clues

As this algorithm is based on finding a lost human or object (as they can be injured) in the minimum possible time, humans must stop unsuccessfully searching for clues after some effort. The number of unsuccessful searches of each human is stored for each human. The unsuccessful search number (USN) is set to 0. Also, whenever a human finds better clues, it is set to 0 for that human, otherwise, it will be updated to 1.

$$\left\{ \begin{array}{ll} USN_i + 1, & \text{if } f(X'_i) < f(X_i), \\ USN_i = 0, & \text{otherwise,} \end{array} \right. \quad (3.54)$$

A solution is left when it cannot be improved after a specific number of searches given by Maximum Unsuccessful Search Number (MU). Then, a new solution replaces using (3.55).

$$X_{i,j} = X_j^{\min} + r_4(X_j^{\max} - X_j^{\min}), \quad (j=1, \dots, D), \quad (3.55)$$

Where $X_{i,j}$ is position of the j^{th} dimension for the i^{th} human, r_4 is a random number for the j^{th} dimension ranging within $[0,1]$. With the increase in search space, the MU also increases.

3.3.6.1.2 Control Parameters of SAR

Social Effect and Maximum Unsuccessful Search Number are the two controlling parameters. In the social phase, SE manages the group members' effects on one another, ranging within $[0, 1]$ and MU ,

ranging within $[0, 2 T_{\max}]$, where T_{\max} is the maximum number of searches done by each human, i.e., the maximum number of iterations. The larger the SE , the higher the convergence rate, elapsed time, and also the decrease in the global search ability of the algorithms. However, the higher the MU value, the less likely humans are to leave traces. Smaller values of this parameter consist of three members in the group finishing searching around the current clue and going to other locations before completely searching around it. However, larger values are searched for around one clue, and the chance of searching for it in other zones is reduced. The SE was set to 0.05 and the value of the MU was obtained using (3.32).

$$MU = 70 * D . \quad (3.56)$$

The Pseudocode algorithm for SAR

1. Begin:
2. The population of $2N$ solutions were randomly initialized ranging X_j^{\max} and X_j^{\min} where, $j=1, \dots, D$.
3. The solutions were in decreasing order and the current best position (X_{best}) was found.
4. The first half of the sorted solutions were used for (X) and others were used for matrix (M).
5. SE and MU was defined and $USN_i = 0$ was set where $i = 1, \dots, N$.
6. While loop, stop if criteria unsatisfied do.
7. For $i=1$ to N do.
8. Using (3.48), (C) was updated.
9. Using (3.49), (SD_i) was generated.
10. For $j=1, \dots, D$ do.
11. The new j^{th} dimension of the i^{th} human was computed using (3.50).
12. Boundary control of the new j^{th} dimension of i^{th} human was updated using (3.51).
13. End of For loop.
14. The n^{th} memory and position of the i^{th} human was updated using (3.53).
15. USN_i was updated using (3.54).
16. Using (3.48), (C) was updated.
17. The i^{th} human position was computed using (3.48).
18. Boundary control for the new position of the i^{th} human was updated using (3.51).
19. The n^{th} memory and human's position was updated using (3.53).
20. (3.33) subjected to (3.16) was updated.
21. USN_i was updated using (3.54).

22. If $USN_i > MU$ do.
23. For $j=1, \dots, D$ do.
24. The j^{th} dimension of the i^{th} human was computed using (3.50).
25. End for loop.
26. Set $USN_i = 0$.
27. End If loop.
28. End for loop.
29. The current best position was found and X_{best} was updated.
30. End while loop.
31. Final X_{best} displayed the minimum possible THD with the corresponding switching angles.
32. End.

3.3.6.2 SAR Application for harmonic compensation in detail

3.3.6.2.1 Angle obtained for RSC and GSC SHEPWM inverter

The angle generation for the inverters was done using the SAR-based SHEPWM technique. The fundamental voltage harmonics amplitude component is equated to modulation index and the other to zero as described in (3.43) and (3.47), three switching angles were achieved and stored offline in the microcontroller memory. It was used to mitigate lower order harmonics, e.g., 5th, 7th, 11th, and 13th, yet the rest of the higher order harmonics, e.g., 17th, 19th, 23rd, 25th, 29th, and so on, would still be present. So, to mitigate existing higher-order harmonics, a proposed series compensation has been executed using a CC.

3.3.6.2.2 Angle generation for compensating SHEPWM converter to mitigate higher orders

In order to ignore the complexity for finding the solution to a transcendental equation, the problem has been converted to an optimization function $t_1(\alpha)$ given in (3.56). The objective function used gives the choice to minimize certain harmonics that would affect the grid. The angles generated for CC to reduce the existing dominant harmonics uses the objective function given as

$$t(\alpha) = K_1 * (b_1 - M)^2 + K_5 * \varepsilon_2^2 + \dots + K_n * \varepsilon_n^2, \quad (3.56)$$

$$\text{Subjected to } 0 < \alpha_1 < \alpha_2 \dots < \alpha_m < \Pi/2.$$

where, $K_1 \dots K_n$ are the values appointed to the harmonics to be reduced in priority, $\varepsilon_1 \dots \varepsilon_n$ are the values that depends upon the amplitude of the particular harmonic to be suppressed. Generally, the values are close to zero but in the present case it is set in the manner in which the higher-order harmonics are to be reduced. This can be illustrated with an example. Suppose the 17th and 25th harmonics are 18% and 34%

of the harmonic amplitude, respectively. So, now the weights have to be kept in accordance with the priority. The 25th is given priority over the 17th in reducing the amplitude. For that, ε_{25} has to be set to 34% value but in the opposite phase to cancel out the 25th harmonic. In this case, the values of weights would be $K_1 = 150$, $K_5 = K_7 = K_{11} = K_{13} = 80$, $K_{17} = 90$, $K_{19} = K_{23} = K_{29} = 80$, and $K_{25} = 140$. Similarly, this works for any harmonic order of whatever amplitude. The objective function (3.33) has been incorporated into the SAR algorithm to particularly remove existing dominant harmonics. The process was redone until convergence was achieved and the desired result was attained. The angles obtained by using (3.33) in the SAR-based SHEPWM technique strictly follow the conditions depicted in (3.12). A conventional technique would reduce the undesired harmonics and monitor the amplitudes of fundamental components. But using the SAR algorithm metaheuristic technique has helped in controlling the lower order harmonics, and higher-order harmonics are reduced or suppressed by the objective function (3.56). These obtained five angles are then fed to the CC, undergoing series compensation with the RSC and GSC as shown in Fig. 3.9. Thus, the selected lower and higher-order harmonics are suppressed by employing the SAR-based SHE technique. So, the THD obtained has been reduced by a substantial amount by using (2.24) in the SAR algorithm.

3.3.7 CONTROL STRATEGY USED

A piecewise mixed model has been used for solving linear and non-linear equations to find the angles. The standard active and reactive power, P^* and Q^* , were compared with the P and Q controllers as shown in Fig. 3.1. The M was computed on the basis of reference voltages V_a^* , V_b^* , and V_c^* found by tuning the PI controller. Then, the stored SHE-PWM-based angles corresponding to M were used, available in the processor memory for optimum voltage THD. The desired switching angles for minimum THD are calculated offline with different modulation indices using SAR algorithm as shown in Fig. 3.9. The higher-order harmonics at the rotor side have a smaller magnitude, so their effect would also be smaller in the stator voltage waveform, but lower orders are significant. For the present scheme, the speed range is computed by a varying slip in the -30% to $+30\%$ range. While computing the triggering pulses through SAR, the objective function (3.56) is adjusted in such a way that it eliminates lower order harmonics and the rest are minimised by three switches per quarter cycle. Similarly, five switches per quarter cycle are adopted for the other speed ranges because of the distortions on the stator side. The switching angles are separately calculated off-line for all three, and five switching methods and stored in the processor memory through mixed model equations for the on-line application shown in Fig. 3.16. The linear and the non-linear equation at each segment of the curve was derived through the mix model equation given in [3.24].

This magnetising curve equations for five switching angles used in the piecewise mixed-model are given below:

In the case of the SAR-based optimization technique,

For, $0.5 \leq MI \leq 0.7$

$$\alpha_1 = -132MI + 64.4,$$

$$\alpha_2 = -120MI + 107.33,$$

$$\alpha_3 = -110MI + 104,$$

$$\alpha_4 = -100MI + 141,$$

$$\alpha_5 = -120.40MI + 105.67.$$

For, $0.71 \leq MI \leq 0.9$

$$\alpha_1 = 525MI^2 - 880MI + 144,$$

$$\alpha_2 = 479MI^2 - 547MI + 200,$$

$$\alpha_3 = -120MI^2 - 140MI + 28, \quad (3.57)$$

$$\alpha_4 = 147MI^2 - 150MI + 100.5,$$

$$\alpha_5 = 400MI^2 - 704.3MI + 300.$$

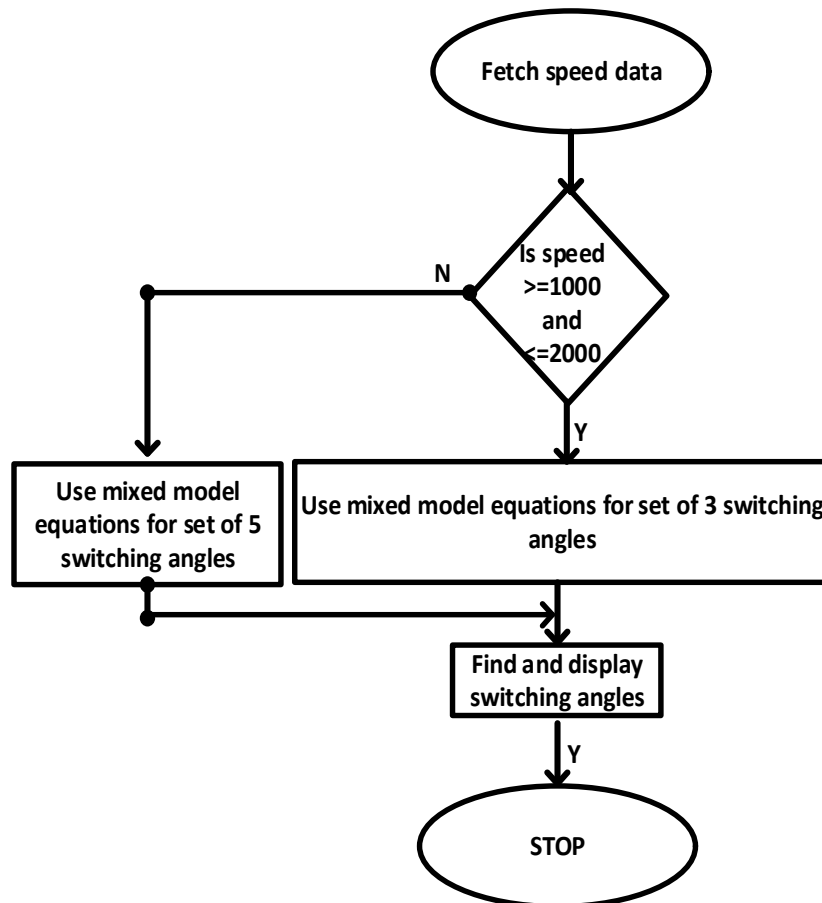


Fig. 3.11 Flowchart for the controller used

Similarly, equations for three or seven switching methods were calculated and stored in processor memory. Gate pulses for the converters are fetched as per the stored data in the microprocessor memory for minimum voltage THD. In the present scenario, to avoid any fluctuation in the stator voltage during the speed transition due to a change in the number of switching angles, a hysteresis of 5 rpm was adopted.

For on-line application, the overall control is governed by the flowchart that can be seen in Fig. 3.3. The RSC controller decides the M to provide the desired magnitude of injected voltage and speed as measured by the speed sensor.

3.3.7.1 Reactive power compensation

Two types of control have been carried out, one at the rotor side and the other at the grid side.

- RSC controller

The job of RSC is to apply voltage to the rotor winding. The active power at stator and torque was controlled by rotor current in the q axis and reactive power was controlled by rotor current in the d axis. It has been also detailed in section 3.2.5.3. These calculations were carried out with the considerations such as resistance winding drop at the stator side was considered to be zero and stator flux as zero [3.43]. The control strategy was applied for converting $a b c$ components of voltage and current to $d q$. The RSC controller has been given in Fig 3.1 (a). In order to transform the rotor voltage and current into d q components using the below equations:

$$P_s = \frac{3}{2} [-i_{qs} V_{qs}] = \frac{3L_m}{2L_s} [i_{qr} w_e \Phi_{ds}] \quad (3.25a)$$

$$Q_s = \frac{3}{2} [i_{ds} V_{qs}] = \frac{3w_e}{2} [i_{ds} \Phi_{ds}] \quad (3.26a)$$

$$T_{em} = \frac{3PL_m}{2*2L_s} [-i_{qr} \Phi_{ds}] \quad (3.29a)$$

The reference voltages at the rotor side for d and q axis has been given in the equation below:

$$V_{dr_ref} = V_{dr}^* - (w_e - w_r) \sigma_s L_r i_{qr} \quad (3.30)$$

$$V_{qr_ref} = V_{qr}^* + (w_e - w_r) \left(\sigma_s L_r i_{dr} + \frac{L_m^2}{L_s} i_{ms} \right) \quad (3.31)$$

- GSC Controller

GSC control strategy control power flow of the DFIG. To carry out the process two components are responsible one is the voltage at the bus and the other is reactive power exchange at the grid for this. The equations at the active and reactive power exchange with the grid is given as follows.

$$P_c = \frac{3}{2} (V_d i_{dg}) \quad (3.32)$$

$$Q_c = -\frac{3}{2} (V_d i_{dg}) \quad (3.33)$$

The path of active power is through RSC to DC link to GSC and then to grid. When the bus voltage is constant active power flow is carried out efficiently and similar is the process for the reactive power flow

and thus pulses are obtained for GSC. The controller has been given in Fig. 3.1 (b). The reference voltages for the grid in d and q axis are given as follows:

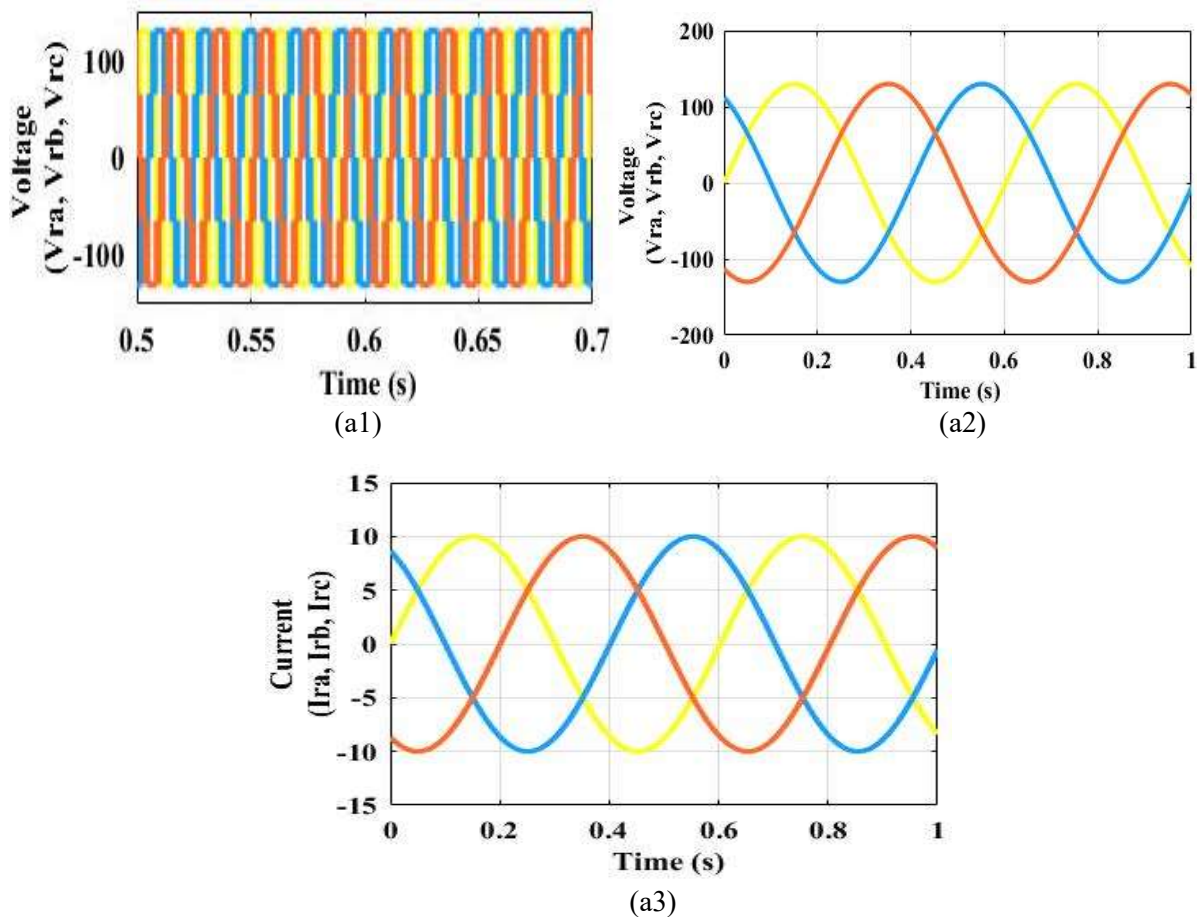
$$V_{dg-re} = -V_{dq}^* + w_e L_{choke} i_{dq} + V_d \quad (3.34)$$

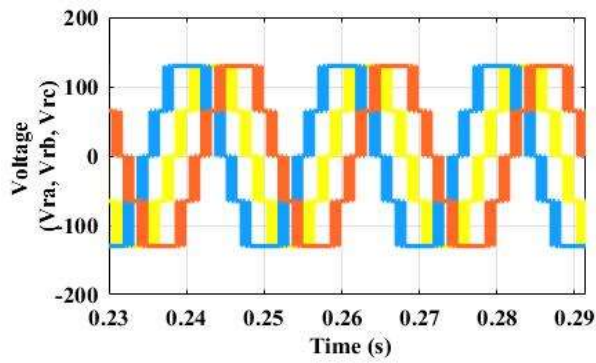
$$V_{qg-ref} = -V_{dq}^* + w_e L_{choke} i_{dq} \quad (3.35)$$

3.3.8 RESULTS

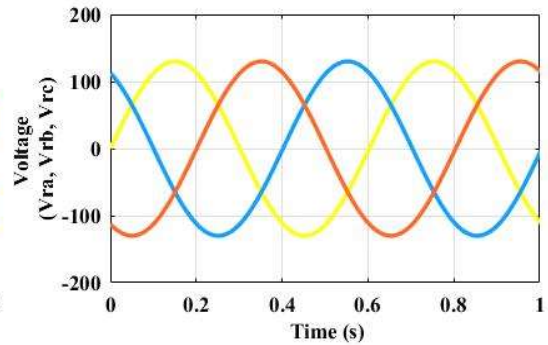
3.3.8.1 MATLAB Simulation results

The simulation was executed in MATLAB 2016b. The stator and rotor voltage and current waveforms in 180° mode and SHE mode under harmonic and non-harmonic conditions are shown in Fig. 3.12. The bipolar switching technique was simpler compared to the unipolar ones, but the THD obtained was less in the latter case. The rotor voltage is shown in Figs. 3.12 (a1), (b1), and (c1) for 180° and SHE in unipolar and bipolar mode, respectively, at a speed of 1250 rpm. This was obtained without eliminating harmonics. Similarly, modified rotor voltages and currents after harmonic elimination up to the 29th harmonic are shown in Figs. 3.12 (a2), (b2), (c2), and Figs. 3.12 (a3), (b3), (c3). The corresponding stator voltage for the 180° and SHE conduction modes is shown in Figs. 3.12 (d1) and (e1) without harmonics elimination. Figs. 3.12 (d2), (e2) and Figs. 3.4 (d3), (e3) show the stator voltage and current after harmonics are removed.

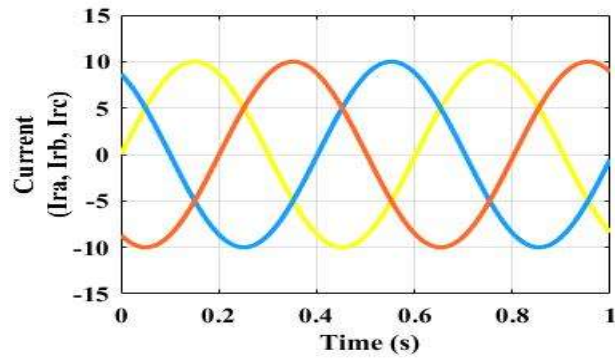




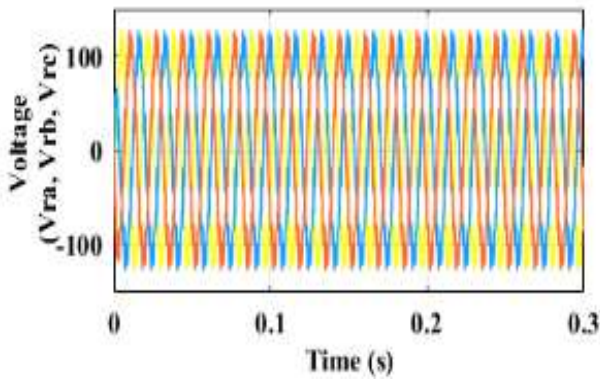
(b1)



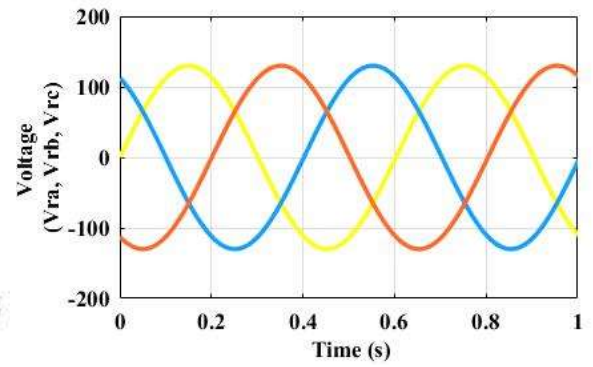
(b2)



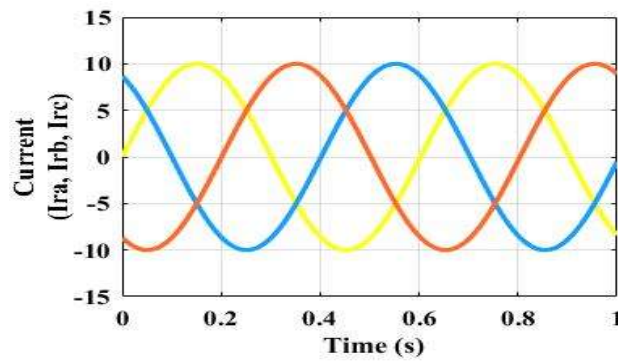
(b3)



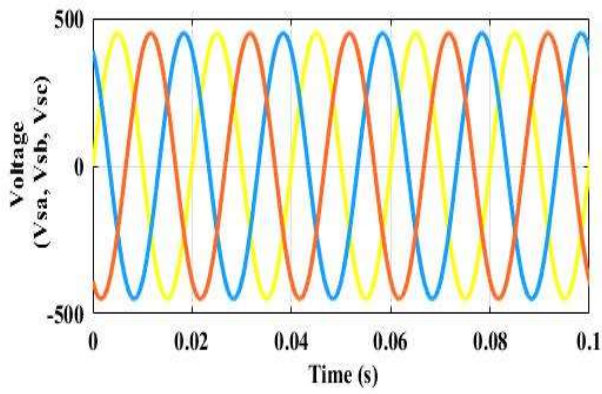
(c1)



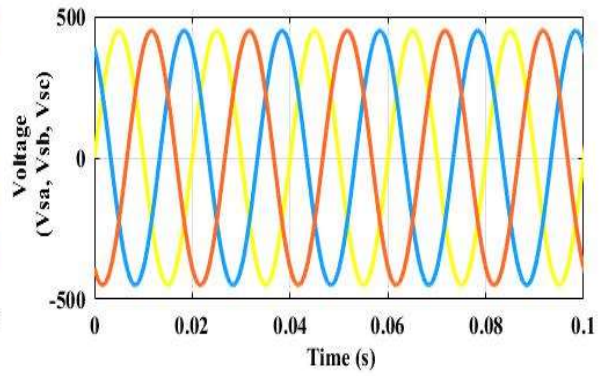
(c2)



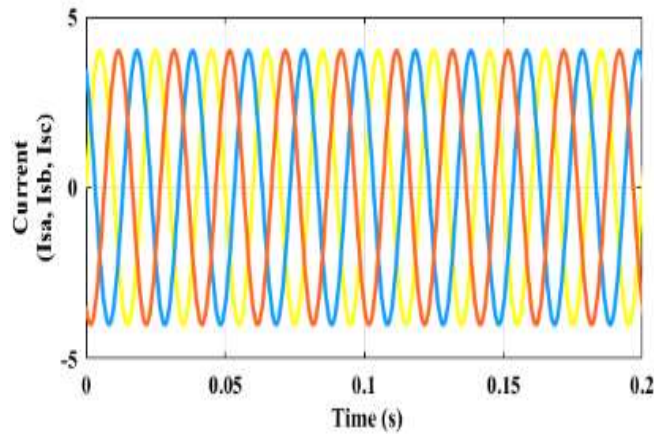
(c3)



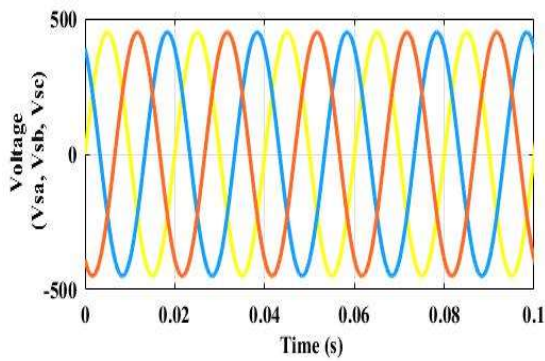
(d1)



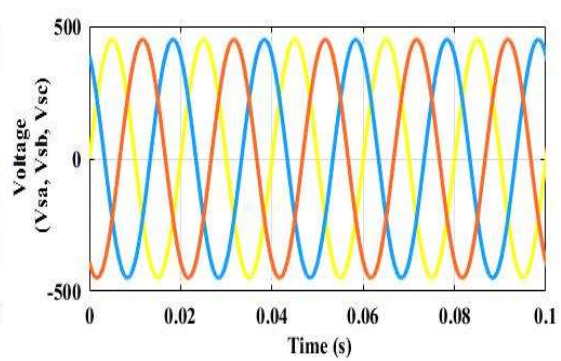
(d2)



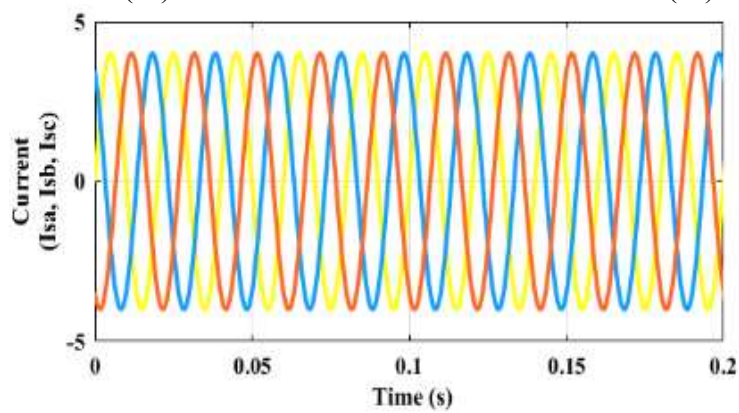
(d3)



(e1)



(e2)



(e3)

Fig. 3.12 DFIG outputs at a speed of 1250 rpm a) Rotor voltage and current in 180° conduction mode (a1) without harmonic elimination (a2) with harmonic elimination (a3) with harmonic elimination b) Rotor voltage and current

in SHE unipolar (b1) without harmonic elimination (b2) with harmonic elimination (b3) with harmonic elimination (c) Rotor voltage and current in SHE bipolar (c1) without harmonic elimination (c2) with harmonic elimination (c3) with harmonic elimination (d) Stator voltage and currents with quasi sine rotor injection in 180° conduction mode (d1) without harmonic elimination (d2) with harmonic elimination (d3) with harmonic elimination (e) Stator voltage and current in SHE (e1) without harmonic elimination (e2) with harmonic elimination (e3) with harmonic elimination

3.3.8.2 Experimental results

A laboratory setup is shown in Fig. 3.13. The stator was coupled with the grid, and the rotor was fixed to the converter system. A set of insulated gate bipolar transistors (IGBT) were used whose gate pulses were given from the microcontroller PIC18F452 based programmer. A driver circuit was made using TLP250H and it was powered by individual rectifier circuits. A PV panel rated at 260 W was used by VIKRAM Solar Company, powered by artificial insolation using incandescent bulbs. The outputs were observed in a Digital Storage Oscilloscope (DSO) by applying a load of 1 kVA at a power factor of 0.8 lag. The ratings used have been mentioned in Table 3.13.

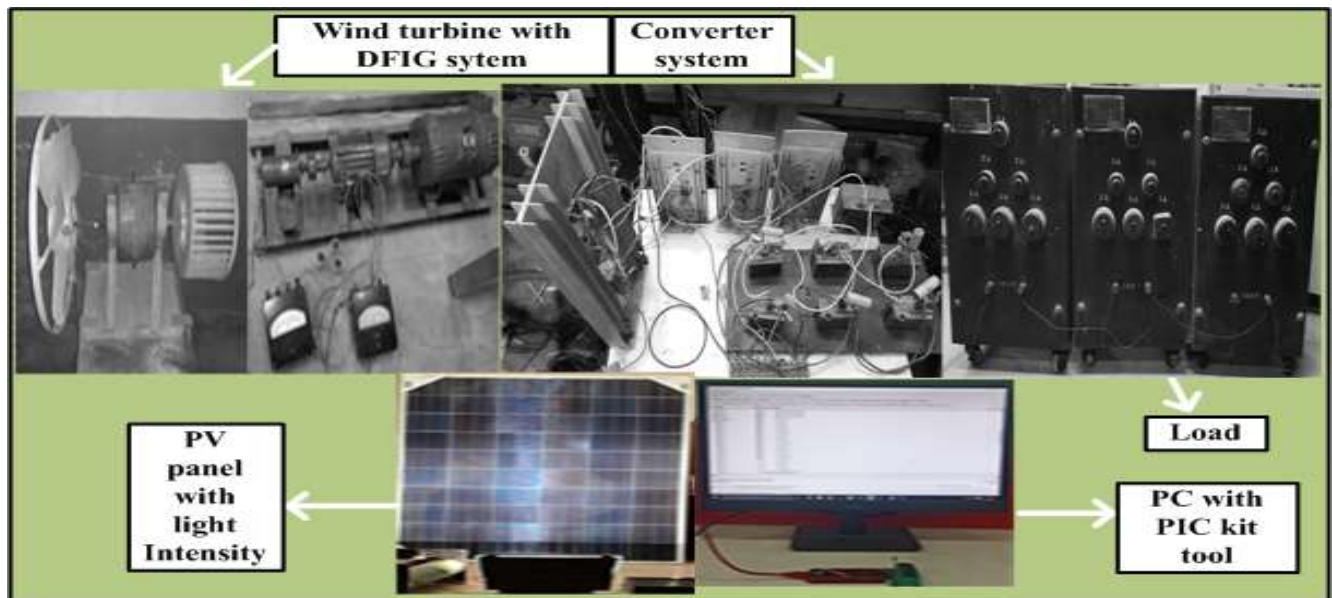


Fig. 3.13 Laboratory setup

Table 3.4 Ratings of the model used

DFIG Specification				Solar Panel Specifications		Grid Specification	
Stator Parameters		Rotor Parameters		Voltage	110 V	Grid voltage	415 V
Supply Voltage	415 V	Rotor Voltage	110 V				
Stator frequency	50 Hz	Resistance	8 Ω	Open Circuit Voltage	35.24 V		
Power	2.8 kW	Rotor speed	1450 rpm	Short Circuit Current	8.57 A		
Inductance	0.06 H	Inductance	0.06 H				

Resistance	9 Ω		
Mutual inductance	0.79 H		

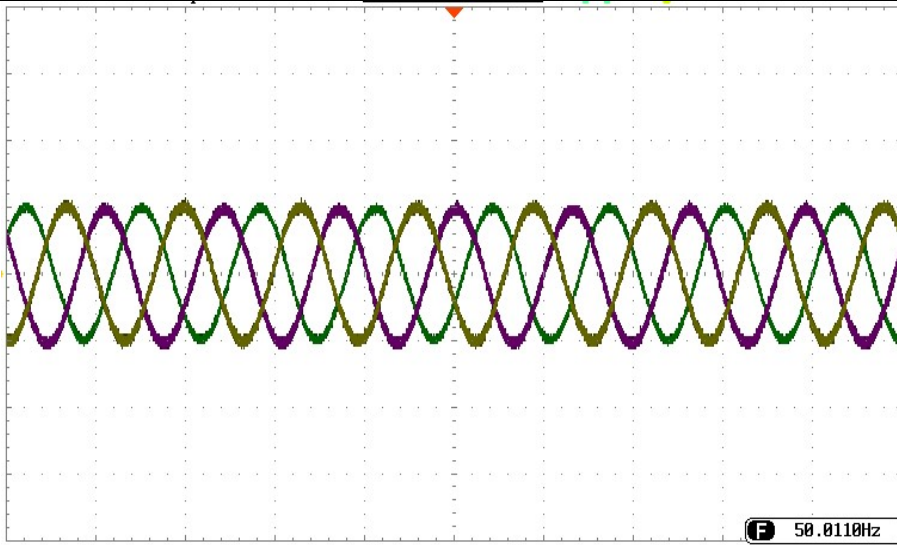
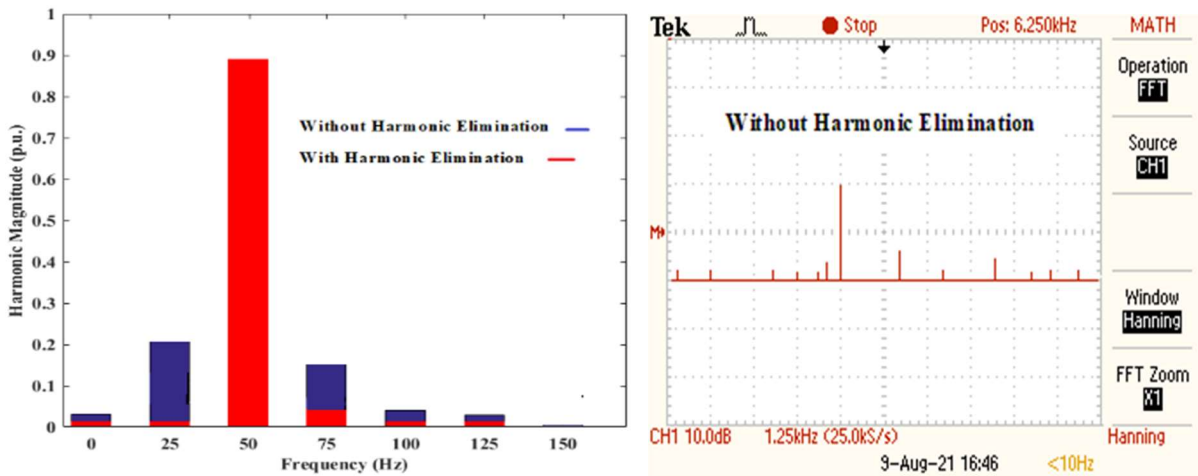


Fig. 3.14 Stator side voltage waveform for three switching (channels 1, 2 and 3: Y-axis: 500 V/div.)



(b(ii))

Fig. 3.15 Voltage harmonic spectra at the stator side a) simulation results b) experimental results i) without harmonic elimination, ii) with harmonic elimination

The hardware results for SHE unipolar at the stator side voltage waveform can be observed in Fig. 3.14. It corroborates with the simulation result shown in Fig. 3.12 (e2). Figs. 3.15 (b (i)) and (b (ii)) show the experimental harmonic spectra at the stator side for three switching per quarter cycle at a speed of 1250 rpm. This has been carried out at the modulation indices of 0.8 where most of the harmonics has been mitigated. It indicates that using the proposed method improves performance and corroborates the simulation results shown in Fig. 3.15 (a). The before and after harmonic spectra of stator voltage are presented in Fig. 3.7. It shows significant improvement after the application of the proposed method. The matching experimental harmonic spectra are displayed in Fig. 3.15, illustrating that the proposed technique validates the simulation results.

3.3.8.3 Comparative analysis of existing schemes with the state-of-the-art

The minimum weighted THD with varying M for 3, 5, and 7-switching per quarter cycle was shown in Fig. 3.16.

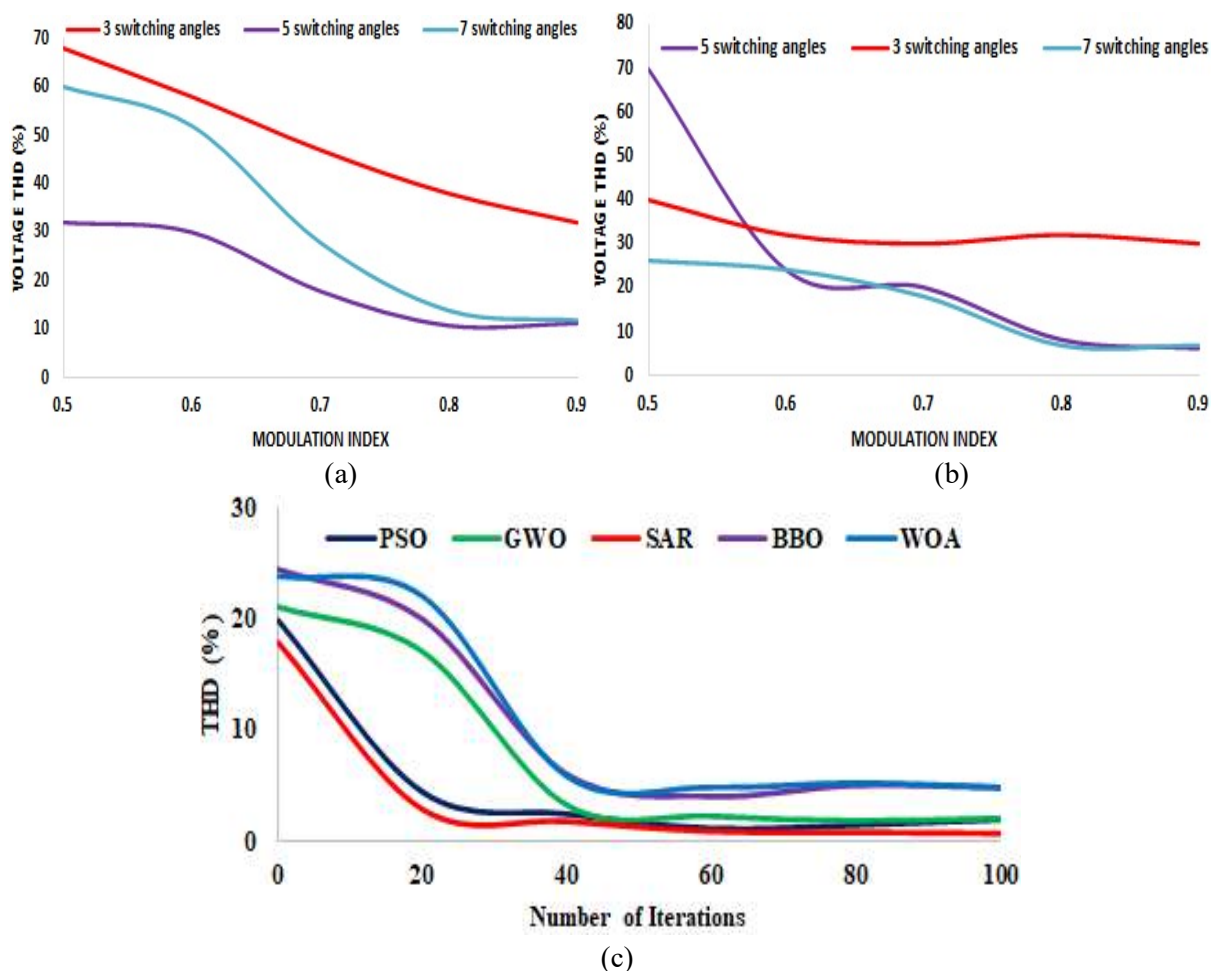


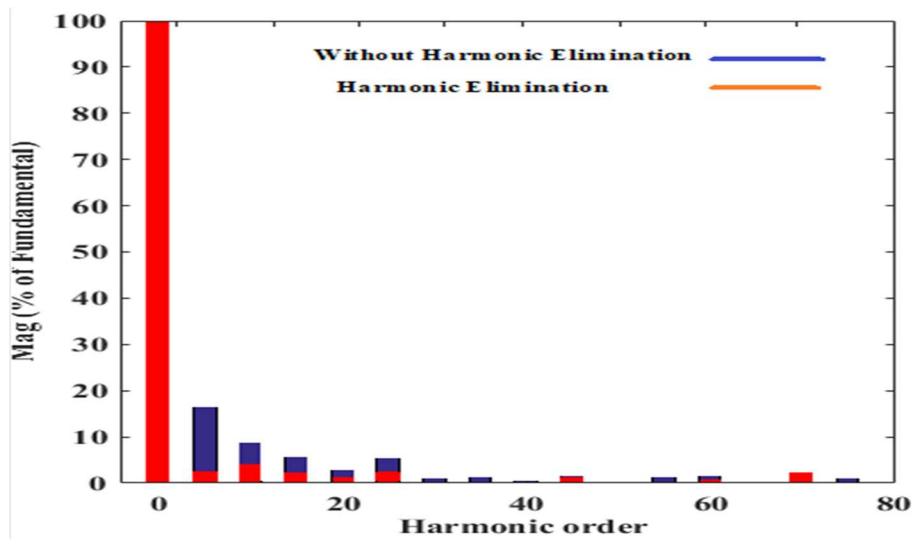
Fig. 3.16 DFIG outputs a) switching angle variation vs. modulation index for 180° conduction mode. b) SHE switching angle vs. modulation index variation c) Plot of voltage THD over variation in iterations

The switching angles for 180° and SHE are given in Fig. 3.16 (a) and (b) respectively. It was observed that by using the objective function (3.33) in SAR algorithm three switching's are capable of reducing THD significantly. Thus, lower number of switching's helps in reducing losses and increasing the life and efficiency of the converters. The performance is better in the case of SHE mode. As shown in Fig. 3.16 (c), SAR-based convergence and THD are much faster than other techniques. The SAR technique being used has faster and more accurate convergence with a smaller number of tuning parameters. The objective function in (3.56) converges to much lower values compared to other algorithms. SAR has been used for the extraction of optimised switching angles for the minimum possible THD, and comparatively, it has been found that in the present prototype, SAR suits better. It has also outperformed other metaheuristic techniques like PSO, GWO, BBO, WOA, etc., as shown later in terms of faster and more accurate convergence with a smaller number of tuning parameters. Thus, with fewer switching losses, system utility is maintained. The details of the parameters used for different evolutionary techniques are given in Table 3.5.

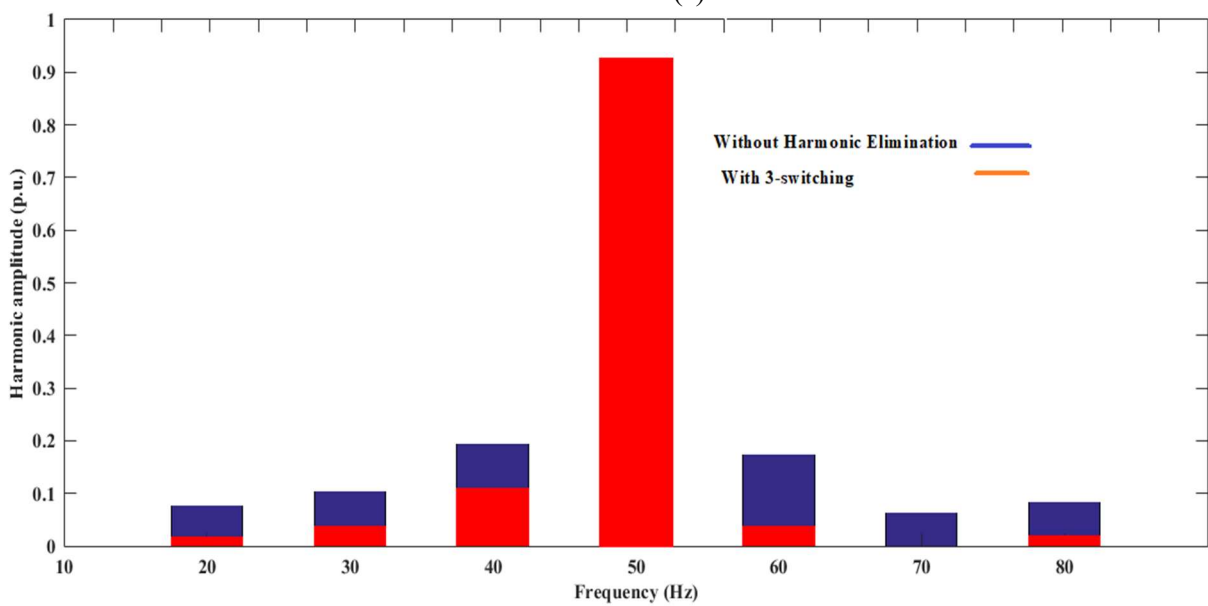
Table 3.5 Different Parameters used for various search-based optimization techniques

PSO		WOA		GWO		BBO		SAR	
Weight (w)	0.4	Population matrix	10*5	Population matrix	10*5	Population size	50	Population size	100
Balance factors c_1, c_2, c_3, c_4	1.3,0.6,1.9, 1.7					Genes in each population	5		
Random variable r_1, r_2	0.6, 0.5	Random variable r_1, r_2	0.7, 0.6	Random variable r_1, r_2	0.7, 0.6	Elitism value	2	Random variable r_1, r_2, r_3, r_4	0.8,0.6, 0.3,0.7
No. of equations	Low	No. of equations	Low	No. of equations	Low	No. of equations	High	No. of equations	Medium
Complexity	Easy	Complexity	Easy	Complexity	Easy	Complexity	Moderate	Complexity	Moderate
Elapse time (s)	0.43	Elapse time (s)	0.22	Elapse time (s)	0.26	Elapse time (s)	0.34	Elapse time (s)	0.19
THD (%)	2.5	THD (%)	2.8	THD (%)	2.98	THD (%)	3	THD (%)	1.8

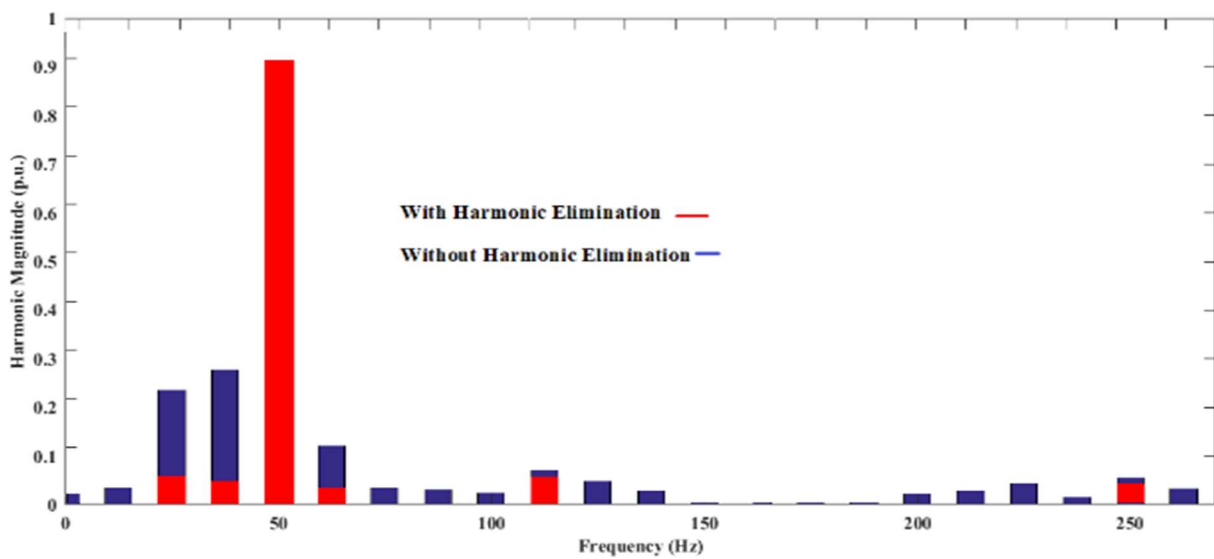
Generally, in these techniques, three switching angles can eliminate the 5th and 7th, five switching angles eliminate the 5th, 7th, 11th, and 13th, and seven switching angles can remove the 5th, 7th, 11th, 13th, 17th and 19th etc. It was found that three switching angles had superior performance over five and seven switching angles. It was able to mitigate higher orders of harmonics with the same seven switches but with three angles. It was capable of eliminating the 5th, 7th, 11th, 13th, 17th, and 19th the same as seven switching does. The objective function (3.56) has been used to achieve the optimized switching angles. The fifth, seventh orders of harmonics and the fundamental voltage amplitude have been set to zero and the desired M , respectively.



(a)



(b)



(c)

Fig. 3.17 FFT analysis of the output voltage at a speed of 1250 rpm for three switching angles a) at the rotor side b) at the stator side for 180° conduction c) at the stator side in SHE

At the modulation index of 0.8, voltage harmonics for 180° conduction and the SHE mode in rotor and stator side are shown in Fig. 3.10. The voltage harmonics spectra have been carried out for each case for both with and without harmonic eliminations. The reduced harmonic magnitude validates the excellence of the proposed scheme. The switching angles obtained from SAR algorithm at m_i of 0.8 are $\alpha_1=30.88^\circ$, $\alpha_2=34.21^\circ$, $\alpha_3=44.01^\circ$; $\alpha_1=23.56^\circ$, $\alpha_2=34^\circ$, $\alpha_3=38.34^\circ$; $\alpha_1=11.88^\circ$, $\alpha_2=20.48^\circ$, $\alpha_3=32.89^\circ$ in the pattern mentioned in (3.56) for the converters. Voltage harmonic amplitude for the standard and proposed technique has been given in Table 3.6.

Table 3.6 Analysis of harmonic amplitudes of the literature survey with the present scheme

Standard Reports used										
Voltage harmonics amplitude on grid synchronization	b ₅	b ₇	b ₁₁	b ₁₃	b ₁₇	b ₁₉	b ₂₃	b ₂₅	b ₂₉	THD (%)
[25]	5	4	3	2.5	1.6	1.2	1.2	1.2	1.06	6.5
CIGRE WG 36-05 [28]	6	5	3.5	3	2	1.5	1.5	1.5	--	8
IEEE-1547 and 2030 [26], [27]										5
Proposed Technique used										
Voltage harmonics amplitude after series compensation	b ₅	b ₇	b ₁₁	b ₁₃	b ₁₇	b ₁₉	b ₂₃	b ₂₅	b ₂₉	THD (%)
Values for SHE unipolar switching mode	0.89	0.27	0.17	0.35	0.5	0.9	0.17	0.08	0.05	1.8
Values for SHE bipolar switching mode	1.12	0.5	0.25	1.1	0.22	1.8	1.8	1.12	2.08	3.58
Values for 180° conduction	1.56	1.2	0.45	0.7	0.78	2	1.3	0.2	0.9	2.9

Table 3.7 Comparison of existing schemes with the State-of-the-Art

Reference	Technique used	THD (%)
[6]	Filter compensation modules	5.1
[7]	UPQC	3.71
[15]	Vol/var/THD control	14.63
[16]	IWOA based MLI	12.42
Proposed Scheme	SAR based SHE	1.8

All the switching methods are verified and any can be used to control the RSC, but the performance of SHE unipolar outperformed in terms of the minimum possible optimised THD. Table 3.7 shows a comparative analysis of the existing and proposed schemes.

3.3.9 CONCLUSION

A modified harmonic suppression technique was proposed using the SAR-based optimization technique. Switching angles were generated using this metaheuristic technique to feed the converters. The present model uses the SAR-based SHEPWM technique, which deals with just three switching angles per half cycle, hence contributing to lower converter losses and an increase in system utility. The proposed series compensation has supported drastically eliminating lower-order harmonics and massively suppressing the higher-order harmonics. The THD obtained from the output voltage waveform was minimized by up to 1.8%, which is within the prescribed international standards of IEEE-519. Also, a comparative analysis has been carried out with different literature and it was found that the present scheme operates with ease and at a low cost, improving efficiency and extending the system's life. At low wind speeds and wide voltage variations, it maintains the voltage on the grid. For storing the generated switching angles from the metaheuristic technique piecewise mixed model approach was implemented for online applications. It was observed that the proposed scheme is efficient in improving power quality along with the series voltage compensation on the AC side. The results of the lab prototype have also been presented to corroborate the simulation results of the proposed scheme. Thus, it can be deduced that the present proposed scheme efficaciously attains the objectives cited in this chapter and, therefore, can be used for the practical purposes.

Publication

- ❖ Suman, S., Chatterjee, D., & Mohanty, R. (2022). Development of improved harmonic compensation technique for PV-wind hybrid distributed generator connected to microgrid. *Electric Power Systems Research*, 210, 108071. [SCI, Q1, Impact Factor 3.41]

References

- [3.22] Hannan, M. A., Lipu, M. H., Ker, P. J., Begum, R. A., Agelidis, V. G., & Blaabjerg, F. (2019). Power electronics contribution to renewable energy conversion addressing emission reduction: Applications, issues, and recommendations. *Applied energy*, 251, 113404.
- [3.23] Al-Quraan, A., and Al-Qaisi, M. (2021), "Modelling, Design and Control of a Standalone Hybrid PV-Wind Micro-Grid System", *Energies*, 14(16), pp. 48-49.
- [3.24] Shahriari, S.A.A. (2020), "Modelling and dynamic state estimation of a doubly fed induction generator wind turbine", *COMPEL - The international journal for computation and mathematics in*

electrical and electronic engineering, 39(6), pp. 1393-1409. DOI: <https://doi.org/10.1108/COMPEL-07-2019-0277>.

[3.25] Alkahtani, A. A., Alfalahi, S. T., Athamneh, A. A., Al-Shetwi, A. Q., Mansor, M. B., Hannan, M. A., & Agelidis, V. G. (2020). Power quality in microgrids including superharmonics: Issues, standards, and mitigations. *IEEE Access*, 8, 127104-127122.

[3.26] Alhato, M. M., & Bouallègue, S. (2019). Direct power control optimization for doubly fed induction generator-based wind turbine systems. *Mathematical and Computational Applications*, 24(3), 77.

[3.27] Khosravi, N., Abdol mohammadi, H. R., Bagheri, S., & Miveh, M. R. (2021). Improvement the harmonic conditions of the AC/DC microgrids with the presence of filter compensation modules. *Renewable and Sustainable Energy Reviews*, 143, 110898.

[3.28] Sarker, K., Chatterjee, D., & Goswami, S. K. (2018). Modified harmonic minimisation technique for doubly fed induction generators with solar-wind hybrid system using biogeography-based optimisation. *IET Power Electronics*, 11(10), 1640-1651.

[3.29] Wu, C., Cheng, P., Ye, Y., & Blaabjerg, F. (2020). A Unified Power Control Method for Standalone and Grid-Connected DFIG-DC System. *IEEE Transactions on Power Electronics*, 35(12), 12663-12667.

[3.30] Reddy, C., Goud, B.S., Aymen, F., Rao, G.S. and Bortoni, E.C. (2021). Power Quality Improvement in HRES Grid Connected System with FOPID Based Atom Search Optimization Technique. *Energies*, 14(18), pp.5812.

[3.31] Aljendy, R., Nasyrov, R.R., Abdelaziz, A.Y. and Diab, A.A.Z. (2019). Enhancement of power quality with hybrid Distributed generation and FACTS device. *IETE Journal of Research*, pp.1-12.

[3.32] Çelik, D. and Meral, M.E., (2019). Current control-based power management strategy for distributed power generation system. *Control Engineering Practice*, 82, pp.72-85.

[3.33] Çelik, D. and Meral, M.E., (2019). A novel control strategy for grid connected distributed generation system to maximize power delivery capability. *Energy*, 186, pp.115850.

[3.34] Çelik, D., (2022). Lyapunov based harmonic compensation and charging with three phase shunt active power filter in electrical vehicle applications. *International Journal of Electrical Power & Energy Systems*, 136, pp.107564.

[3.35] Patel, R., Hafiz, F., Swain, A. and Ukil, A., (2021). Nonlinear rotor side converter control of DFIG based wind energy system. *Electric Power Systems Research*, 198, pp.107358.

[3.36] Krishnamurthy, K., Padmanaban, S., Blaabjerg, F., Neelakandan, R. B., & Prabhu, K. R. (2019). Power Electronic Converter Configurations Integration with Hybrid Energy Sources—A Comprehensive Review for State-of-the-Art in Research. *Electric Power Components and Systems*, 47(18), 1623-1650.

- [3.37] Reddy, A. K. V. K., & Narayana, K. V. L. (2020). Optimal total harmonic distortion minimization in multilevel inverter using improved whale optimization algorithm. *International Journal of Emerging Electric Power Systems*, 21(3), pp. 20200008, DOI: <https://doi.org/10.1515/ijeeps-2020-0008>.
- [3.38] Kundu, S., Burman, A. D., Giri, S. K., Mukherjee, S., and Banerjee, S. (2020), "Selective harmonics elimination for three-phase seven-level CHB inverter using backtracking search algorithm", *International Journal of Power Electronics*, 11(1), pp. 1-19.
- [3.39] Antonio-Ferreira, A., Collados-Rodriguez, C. and Gomis-Bellmunt, O., (2018). Modulation techniques applied to medium voltage modular multilevel converters for renewable energy integration: A review. *Electric Power Systems Research*, 155, pp.21-39.
- [3.40] Zhou, D., & Blaabjerg, F. (2017). Bandwidth oriented proportional-integral controller design for back-to-back power converters in DFIG wind turbine system. *IET Renewable Power Generation*, 11(7), 941-951.
- [3.41] Sarker, K., Chatterjee, D., & Goswami, S. K. (2021). A modified PV-wind-PEMFCS-based hybrid UPQC system with combined DVR/STATCOM operation by harmonic compensation. *International Journal of Modelling and Simulation*, 41(4), 243-255.
- [3.42] Soued, S., Chabani, M. S., Becherif, M., Benchouia, M. T., Ramadan, H. S., Betka, A., ... & Zouzou, S. E. (2019). Experimental behaviour analysis for optimally controlled standalone DFIG system. *IET Electric Power Applications*, 13(10), 1462-1473.
- [3.43] Chhipa, A. A., Chakrabarti, P., Bolshev, V., Chakrabarti, T., Samarin, G., Vasilyev, A. N., ... & Kudryavtsev, A. (2022). Modeling and Control Strategy of Wind Energy Conversion System with Grid-Connected Doubly-Fed Induction Generator. *Energies*, 15(18), 6694.
- [3.44] Shabani, A., Asgarian, B., Gharebaghi, S. A., Salido, M. A., & Giret, A. (2019). A new optimization algorithm based on search and rescue operations. *Mathematical Problems in Engineering*, 2019.
- [3.45] Chatterjee, D. (2011). A novel magnetizing-curve identification and computer storage technique for induction machines suitable for online application. *IEEE Transactions on Industrial Electronics*, 58(12), 5336-5343.
- [3.46] Cleveland, F. M. (2008). IEC 61850-7-420 communications standard for distributed energy resources (DER). In *2008 IEEE Power and Energy Society General Meeting-Conversion and Delivery of Electrical Energy in the 21st Century* (pp. 1-4). IEEE.
- [3.47] Blooming, T. M., & Carnovale, D. J. (2006). Application of IEEE Std 519-1992 harmonic limits. In *Conference Record of 2006 Annual Pulp and Paper Industry Technical Conference* (pp. 1-9). IEEE, DOI: 10.1109/PAPCON.2006.1673767.

[3.48] Basso, T. (2014). *IEEE 1547 and 2030 standards for distributed energy resources interconnection and interoperability with the electricity grid* (No. NREL/TP-5D00-63157). National Renewable Energy Lab. (NREL), Golden, CO (United States), DOI: <https://doi.org/10.2172/1166677>.

[3.49] Beaulieu, G., Bollen, M. H., Malgarotti, S., & Ball, R. (2002). Power quality indices and objectives. Ongoing activities in CIGRE WG 36-07. In *IEEE Power Engineering Society Summer Meeting, 2*, pp. 789-794). IEEE.

CONCLUSION**4.1 INTRODUCTION**

This chapter summarises the contributions made by the dissertation work. It also describes the future scope of work that can be carried out further for maintaining power quality in microgrid connected hybrid system.

4.2 OUTLINE OF THE CONTRIBUTIONS

It is very important to understand every aspect of the topic clearly to achieve the objective of the thesis successfully. The aspects that are to be taken care of in the chronology are the source of renewable energy, components used like proper converters and their control design, maintaining the power quality by harmonic reduction on grid connection as well as practical implementation and then finally heading to the achievement of ultimate proposed design.

In the present thesis different topologies have been developed and discussed in detail. The contributions made for the present dissertation are as follows:

The thesis presents a PV integrated grid system the use of series compensation under PSC, has possibly eliminated harmonics and improved voltage profile. The obtained results were compared with the standard and the existing reports. It was found that these results have not only mitigated significant number of harmonics but also regulates wider voltage variations. The experimental results of the prototype have also been presented to verify the simulated outputs. The performance of three switching angles obtained from IJFA was equivalent to nine switching angles per quarter cycle in reducing harmonics, resulting in lower losses and improved system efficiency. A piecewise mixed-model approach has been used to store angles offline in the micro-controller for the online applications. Its application can be found in large power plants for effective control of output voltage as well as output harmonics. This research can be helpful in improving the quality of life in the remote grid-secluded regions.

Subsequently the thesis has introduced a topology based on harmonic suppression using the SAR-based optimization technique. A comparison of different optimization technique has been carried out in which SAR outperformed. The scheme deals with just three switching angles per half cycle, hence contributing to lower converter losses and an increase in system utility. The proposed series compensation has supported drastically eliminating lower-order harmonics and massively suppressing the higher-order harmonics. Also, a comparative analysis has been carried out with different literature and it was found that the present scheme has improved performance over others to achieve the aims mentioned. Also, at low

wind speeds and wide voltage variations, it maintains the voltage on the grid. The results of the lab prototype corroborate the simulation results of the proposed scheme.

Further, a PV-Wind hybrid model was introduced in which MWOA optimization technique was used. It reduces the lower and higher-order harmonics obtained at the stator and rotor side of the DFIG system. The best performance of all was that of MWOA, considering factors such as convergence time, minimum THD possible, etc. The angles obtained from the evolutionary techniques were stored offline in the microcontroller memory for online usage. Here, five switching angles gave equivalently good results as that of seven switches. A test system was also modelled for this scheme. Also, the other part of the chapter deals with the purpose of controlling the converters at higher wind speed. The aim was to achieving constant generated voltage at different wind speed was obtained. GWO search based algorithm was used to find out the angles for SHEPWM inverters. This paper also achieves the purpose of harmonic mitigation efficiently by the implementation of SHEPWM technique at any wind speed within the speed limit. This paper successfully achieves the purpose of controlling the converters at high wind speed and has satisfactorily met every aspect. Table 4.1 shows the comparison carried out between various schemes used in the present thesis.

Table 4.1 Comparison of different proposed schemes proposed in this thesis.

Parameters	Chapter 2		Chapter 3	
	Scheme 1	Scheme 2	Scheme 1	Scheme 2
Objectives	Inverter comparison carried out to find which performs the best out of all	To deal with wider voltage variation, harmonics reduction and PSC	Focusses on harmonics reduction thus reducing its corresponding THD.	To deal with wider voltage variation, harmonics reduction and PSC
PV-wind Hybrid System	No	No	No	Yes
Series Compensation	No	Yes	No	Yes
Metaheuristic technique used	PSO, GWO	IJFA	MWOA	SAR
Triggering angles used	5	3	5	3
Performance	Good	Best	Good	Best
THD	1.56	1.32%	1.6%	1.8

Experimental Validation	Not done but can be carried out easily	Yes	Not done but can be carried out easily	Yes
----------------------------	---	-----	---	-----

Proper converters are required for the efficient conversion of DC to AC. Therefore, lastly a detailed comparative analysis of different switching methods for inverters was carried out to analyze which outperforms for the PV integrated microgrid system. For SHEPWM and CHB-MLI H-bridge inverters, GWO switching scheme works better for removing undesirable harmonics. The controller adjusts itself with the variation in load. The proposed method shows benefits in terms of power quality and switching frequency and the complex circuit designs thus, reducing the overall costing. Later, a comparison of PSO and GWO algorithms has been done on the basis of smoother and faster convergence, efficiency, THD minimization, and harmonic compensation etc. for calculation of optimum switching angled for minimum THD for three-levelled inverter. GWO outperformed PSO under wide range of modulation index for three levelled inverters. The switching angles are calculated offline by PSO and GWO technique and hence stored in controller memory in the form of look up table. The study has been carried out using MATLAB simulation.

4.3 RECOMMENDATION FOR FUTURE WORK

Various proposed schemes have been studied for improving and maintain power quality. There were new topologies are developed based on the existing topologies after modifying them in order to develop better topologies. Based on completed research work and report, possible area for further investigation is presented here:

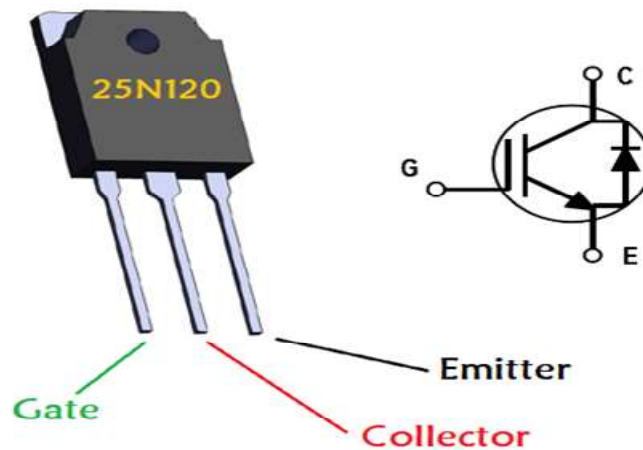
- Application of GaN-FET and or some other advanced electronic compensators tools in order to improve the power handling capability with lower losses along with reactive power compensation.
- Also, this research can be extended to faulty conditions such as in grid faults (e.g., voltage unbalance, power and frequency fluctuation) and inverter faults.

APPENDICES

Appendix A

Various materials used to develop the hardware in chapter 2

- Pin diagram for power IGBT “FGA25N120” (Courtesy: Google Image).



The ratings of the IGBT FGA25N120 used are given as follows:

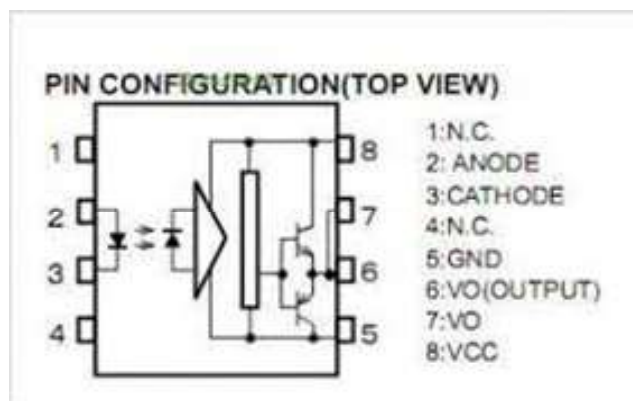
Collector- emitter voltage: $V_{ces} = 1200V$

Collector current: $I_c = 40A$ @ $T_c = 25^\circ C$

Maximum Power dissipation: $P_D = 310W$ @ $T_c = 25^\circ C$

Where, T_c is case temperature.

- Pin diagram for driver TLP 250H of 1636 series (Courtesy: Google Image).



➤ Pin diagram of PIC18F452 micro-controller (Courtesy: Google Image).

